PUBLIKACIJE ASTRONOMSKE OPSERVATORIJE U BEOGRADU
PUBLICATIONS OF THE ASTRONOMICAL OBSERVATORY OF BELGRADE
Sv. **97** No. **97**

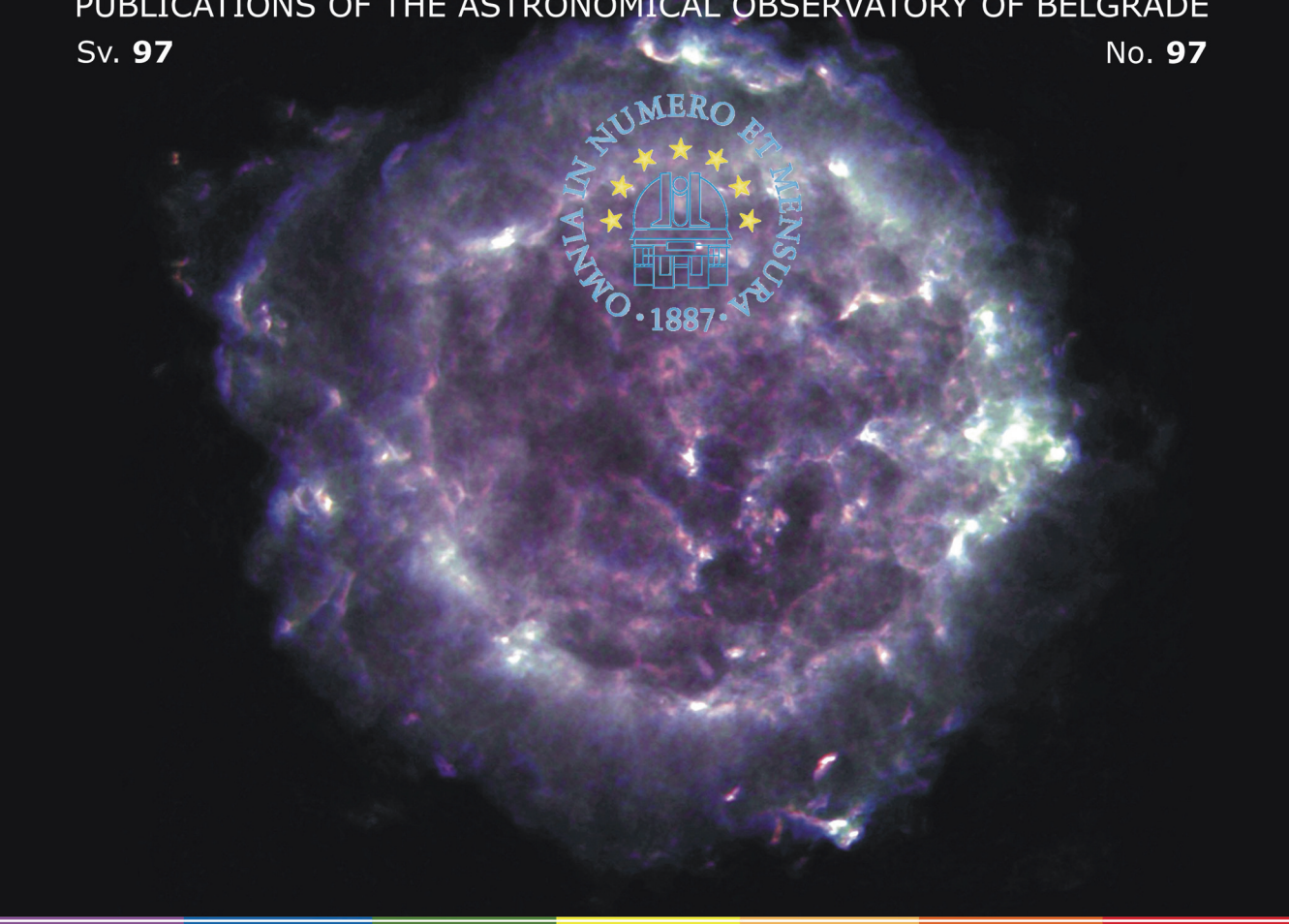

Bojan Arbutina

EVOLUTION OF SUPERNOVA REMNANTS

PUBL. ASTRON. OBS. BELGRADE No. 97, 1-92 BELGRADE, DECEMBER 2017

UDC 524.352 : 524.54 ISSN 0373-3742

ПУБЛИКАЦИЈЕ АСТРОНОМСКЕ ОПСЕРВАТОРИЈЕ У БЕОГРАДУ
PUBLICATIONS OF THE ASTRONOMICAL OBSERVATORY OF BELGRADE

Св. 97 **No. 97**

BOJAN ARBUTINA

EVOLUTION OF SUPERNOVA REMNANTS

Б Е О Г Р А Д
2017

PUBL. ASTRON. OBS. BELGRADE No. 97, 1-92 BELGRADE, DECEMBER 2017

PUBLICATIONS OF THE ASTRONOMICAL OBSERVATORY OF BELGRADE

FOUNDED IN 1947

Published and copyright © by Astronomical Observatory, Volgina 7, 11160 Belgrade 38, Serbia

Director of the Astronomical Observatory: Dr. Gojko Djurašević

Typesetting and cover design: Bojan Arbutina

Language editing: Dragana Momić

Cover image: Supernova remnant Cas A in radio (Image courtesy of National Radio Astronomy Observatory / Associated Universities, Inc.)

Internet address: `http://www.aob.bg.ac.rs`

ISBN 978–86–80019–83–3

The publication of this issue is financially supported by the Ministry of Education, Science and Technological Development of the Republic of Serbia.

Number of copies / тираж : 150

Production: Donat Graf, Vučka Milićevića 29, 11000 Belgrade, Serbia

Bojan Arbutina

Evolution of Supernova Remnants

BELGRADE, 2017

This book, both a monograph and a graduate textbook, is based on my original research and partly on the materials prepared earlier for the 2007 and 2008 IARS Astrophysics Summer School in Istanbul, AstroMundus course 'Supernovae and Their Remnants' that was held for the first time in 2011 at the Department of Astronomy, Faculty of Mathematics, University of Belgrade, and a graduate course 'Evolution of Supernova Remnants' that I teach at the aforementioned university. The first part *Supernovae* (introduction, thermonuclear supernovae, core-collapse supernovae) provides introductory information and explains the classification and physics of supernova explosions, while the second part *Supernova remnants* (introduction, shock waves, cosmic rays and particle acceleration, magnetic fields, synchrotron radiation, hydrodynamic and radio evolution of supernova remnants), which is the field I work in, is more detailed in scope i.e. technical/mathematical. Special attention is paid to details of mathematical derivations that often cannot be found in original works or available literature. Therefore, I believe it can be useful to both, graduate students and researchers interested in the field.

I would like to thank the referees Dejan Urošević, Srdjan Samurović and Aşkin Ankay for reading and commenting on the manuscript, as well as my colleagues and friends: Dragana Ilić, Tijana Prodanović, Dušan Onić, Branislav Vukotić, Milica Vučetić, Aleksandra Ćiprijanović, Jovana Petrović, Vladimir Zeković and Marko Pavlović, for numerous stimulating discussions. At the end, it remains only to thank Ministry of Education, Science and Technological Development of the Republic of Serbia for a grant towards printing expenses.

Belgrade, December 2017 B. A.

Contents

1 Supernovae

1.1 Introduction

Supernovae (SNe) are probably the strongest explosions in the Universe which mark the endpoint of life for some stars. They are quite rare events. The oldest records of SNe are found in the ancient Chinese chronicles, and the last two SNe observed in our Galaxy were discovered by Tycho Brahe and Johannes Kepler in 1572 and 1604, respectively (Table 1). There are some indications that the SN of the remnant Cas A, the strongest radio source in the sky, was recorded as a faint star by the first Astronomer Royal John Flemsteed around 1680 (Green & Stephenson 2002), but this remains uncertain. Today, there are thousands of extragalactic SNe discovered (see Barbon et al. 1999). The first, S And, was discovered by Ernst Hartwig in 1885 in the Andromeda's galaxy M31, and the closest was the well-known SN 1987A in the Large Magellanic Cloud. The term *super-novae* was introduced only in 1934 by Walter Baade and Fritz Zwicky, to distinguish this phenomenon from much less spectacular "classical" novae (Baade & Zwicky 1934). They suggested that SNe are explosions of stars and that in these explosions neutron stars are born.

Table 1: Historical supernovae and their remnants (see Green & Stephenson 2002). The last in this table is the first extragalactic supernova S And.

Date	Source	Constellation	Remnant
AD 185?	Chinese chronicles	Centaurus	G315.4-2.3?
AD 1006	Monks in Switzerland and Italy	Lupus	G327.6+14.6
AD 1054	Chinese chronicles, Arabian astronomers	Taurus	Crab
AD 1181	Chinese chronicles	Cassiopeia	3C58
AD 1572	Tycho	Cassiopeia	G120.1+2.1
AD 1604	Kepler	Ophiuchius	G4.5+6.8
AD 1680?	Flamsteed?	Cassiopeia	Cas A
AD 1885	Hartwig	Andromeda	(S And)

There are actually two main classes of SNe: SNe Ia representing the thermonuclear explosion of a white dwarf in a close binary system (CBS), and core-collapse SNe (II, Ib/c) resulting in the gravitational collapse of massive stars and believed to leave a compact stellar remnant, a neutron star or a black hole. Stripped-envelope SNe Ib/c represent a particular class of core-collapse SNe. They occur with stars stripped of their hydrogen/helium envelope in CBS and/or due to the strong stellar wind. Recently there were three SNe discovered: SN 1997ef, 1998bw, 2002ap, which might form a new subclass Ic pec corresponding to the hypernovae, possibly connected to some gamma-ray bursts (Hamuy 2003).

Historically, classification of SNe began by recognizing SNe I, with no hydrogen lines, and SNe II which do show hydrogen in their spectra (Minkowski 1941, see Fig. 1). SNe II make a quite heterogeneous class and can be further classified as SNe II-L whose light curves linearly decrease after maximum, and SNe II-P with a plateau on the light curves, due to the recombination of H (Fig. 2). Newer classes are IIb with low H and IIn showing narrow emission lines and probably interacting with dense circumstellar medium (CSM). There are also peculiar SN II like SN 1987A and Zwicky's types III, IV, V. A rather

homogeneous class SN I was shown later to consist of two spectroscopically and photometrically distinct subclasses: Ia as the only located in ellipticals and Ib found in H II regions and spiral arms, which strongly suggested that their progenitors were massive young stars with their H envelopes stripped. SNe Ic, discovered later, show no helium lines either, and thus correspond to massive stars stripped of their H and He envelopes. In addition, SN Ic pec (peculiar Ic, hypernovae) show smooth spectra with very broad lines due to the high expansion velocity i.e. high explosion energy.

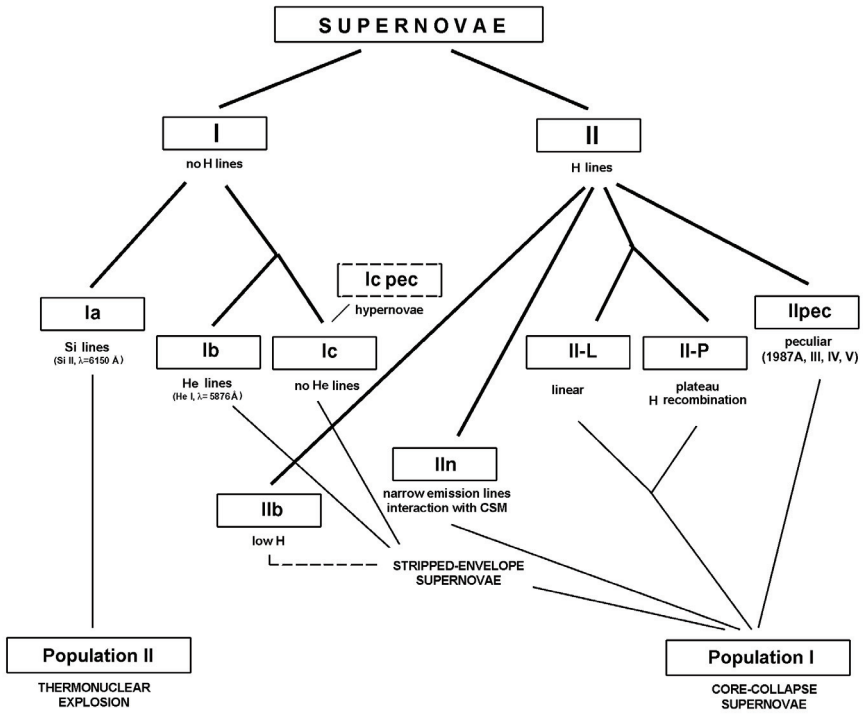

Figure 1: Classification of supernovae (from Arbutina 2005).

After a brief introduction to SN taxonomy, we shall finish this subsection with nomenclature i.e. naming conventions. The name is usually formed by combining the prefix SN, the year of discovery and a one- or two-letter designation. The first 26 SNe of the year get an upper case letter from A to Z, while the others get a pair of lower-case letters: aa, ab, ac, etc. SN 1885A and SN 1987A are thus the first SNe discovered in 1885 and 1987, respectively. The discovery is reported to the International Astronomical Union (IAU), which after confirmation, sends a telegram announcing discovery to the astronomical community. Nowadays, automated searches and a growing number of discoveries have resulted in the fact that not all SNe (not even the majority, see Gal-Yam et al. 2013) are being reported to IAU, and have lead some groups and projects, such as Catalina Real Time Survey, Robotic Optical Transient Search Experiment or Palomar Transient Factory, to develop their own naming conventions with prefixes such as CSS, ROTSE, PTF.

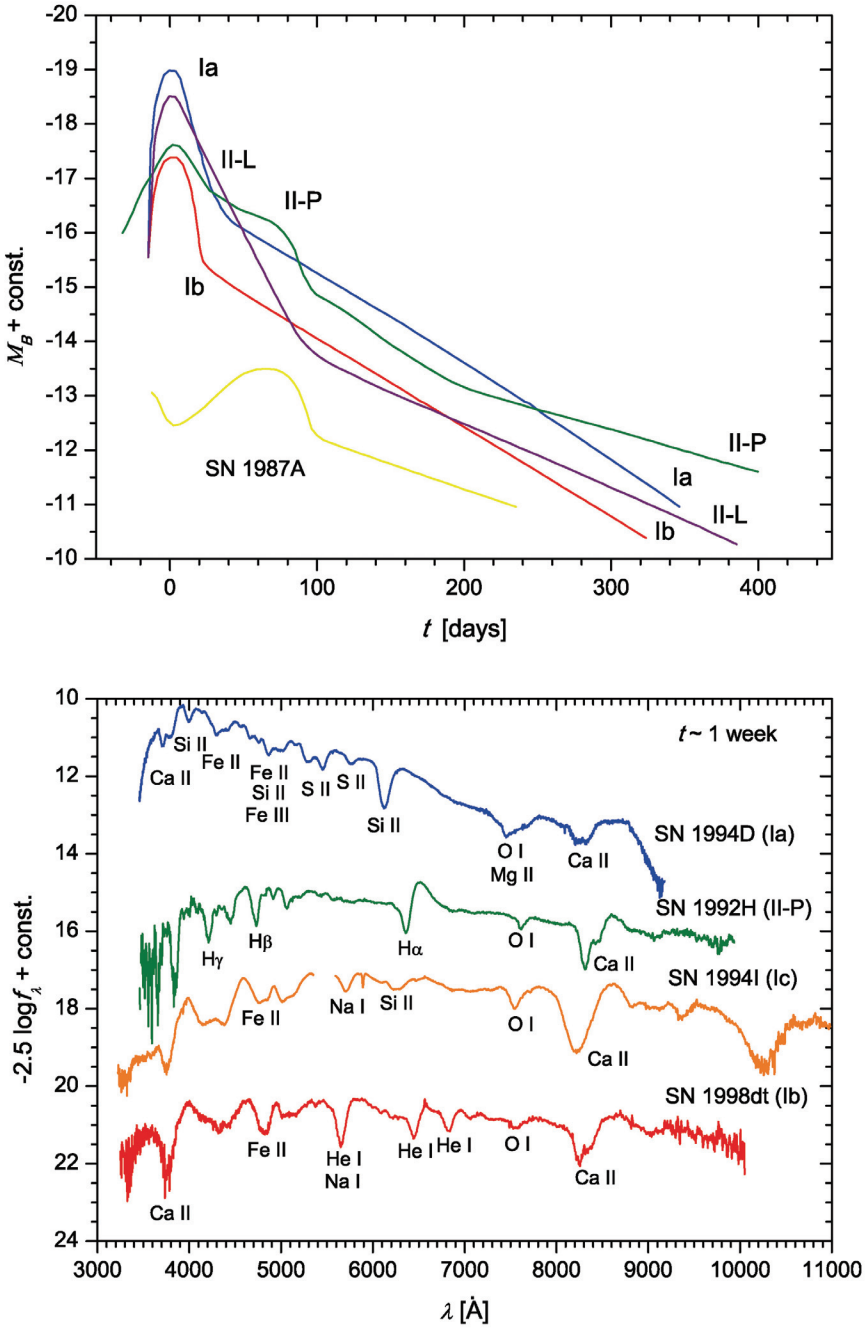

Figure 2: Up: sketch of light curves in B band for different types of SNe, adapted from Filippenko (1997) (after Wheeler 1990). Down: supernova spectra (from Caroll & Ostlie 2006, data by Thomas Matheson, National Optical Astronomy Observatory, and Alexei Filippenko, University of California, Berkley). t is time after maximum light and λ is the rest wavelength.

1.2 Thermonuclear explosions

SNe type Ia are widely used by astronomers as distance indicators or the so-called "standard candles". This is because they are bright, their absolute magnitude at maximum light reaches $M_V \approx M_B \approx -19$, and they represent a rather homogenous class when compared to other SN types.[1]

The standard model for type Ia SN is thermonuclear explosion (Hoyle & Fowler 1960), i.e. (delayed) detonation or deflagration (in the former case the nuclear burning front is supersonic, while in the latter case it is subsonic) of a carbon-oxygen white dwarf in CBS. In this scenario, when the secondary star in CBS has evolved enough to fill its Roche lobe, it will start to transfer mass to the white dwarf companion. The accreted matter may form a shell at the surface of white dwarf and if temperature in the shell rises high enough a thermonuclear flush may happen. This is the typical mechanism for novae outbursts.

However, if the mass transfer rate is high and the white dwarf has a mass close to the Chandrasekhar's limit, $\mathcal{M} \approx 1.4\ \mathcal{M}_\odot$, additional mass will cause instability and collapse which will lead to a rise of temperature and ignition of carbon and oxygen. In normal, main sequence stars supported by thermal pressure of gas and radiation, the pressure would rise and material would expand and cool to reestablish equilibrium. But since in the equation of state of degenerate gas the pressure is independent of temperature, there is no "safety valve" – the rise in temperature will not be followed by the rise in pressure and this is why nuclear burning processes in degenerate conditions tend to be explosive. In the case of white dwarfs, this will lead to a complete disruption of star.

Typical SN type Ia release in total the energy of about 10^{51} ergs. The explosion is usually so fast (takes about a second) and violent that for a few weeks the star can outshine its parent galaxy. Type Ia SNe light curves are powered by the decay of radioactive elements created in nuclear reactions (Arnett 1996), namely

$$^{56}\mathrm{Ni} \rightarrow {}^{56}\mathrm{Co} \rightarrow {}^{56}\mathrm{Fe},$$

which explains the characteristic shape of the light curve, its peak (nickel decay) and tail (decay of cobalt). The initial rise to a peak takes about two weeks, followed by a gradual decrease over the period of months. Their main spectral characteristic is a strong line of ionized silicon in early spectra, but also magnesium, sulfur and calcium, and iron in later phases.

Type Ia SNe are the only SNe whose progenitors are old, population II stars. We know from stellar evolution theory that massive stars mainly occur and remain in dense environments (such as molecular clouds) owing to their shorter lifetimes, while the longer-lived lower-mass stars tend, on average, to be found in less dense environments such as inter-arm regions of spiral galaxies or high above the galactic plane (see Fig. 3). These are the only SNe located in gas-deficient elliptical galaxies.

Most commonly used deflagration model for SNe Ia with detailed nucleosynthesis is W7 (Nomoto et al. 1984). The density profile for model W7 one day after the explosion is given in Fig. 4. The maximum velocity is around $v \sim 22000$ km s^{-1}. The inner part is often approximated by a flat and the outer

[1] This is not entirely true, because more careful observations have revealed differences among them. Events that are intrinsically dimmer near maximum light tend to decline more rapidly, but for most SNe Ia this is quantifiable, though there are some exceptions (Gonzalez Gaitan 2011).

Figure 3: Type Ia supernova SN 1994D in spiral galaxy NGC 4526 in Virgo cluster (NASA/ESA, The Hubble Key Project Team and The High-z Supernova Search Team).

part by a steep power-law $\rho t^3 \propto v^{-n}$, where $v = r/t$ is mass element's velocity and n is usually taken to be 7 for SNe type Ia, but it can also be well approximated with an exponential function $\rho t^3 \propto e^{-v/v_e}$, v_e being e-folding velocity (Jeffery 1999).

There is also an alternative model for SN Ia, the so-called double degenerate scenario (Iben & Tutukov 1984, Webbink 1984), which involves a merger of two white dwarfs in a CBS, rather than the explosion of one Chandrasekhar white dwarf in a cataclysmic variable – single degenerate scenario (Whelan & Iben 1973). For example, SN 2007if ejecta might have 2.4 $\mathcal{M}_\odot$ (Scalzo et al. 2010). Compact double white dwarf systems are believed to had gone through two stages of common envelope phase, during which a more evolved star practically engulfs its companion. In compact white dwarf systems this phase happens for the first time when the more massive primary to become a white dwarf engulfs the secondary star, and for the second time when during the curse of evolution the secondary expands and engulfs the already formed white dwarf. During the

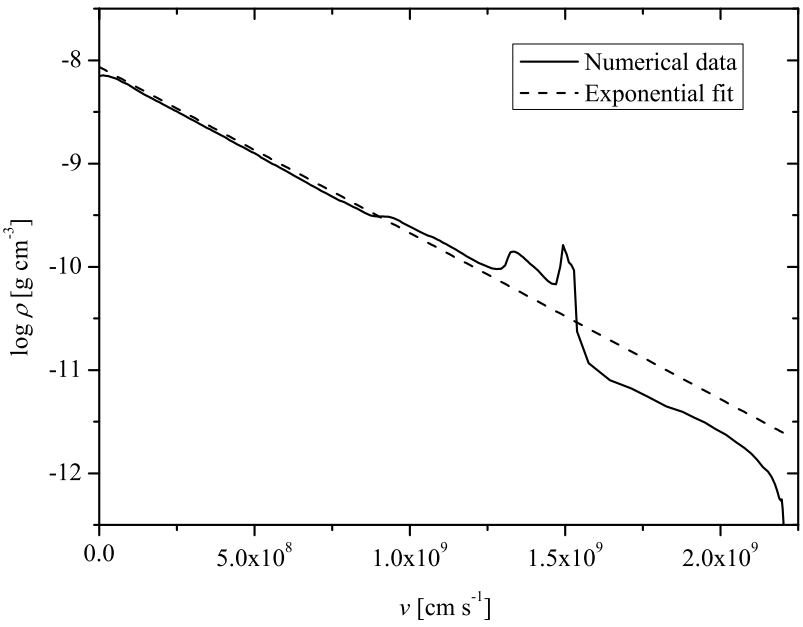

Figure 4: Density profile for W7 model 1 day after the explosion: numerical data and exponential fit.

common envelope phase a more compact star orbiting inside the envelope of the giant will lose energy due to friction and will slowly spiral-in towards the giant's core. This will produce heat and thus the orbital energy of the binary will practically be used to expel the envelope of the giant, leaving a compact binary system with two white dwarfs at the end of the second stage. The system will continue to lose energy due to the emission of gravitational waves or other mechanisms, and the stars will continue to spiral toward each other and will ultimately merge. If the total mass of the compact binary is greater than Chandrasekhar's mass, the merger can lead to type Ia SN explosion.

It is hard for astronomers to say which model for SN Ia is more favorable. No progenitor of type Ia SN has been seen so far. If the single degenerate scenario is correct, we may expect to find a runaway giant close the center of type Ia supernova remnant (SNR). This search has turned out to be negative for Kepler SNR which is believed to be type Ia (and some other remnants), at least for the surviving red giant companion (Kerzendorf et al. 2014). On the other hand, Krause et al. (2008) detected a light echo of Tycho's SN and spectrally confirmed that it was type Ia, while Ruiz-Lapuente et al. (2004) identified the so-called Tycho G star moving at more than three times the mean velocity of surrounding stars, as the possible surviving companion of Tycho's SN.

SNe type Ia are rare events, by human criteria. They make about 25 per cent of all SNe in spiral and irregular galaxies and the exact rate depends on galaxy luminosity or mass (Mannucci et al. 2005), but in a galaxy like ours one SN explodes every few hundred years. Tycho and Kepler SNe were the last two observed in our Galaxy, but this does not mean that SNe did not happen.

G1.9+0.3 is the youngest Galactic SNR, believed to be type Ia, only 130 years old (Reynolds et al. 2008). A large amount of gas and dust toward the Galactic center where it resides prevented astronomers from seeing this SN explosion.

1.2.1 Cosmological supernovae

Because of their high luminosity, SNe Ia are seen at very large cosmological distances of thousands megaparsecs. They played a crucial role in the discovery of acceleration of the Universe in the late 1990s for which Saul Perlmutter (Supernova Cosmology Project), Adam Riess and Brian Schmidt (High-z Supernova Search Team) were awarded the Nobel prize in physics for 2011 (Riess et al. 1998, Perlmutter et al. 1999).

Simply put, if all SNe Ia have nearly the same luminosity or absolute magnitude at maximum light, we can measure their apparent magnitudes and determine distances to their host galaxies. We know from Hubble's time the Universe is expanding and that the other quantities that we can measure are galaxies' redshifts z. In cosmology we can define distance in multiple ways. If we use objects whose dimensions are known – the so-called "standard rulers", and measure their angular dimensions, the distance obtained in this way is called angular-diameter distance d_A and it can be shown that Hubble's law for small z takes the form

$$H_0\ d_A = \frac{c}{1+z}(z - \frac{1+q_0}{2}z^2 + \ldots), \tag{1}$$

where Hubble constant is H_0 and deceleration parameter q_0 is supposed to be positive if the Universe is decelerating, which is what we expect if the only relevant force – the gravity is attractive. If, on the other hand, we use "standard candles" like SNe Ia, then we are talking about luminosity distances d_L and Hubble's law is

$$H_0\ d_L = c(1+z)(z - \frac{1+q_0}{2}z^2 + \ldots), \tag{2}$$

$$H_0\ d_L \approx c(z + \frac{1-q_0}{2}z^2 + \ldots). \tag{3}$$

In both cases, for local Universe $z \to 0$, we obtain the well-known linear Hubble's law $v = z \cdot c = H_0\ d$.

Table 2: Data adopted from Ned Wright's page* (Riess et al. 2007 dataset).

z	d_L
0.015	0.063
0.033	0.142
0.071	0.321
0.207	1.007
0.322	1.635
0.423	2.338

*`http://www.astro.ucla.edu/~wright/sne_cosmology.html`

If we use data from Table 2 and perform the least squares fit, we obtain $H_0 \approx 73$ km s^{-1} Mpc^{-1} and $q_0 = -0.569$ – the negative value suggesting the

action of some repulsive force commonly known as cosmological constant Λ or dark energy. Deceleration parameter can be expressed as

$$q = \frac{1}{2}\Omega_{\rm m} + \Omega_{\rm r} - \Omega_\Lambda, \tag{4}$$

where $\Omega_{\rm m}$, $\Omega_{\rm r}$ and Ω_Λ are mass-energy contributions from matter (including dark matter), radiation and dark energy, respectively. For the flat Universe (curvature constant $k = 0$) we have

$$\Omega_{\rm m} + \Omega_{\rm r} + \Omega_\Lambda = 1, \tag{5}$$

and if we further set $\Omega_{\rm r} = 0$, the last two equations give us $\Omega_\Lambda \approx 0.71$ and $\Omega_{\rm m} \approx 0.29$ which are close to the real values.

1.3 Core-collapse supernovae

Core-collapse SNe are believed to follow the gravitational collapse of massive stars at the end of their evolution, and the formation of neutron stars and black holes. This is the most probable scenario for stars with initial masses $\mathcal{M} \gtrsim 8\ \mathcal{M}_\odot$ (Nomoto 1984).

Stellar lifetime is primarily based on thermonuclear reactions in their cores. Massive stars will consume nuclear fuel more rapidly which will result in their shorter lifetimes. When hydrogen in stellar core is exhausted, a star will successively burn heavier and heavier elements – a process that for the most massive stars ($\mathcal{M} \gtrsim 12\ \mathcal{M}_\odot$) will end with iron. The collapse is usually triggered when the core reaches the mass $\gtrsim 1.4\ \mathcal{M}_\odot$ that degenerate electrons cannot support. What follows is the photodisintegration of iron at high temperatures

$$^{56}\mathrm{Fe} + \gamma \rightarrow 13\ ^4\mathrm{He} + 4\ \mathrm{n}$$

and electron capture $\mathrm{p} + \mathrm{e} \rightarrow \mathrm{n} + \nu$, on iron-group elements in a core (Fowler & Hoyle 1964, Woosley & Weaver 1986).

These processes basically cancel out millions of years of chemical evolution, leading to the loss of pressure support and implosion of the core. The iron core takes about a second to implode. The subsequent explosion in the envelope is the process that is still not understood well.

It is quite certain that the explosion is not dominantly thermonuclear, but a consequence of core collapse. Electron capture by protons will create more and more neutrons. As the pressure of degenerate neutrons increases, the collapse of the core is at some point halted and a neutron star is born. At the same time, the still infalling matter will bounce off the surface of this proto-neutron star and a strong supersonic shock wave will propagate back through the envelope. It is, however, questionable whether the shock will have enough energy to reach the outer layers of the star. In this situation the shock wave can stall, but the matter will continue to fall onto the neutron star and with enough matter it can crush into a black hole. Current calculations thus show that core bounce and shock formation alone are not sufficient to cause an explosion (see Wheeler 2003 and references therein).

However, each electron capture reaction, along with a neutron, creates a neutrino. Neutrinos will actually carry away most of the binding energy of a neutron star, $\sim 10^{53}$ ergs. While normal matter is transparent to neutrinos,

since they only interact through the weak force, neutron star matter is so dense that it can trap a small fraction of them and their energy may be enough to invigorate the shock and yield an explosion. Aside from neutrinos, important part in core-collapse SN explosions may be played by rotation and magnetic fields.

The majority of core-collapse SNe are type II with outer hydrogen layers still preserved. They make around 60 per cent of all SNe in spiral and irregular galaxies (Mannucci et al. 2005). No SN II has been observed in an elliptical. Spectroscopically, most SNe II around maximum, along with hydrogen absorption lines show solar abundances in ejected material approximately. An important subclass – type IIb, however, show weak hydrogen lines, and another one – type IIn, show narrow emission lines and other evidence of interaction with curcumstellar matter shed by progenitor star before explosion. In the later phases, when ejecta has expanded enough to become optically-thin, type II SNe show strong emission lines of hydrogen, but also oxygen, magnesium and calcium, characteristics of the evolved interiors of massive stars.

Photometrically, SNe II can be divided into two main subclasses, type II-P and type II-L. Their absolute magnitude at maximum light is around $M_B \approx -17$ to -18 with a large dispersion. The optical light curves of type II-P SNe show a rise to a peak brightness in a week or two, then a drop followed by period of a month or two when the light output is nearly constant – the plateau, after which luminosity goes further down. This photometric behavior is the basis for the so-called Expanding Photosphere Method (EPM, see Kirshner & Kwan 1974) for distance determination. The plateau is generally considered to be a consequence of the recombination of hydrogen in the envelope. Ionized hydrogen has a very high opacity, while neutral hydrogen has a very low opacity (except at a few special wavelengths). In stars, hydrogen starts to recombine at around 10000 K. In the outer layers of a SN, the densities are considerably lower than those in the photosphere of a typical star and thereby recombination occurs at around 6000 K. By a convenient coincidence, density and temperature of the gas at the opaque/transparent boundary – the effective photosphere – remains roughly constant. In a typical type II-P SN, thus, there is a period of several weeks to months during which we see an expanding photosphere of roughly constant temperature. If we combine equations

$$R = v \cdot t, \tag{6}$$

$$L = 4\pi R^2 \sigma T^4, \tag{7}$$

where σ is Stefan-Boltzmann constant, with photometric relation

$$M = m + 5 - 5 \log d, \tag{8}$$

by measuring v, t and apparent magnitude m, we can obtain luminosity L, absolute magnitude M and, finally, distance d. From Eq. (7) it is obvious that for to have such a large luminosity, with a temperature of only few thousands K, the SN must be huge – which is consistent with type II SNe dominantly being explosions inside red giants. Unlike type II-P, type II-L SNe after the peak brightness show a steady (linear) decline, implying a mass loss and expulsion of a large portion of the H envelope of the progenitor star. Light curves of both II-P and II-L SNe are powered by deposited SN energy rather than by the

radioactive decay of nickel. Only the long tail subsequent to the decline from the plateau in type II-P SNe is consistent with the radioactive decay of a small amount of cobalt.

The brightest SN detected since the invention of telescope was SN 1987A in the outskirts of the 30 Doradus (or Tarantula Nebula) in the Large Magellanic Cloud (Fig. 5). This SN is one of the most extensively observed object in the history of astronomy. It was observed in all wavelengths, from γ-rays to radio, and for the first time neutrinos were detected from an astronomical source other than the Sun, a couple of hours before the visible light. SN 1987A was, however, a very peculiar type II SN. Unlike most type II SNe, its light curve was powered by radioactive decay, but because only a small amount of nickel is synthesized in core-collapse SNe, SN 1987A was not very luminous. Furthermore, due to its proximity it was possible to identify progenitor star in archival images and it was shown that it was, surprisingly, a blue supergiant. Subsequent observations have not detected a neutron star either. SN 1987A is surrounded by three bright rings – inner and two outer rings, ionized by ultraviolet emission from SN. What we will observe in the following years is the early evolution of SNR – ejected material interacting with CSM, including the innermost ring already reached by the shock.

Density profiles of type II SNe can be very different due to their heterogeneity. It is sometimes assumed that they can be roughly approximated with a broken power-law, the outer part being described by a steep power-law with $n = 12$, but also with piecewise exponentials (Pizzochero 1990).

1.3.1 Stripped-envelope supernovae

It is important to recall that although stripped-envelope SNe phenomenologically belong to type I SNe (no hydrogen), they are physically core-collapse SNe whose progenitors are young stars i.e. population I objects. SNe Ib are those showing strong helium absorption lines in their early-time photospheric spectra, whereas SNe Ic are those in which there are very weak or no helium lines at all (see Filippenko 1997). SNe Ib/c light curves, as the ones for SNe Ia, are believed to be powered by radioactive decay. However, since type Ia SNe are generally brighter, they must produce more nickel, of order $1/2-1\ \mathcal{M}_\odot$, while for types Ib and Ic, the amount of nickel required to power the light curve is only $\sim 0.1\,\mathcal{M}_\odot$ consistent with the amount synthetized when the shock wave produced during core-collapse impacts the layer of silicon surrounding the iron core (Wheeler 2003). Absolute magnitude for type Ib/c SNe at maximum light varies, but the average value corrected for extinction might be $M_B \approx -18$ (Arbutina 2007).

Since SNe type Ib show no hydrogen and type Ic no helium either, they are thought to occur with stars stripped of their hydrogen/helium envelope due to mass loss either because of the strong stellar wind or mass transfer/loss in CBS. According to Nomoto et al. (1994) the progenitor of type Ic SN might be a massive CO star in CBS formed after two stages of mass transfer/common envelope evolution during which both H and He were removed. Similarly, Woosley et al. (1995) modelled progenitors of type Ib SNe as helium, Wolf-Rayet stars in CBS – only one phase of mass transfer was invoked.

SN 1993J was a SN observed in the M81 galaxy, showing features typical of type II SNe near the maximum light, but with the strong helium lines characteristic of type Ib SNe at later times (Schmidt et al. 1993). This implies that

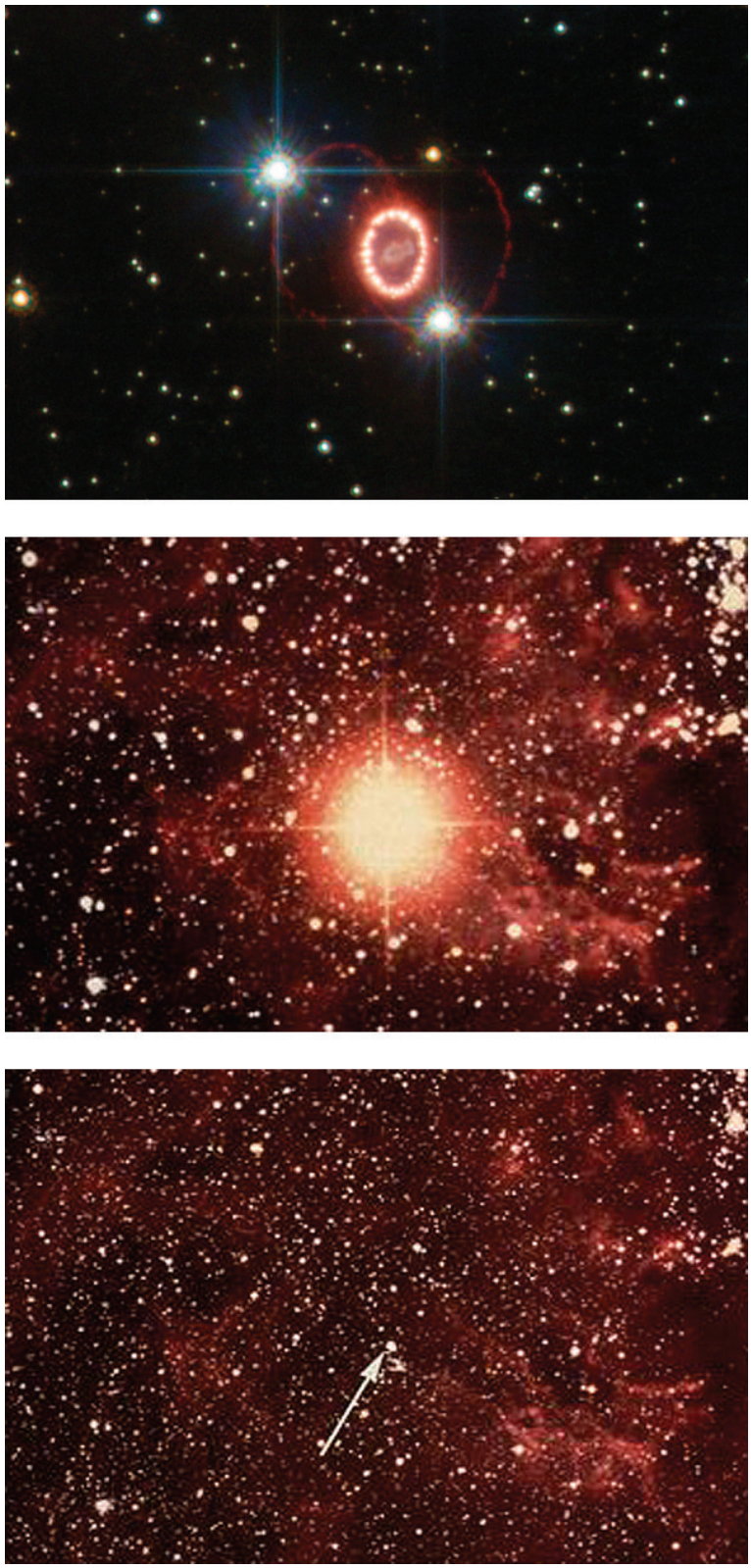

Figure 5: SN 1987A before (left), at the moment of (center) and 24 years after the explosion (right). (Image credit: Anglo-Australian Observatory/David Malin (left, center) & ESA/Hubble Space Telescope, NASA (right))

the progenitor star had an unusually thin hydrogen envelope. Hence, the SN has been classified as a type IIb, an intermediate class between type II and type Ib. Since M81 is relatively close, it was possible to identify the progenitor as a K supergiant star, and later even the presence of the long suspected B supergiant companion (Maund et al. 2004).

A typical type Ic SN is SN 1994I in the Whirlpool galaxy, M51. In the following years there were three SNe discovered: SN 1997ef, 1998bw, 2002ap, which are now considered to form a new subclass, Ic pec, corresponding to the hypernovae (Paczyński 1998), possibly connected to some gamma-ray bursts (see Hamuy 2003). These SNe have smooth spectra with broadened lines due to high expansion velocity i.e. explosion energy $\sim 10^{52}$ ergs, at least an order of magnitude higher than usual. Hypernovae and long gamma-ray bursts (GRBs) are frequently associated with the collapsar model (MacFadyen & Woosley 1999). A star with a core mass $\gtrsim$ 10-15 $\mathcal{M}_\odot$ (or main-sequence mass $\gtrsim$ 30-40 $\mathcal{M}_\odot$) ultimately collapses into a black hole. If such a star is rotating slowly, it will produce a failed SN, but if the star is rotating fast enough, the accretion disk will form and powerful jets may be produced. During its propagation through the star, the jet deposits enough energy to explode, eventually, all the star that has not already collapsed to the disk. After the jet breaks through the surface of the star, a highly relativistic flow can emerge. Physical details behind these processes and observational effects such as inclination i.e. viewing angle can lead to many possible outcomes, ranging from bright GRBs to faint GRB-SNe like SN 1998bw.

1.3.2 Some special supernovae

At the lower end of the mass range for core-collapse SNe, $\mathcal{M} \sim$ 8-12 $\mathcal{M}_\odot$, evolution might look differently than in the standard scenario described in the previous section. In these stars carbon burns to create neon and magnesium, but oxygen does not get hot enough to burn. The collapse may thus start before the iron core had been formed. Such SNe are known as electron-capture SNe, in which e^- capture by Ne and Mg lowers the pressure and inaugurates the collapse. During the collapse, the remaining nuclear fuels are converted to iron, so the net result is a collapsing iron core, as before, but there may be some differences that could affect the explosive outcome (Wheeler 2003). These SNe are thought to be less energetic, $\sim 10^{50}$ ergs, but their observational features are not completely clarified yet.

At the high-mass end we may see the so-called pair-instability (or pair-production) SNe which are presumed to be the final stage of the evolution of extremely massive stars, $\mathcal{M} > 100\mathcal{M}_\odot$, in whose cores the temperature is so high that electron-positron pairs are created from high energy γ-ray photons. The process will lower the pressure and induce a partial collapse followed by oxygen ignition. Fusion releases nuclear energy that heats the material further, which in turn speeds up the fusion, in a runaway reaction. The explosion is believed to disrupt the whole star (no compact stellar remnant). It would also form a huge amount of nickel. A good candidate was found in SN 2006gy which was after hundred days more luminous than the brightest SNe Ia, but afterward faded too quickly to have been powered by radioactivity. Nevertheless, another extremely luminous supernova, SN 2007bi, showed the right characteristics and probably is a pair-instability SN (Gal-Yam 2012). Very massive high metallicity

stars are probably unstable due to the Eddington limit, so pair-instability SN are presumed to occur primarily in Population III stars – the first stars in the Universe.

2 Supernova remnants

2.1 Introduction

While SN events happen quite suddenly and last for a relatively short time, in astronomical standards (historical SNe were visible for about a year), SNRs – the material ejected in an explosion, continue their life through the interaction with the surrounding interstellar medium (ISM) for thousands, and in extreme cases up to a million years. SNRs are responsible for enrichment of ISM with heavier elements produced in nucleosynthesis in stars and for creating turbulence in ISM from which the second generation stars, like our Sun, have been born. SNe and SNRs thus might be indirectly responsible for our own, human existence (as a carbon-based life).

SNRs are generally characterized by the interaction of SN ejecta with the surrounding ISM. In some cases the ejected material primarily interact with the dense CSM in the vicinity of the star during the phase known as the radio SN. The main features of SNRs are strong shock waves, amplified magnetic field, ultra-relativistic particles (cosmic rays) generation and associated synchrotron radiation. Synchrotron radiation is dominant at radio frequencies, which is why most SNRs are identified in radio (Urošević et al. 2005, Green 2014).

In optical search for SNRs we use the fact that the optical spectra of SNRs have elevated [S II]/Hα emission-line ratios, as compared to the spectra of normal H II regions. So far, through this technique, more than 1000 optical extragalactic SNR candidates have been detected (Vučetić et al. 2015). This emission ratio has proven to be an accurate means of differentiating between shock-heated SNRs (ratios > 0.4, but often considerably higher) and photoionized nebulae (0.4, but typically < 0.2). The physical basis for this is that in typical H II regions, sulfur exists mainly in the form of S III, yielding low [S II] 6717,6731 nm to Hα emission ratios. After the shock wave from an SN explosion has propagated through the surrounding medium and the material has cooled sufficiently, a variety of ionization states are present, including S II. This accounts for the increased ratio [S II]/Hα observed in SNRs (Blair & Long 2004). Generally, the material in H II regions is too ionized to produce forbidden lines of [O I], [N II] or [S II], while in SNRs both, models (Allen et al. 2008) and observations show optical spectra containing these lines (Long 2016).

SNRs can be broadly classified as shell-type or plerions (filled-center). Mathewson et al. (1983) classified SNRs into four categories based on their optical features: Balmer-dominated, oxygen-rich, plerionic/composite, and evolved SNRs. It has been suggested (van den Bergh 1988) that Balmer-dominated SNRs are connected to type Ia SNe – deflagration of a CO white dwarf, and are remnants with high velocity, non-radiative, collisionless shock interacting with ISM, while oxygen-rich SNRs originate in the type Ib (Ic) event – explosion of a massive O or a Wolf-Rayet (W-R) star, and have emission arising from a shock interacting more with the circumstellar material lost by the progenitor in the last stages of the stellar evolution. Similarly, plerionic/composite SNRs originate in type II events – explosion of a massive B star, and derive their energy from the rotational energy losses of a stellar remnant – neutron star (pulsar driven plerions), plus the shock wave powered shell (in the case of composite type). All three of these classes eventually become evolved remnants. This picture is probably oversimplified. Although, in some oxygen-rich SNRs like Pup A and

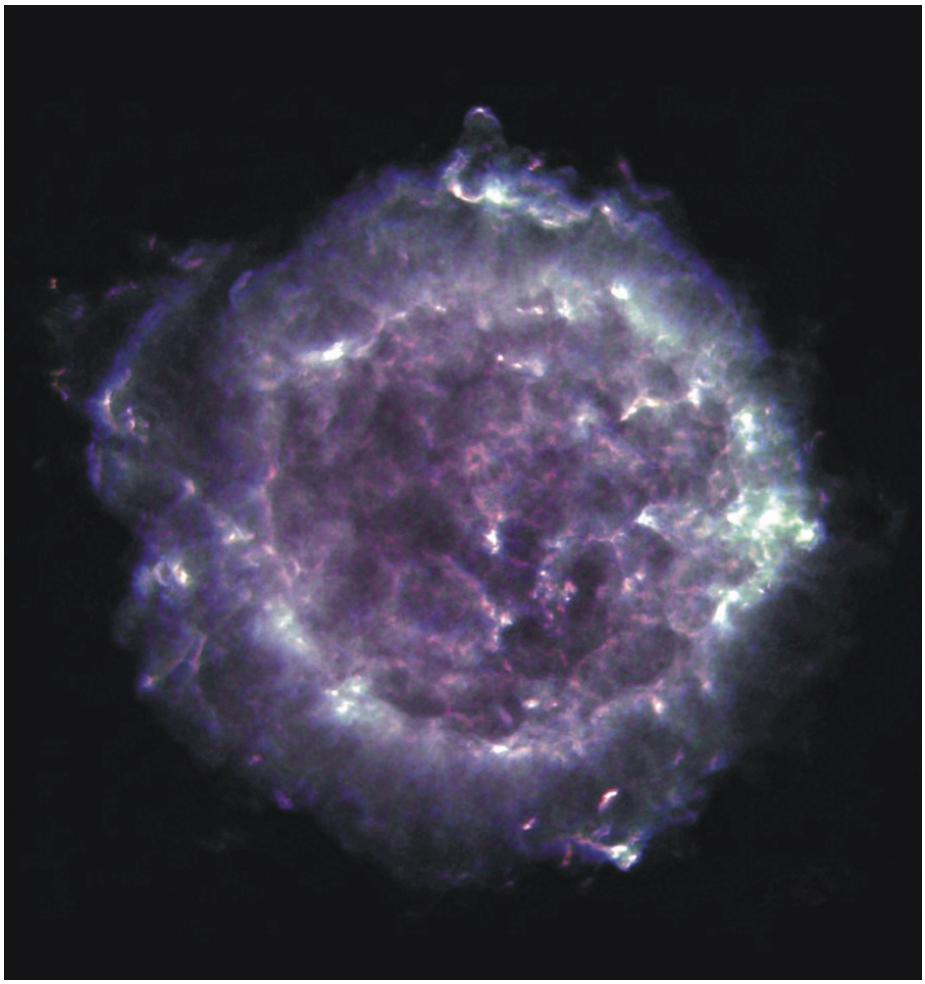

Figure 6: Supernova remnant Cas A in radio (Image courtesy of National Radio Astronomy Observatory / Associated Universities, Inc. Investigators: L. Rudnick, T. Delaney, J. Keohane and B. Koralesky, image composite by T. Rector).

Cas A (Fig. 6) radio-quiet neutron stars have been discovered, some do show pulsars and plerions. It is quite difficult to deduce SN type from observations of its remnant, and especially to separate type Ib/c and type II SNRs. X-ray emission lines diagnostics has been a valuable tool in performing this task.

Owing to an increasing number of space observatories in recent decades (ROSAT, ASCA, Chandra, XMM-Newton), many SNRs have been observed in X-rays (Fig. 7). A large number of SNRs emit "soft" X-ray ($\lesssim 10$ keV) thermal *bremsstrahlung* radiation (free-free emission). Older remnants evolving in dense environment (with hydrogen number density $n_{\mathrm{H}} \sim 300$ cm^{-3}) may also emit thermal bremsstrahlung in radio domain (Urošević & Pannuti 2005, Onić et al. 2012, Onić 2013). On the other hand, there are considerable efforts nowadays in detecting and analyzing non-thermal X-rays in younger remnants. Non-thermal X-rays are likely synchrotron or non-thermal bremsstrahlung emission, while

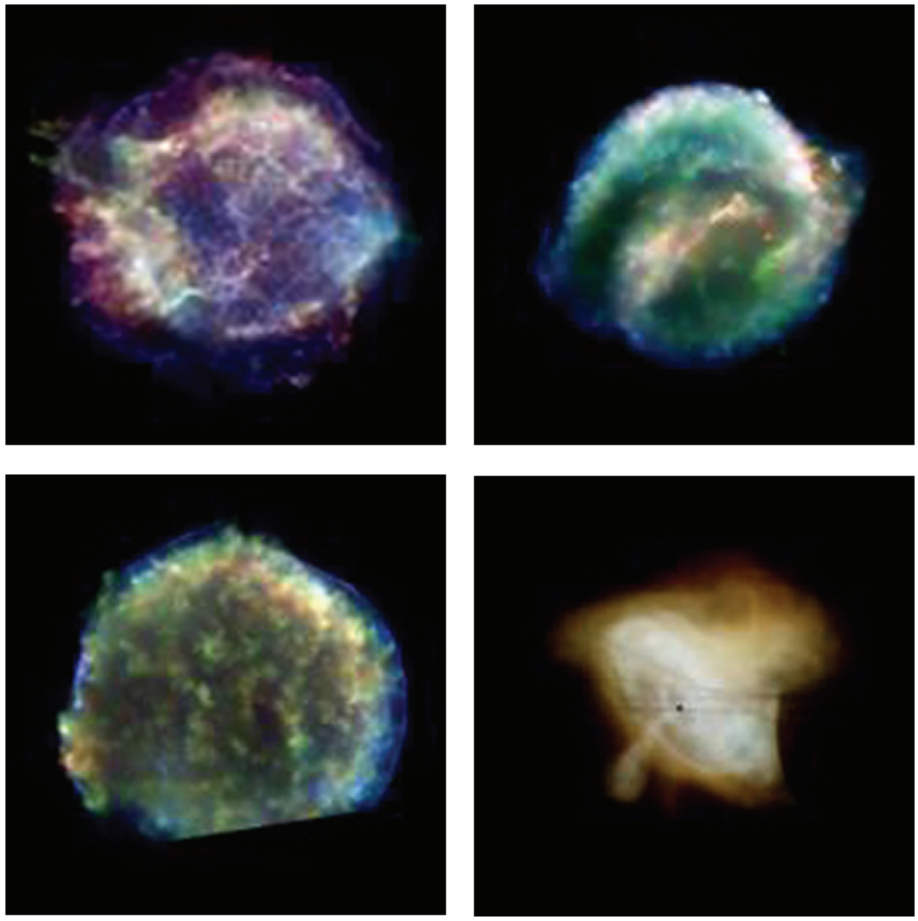

Figure 7: Supernova remnants in X-rays. Top-down and left-right: Cas A, Kepler, Tycho, Crab (Chandra X-ray Observatory / Harvard Smithsonian Center for Astrophysics / NASA).

thermal emission may be bremsstrahlung, recombination continuum (free-bound emission), and two-photon emission (see an excellent review by Vink 2012).

Morphologically, SNRs in X-rays resemble their radio counterparts and have a visible emitting shell. There is, however, a special class of SNRs, not completely understood, the so-called mixed-morphology SNRs with a radio shell with flat radio spectra and thermal X-rays emitting interior (see Onić 2013).

SNe release about $E_o \approx 10^{51}$ ergs in the form of kinetic and thermal energy (in the case of hypernovae this number is larger, $\geq 10^{52}$ ergs).[2] Only about one per cent of this energy is radiated in the form of light and seen as a SN event. The ejected mass is of order $\mathcal{M}_o \approx 1 - 10\ \mathcal{M}_\odot$ (or even more) depending on SN type. Typical SN expansion velocities $v^2 \sim E_o/\mathcal{M}_o$ range from a few thousand to a few tens of thousand km s^{-1}. These are also the initial shock velocities in SNRs.

[2]Most of the energy is, of course, taken away by neutrinos, about 10^{53} ergs, for a typical core-collapse SN.

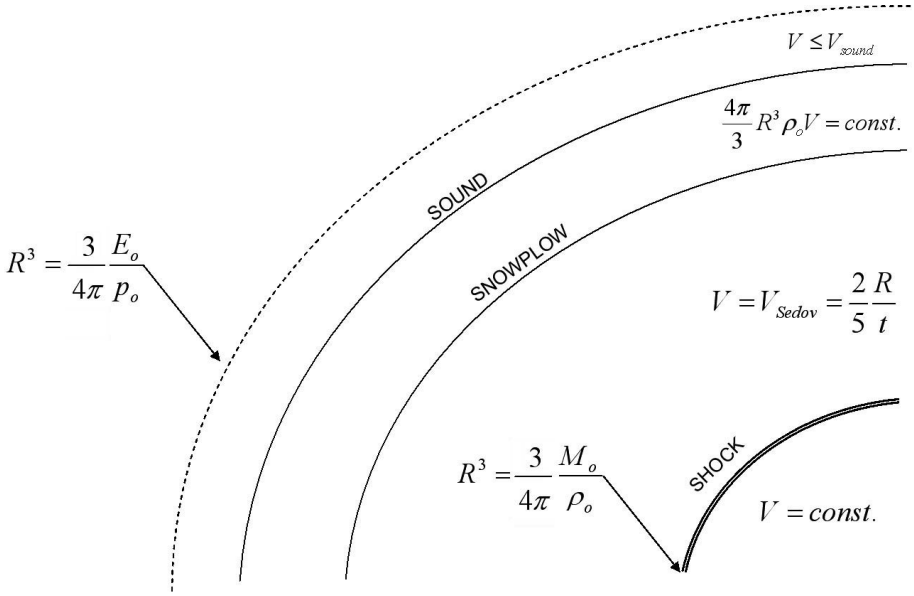

Figure 8: Evolution of supernova remnants (Arbutina 2005).

The standard picture of evolution of SNRs (Figs. 8 and 9), from the explosion to the end of expansion, involves four different phases[3] (Woltjer 1972):

(i) free expansion,

(ii) adiabatic i.e. Sedov's phase (Sedov 1959),

(iii) radiative phase, and

(iv) dissipation.

During the first phase, after the explosion, ejected material expands practically in vacuo with the constant velocity $v_s^2 = (dR/dt)^2 \propto E_o/\mathcal{M}_o$, i.e.

$$R \propto (E_o/\mathcal{M}_o)^{1/2} t, \tag{9}$$

where R and t are the radius of SNR and the time since the explosion, respectively, E_o is SN energy and $\mathcal{M}_o$ is the mass of the ejecta. In terrestrial explosions we expect a shock wave to form in collisions between the ejected and the surrounding particles. In space conditions where hydrogen density is as low as $n_{\rm H} \sim 1$ cm^{-3} and ejected material velocity is typically $v \sim 10\,000$ km s^{-1}, shock wave in collision processes would never form. The key role in these collisionless shock waves is taken over by the magnetic field which serves a massless barrier between the SN ejecta and the swept-up ISM (Rohlfs & Wilson 2004). The term free expansion for this first phase of evolution of SNRs is more historical, since there may be significant deceleration even in this phase. Transition from this to the subsequent phase in the evolution of SNRs is often described with the solutions given by Chevalier (1982).

[3]We shall focus on shell-type SNRs. In the case of plerions, the pulsar presence can significantly complicate this simple four-phase picture.

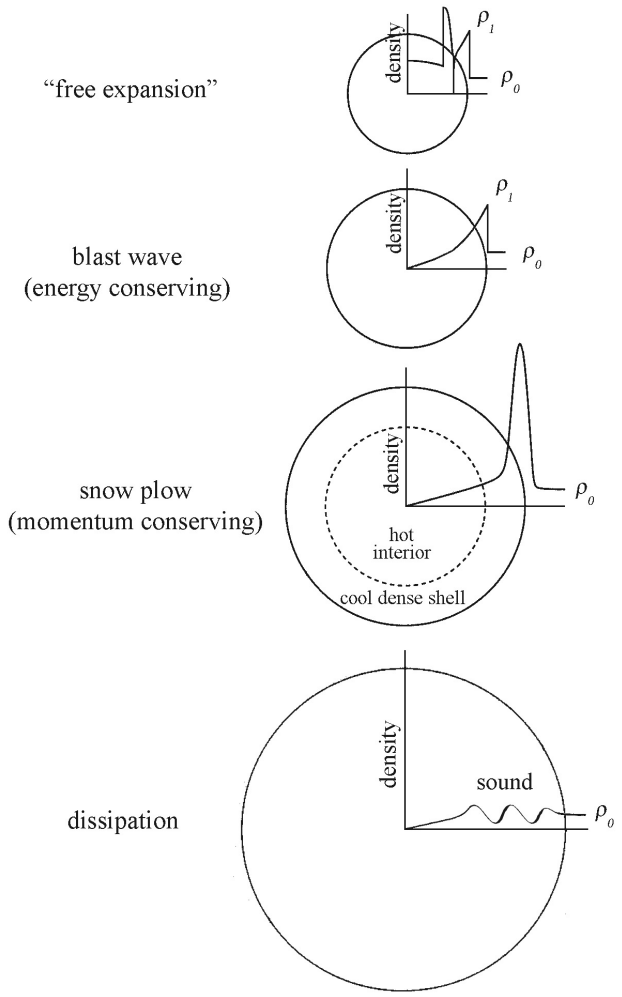

Figure 9: Density profile of supernova remnants in different phases. Adapted from Shu (1992).

When the shock wave sweeps-up enough space so that the ISM mass many times exceeds the mass of SN ejecta $4\pi R^3\rho_o/3 \gtrsim \mathcal{M}_o$, a SNR enters the second phase of evolution. During this phase the shock wave decelerates according to the law $v_s = dR/dt = 2R/(5t)$, i.e.

$$R = 1.15\ (E_o/\rho_o)^{1/5} t^{2/5}, \tag{10}$$

which is given in the analytical solution of Sedov (1959), for a point-like explosion in the uniform medium with density ρ_o. Sedov phase is approximately energy-conserving ($\int (dE/dt)_{\rm rad} dt \ll E_o$) i.e. the expansion is nearly adiabatic.

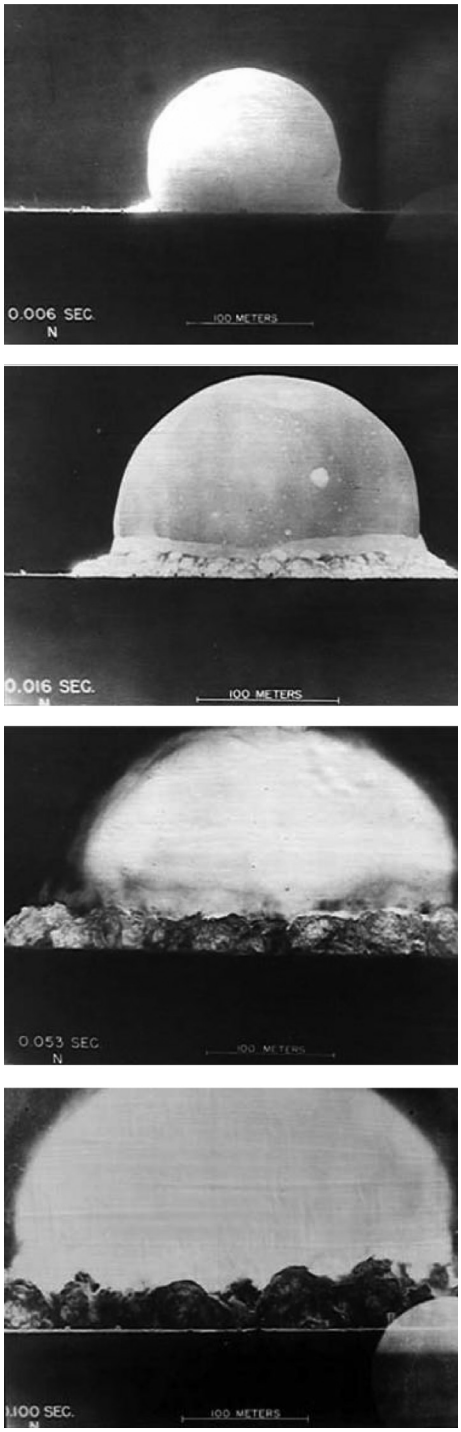

Figure 10: Trinity test, Alamogordo atomic bomb probe, New Mexico, 1945 (Los Alamos National Laboratory).

Independently of Sedov, this solution was found numerically by Taylor (1950), who used it to deduce the energy released in the Alamogordo atomic bomb probe. In 1950, by analyzing old photographs and applying his blast wave solution, Taylor calculated and published the explosion energy of the first atomic bomb, which was considered as classified information at the time! From Fig. 10 we estimate that at $t = 0.006$ seconds the radius of the shock wave was approximately $R \approx 80$ meters. From $E_o \approx (R^5\rho_o)/t^2$ we can estimate $E_o \sim 10^{21}$ ergs ~ 25 kilotons (1 g of TNT $= 4 \times 10^{10}$ erg, air density is about $\rho_o = 1.2$ kg m^{-3}).

When the temperature behind the shock drops, the energy losses due to the thermal radiation become significant and a remnant enters the radiative phase of evolution. The strict radiative phase last short since the gas cools quickly and loses all the energy. It is expected in this epoch that SNR undergoes a phase of dense shell formation. Afterwards the remnant continues to expand on account of the internal pressure behind the shell, as a pressure-driven snowplow: $R \propto t^{2/7}$ (McKee & Ostriker 1977, Bandiera & Petruk 2004).[4]

Finally, when the expansion velocity becomes comparable with the sound speed in the surroundings, $v_s^2 \sim c_s^2 = \gamma P_o/\rho_o$, the SNR will merge into the interstellar medium and the evolution ends. If we neglect the radiative losses (which may have some justification for SNR in low-density ISM) and assume that all the energy was spent for work against external pressure, $4\pi R^3 P_o/3 \lesssim E_o$ can give us some estimate of the largest radius up to which the remnant had expanded.

A problem in hydrodynamical description of the evolution of SNRs is the fact that all exact solutions of Euler's equations are obtained by similarity methods where we introduce dimensionless variable

$$\xi = crt^{-\lambda}, \tag{11}$$

from which follows the law $R \propto t^\lambda$, i.e. $v \propto R^{1-1/\lambda}$. Only for this power law expansion can we obtain a complete solution for an SNR, from the shock wave position to the center of explosion. The division into evolutionary phases is thus a necessity if we want to obtain analytical or semi-analytical results.

2.2 Shock waves

Shock waves are very important in astrophysics. They appear in many astrophysical objects and phenomena, such as SNe and SNRs, but also in the solar corona, where they might be responsible for heating, and let us not forget planetary and stellar bow shocks.

We know from standard courses of fluid dynamics that small-amplitude acoustic disturbances in isentropic (constant specific entropy) fluid will propagate with the adiabatic speed of sound $c_s^2 = \gamma \frac{P}{\rho}$. If magnetic field is present, equations of "ideal" magnetohydrodynamics (MHD) (when conductivity $\sigma \to \infty$)

$$\frac{\partial \rho}{\partial t} + \nabla \cdot (\rho \mathbf{v}) = 0, \tag{12}$$

[4]There is a possibility that SNR from the energy-conserving ends in the momentum-conserving phase $4\pi R^3 \rho_o v_s/3 = \text{const}$, as a momentum-conserving snowplow: $R \propto t^{1/4}$ (Bandiera & Petruk 2004).

$$\rho\frac{D\mathbf{v}}{Dt} = -\nabla P + \frac{1}{c}\mathbf{j}\times\mathbf{B} \qquad (\mathbf{j} = \frac{c}{4\pi}\nabla\times\mathbf{B}), \tag{13}$$

$$\frac{\partial}{\partial t}\Big(\rho(\frac{1}{2}v^2+\varepsilon)+\frac{1}{8\pi}B^2\Big)+\nabla\cdot\big(\rho\mathbf{v}(\frac{1}{2}v^2+h)+\mathbf{S}\big)=0 \tag{14}$$

$$\big(\mathbf{S}=\frac{c}{4\pi}\mathbf{E}\times\mathbf{B},\ \mathbf{E}=-\frac{\mathbf{v}}{c}\times\mathbf{B}\big),$$

$$\frac{\partial\mathbf{B}}{\partial t} = \nabla\times(\mathbf{v}\times\mathbf{B}), \tag{15}$$

will also give rise to Alfvén, fast and slow magneto-acoustic waves. In the last set of equations we used material or Lagrange derivative: $\frac{D}{Dt} = \frac{\partial}{\partial t} + (\mathbf{v}\cdot\nabla)$, $\mathbf{j}$ is current density, $\mathbf{S}$ is Poynting vector, $\mathbf{E}$ and $\mathbf{B}$ electric and magnetic field, respectively, $\varepsilon = \frac{u}{\rho}$ is energy per unit mass, $u = \frac{1}{\gamma-1}P$ energy density (energy per unit volume) and $h = \varepsilon + \frac{P}{\rho} = \frac{\gamma}{\gamma-1}\frac{P}{\rho}$ the specific enthalpy. Of course, we also have $\nabla\cdot\mathbf{B} = 0$ – the magnetic field lines are closed i.e. the field is "sourceless". Eq. (15) is differential equation form of Alfvén's theorem that magnetic field lines are practically "frozen" in ideal plasma. If $\mathbf{B} = 0$ we get Euler equations. Energy equation can be replaced with internal energy conservation (the first law of thermodynamics for adiabatic conditions):

$$\frac{D\varepsilon}{Dt} + P\frac{D}{Dt}\Big(\frac{1}{\rho}\Big) = 0. \tag{16}$$

Let us go back to sound propagation. If we ignore dissipation (action of viscosity) acoustic waves having finite amplitude of any waveform will always steepen. This is because acoustic sine waves are obtained by linearization of Euler equations (all higher order terms were neglected). Nonlinear acoustic waves cannot maintain a constant form. A part of the wave that has a density excess has a sound speed larger than the undisturbed speed of sound $c_s^2 = \gamma P_o/\rho_o$, and a part with the density deficit travels slower. The crest of the wave thus tends to catch up with the through, which will distort a sine wave, eventually producing a front – a "surface" at which density rises almost instantaneously. Of course, viscosity will make this discontinuity layer to have some finite thickness, but on the length scale of interest we will not see any smooth variations. High density (and high pressure) region will continue to push the front ahead faster than the undisturbed sound speed and eventually front completely overruns the trough of the wave propagating at supersonic speed through the undisturbed medium. At the same time, the tail of the wave will begin to lag behind the front, so that the profile gets stretched.

What we have just described is the steepening of acoustic waves into shock waves (Shu 1992). Unlike a steady shock wave driven by a constant source of momentum and energy (such as an airplane), shock waves created by explosion (an initial input of energy) are usually called blast waves.

There are actually two types of discontinuities in fluids: stationary (tangential and contact) and shocks. In stationary discontinuities there is no fluid flow across the surface i.e normal component of fluid velocity is zero. In tangential discontinuities normal component of magnetic field, with respect to the surface, is also zero, while in contact discontinuities it is not.

2.2.1 Adiabatic shocks

Adiabatic shock is actually a misnomer for energy conserving i.e. non-radiative shock. The term "adiabatic" refers to "entropy-conserving", while entropy is precisely what is not conserved in strong shocks.

Case $\mathbf{B} = 0$

We will first consider the case when $\mathbf{B} = 0$ and take a look at Euler equations for one-dimensional stationary flow (ρ, P, $v \neq f(t)$)

$$\frac{\partial}{\partial x}\big(\rho v\big) = 0 \quad \Rightarrow \quad \rho v = \text{const}, \tag{17}$$

$$\rho v \frac{\partial v}{\partial x} = -\frac{\partial P}{\partial x} \quad \Rightarrow \quad \rho v^2 + P = \text{const}, \tag{18}$$

$$\frac{\partial}{\partial x}\Big(\rho v\big(\frac{1}{2}v^2 + \varepsilon + \frac{P}{\rho}\big)\Big) = 0 \quad \Rightarrow \quad \frac{1}{2}v^2 + \frac{\gamma}{\gamma - 1}\frac{P}{\rho} = \text{const}. \tag{19}$$

Let us assume that there is instantaneous jump in density, pressure and velocity caused by a shock of velocity v_s passing through the undisturbed medium at rest, and that we are working in a frame of reference attached to the shock so that in this frame the gas is flowing into the shock with velocity $v_1 = -v_s$ (see Fig. 11). Eqs. (17)–(19) state that mass, momentum and energy must be conserved across the shock, i.e they must be the same ahead of the shock i.e. "upstream" (for which we will use index 1) and behind the shock i.e. "downstream" (for which we will use index 2). Thus, we have

$$\rho_1 v_1 = \rho_2 v_2, \tag{20}$$

$$\rho_1 v_1^2 + P_1 = \rho_2 v_2^2 + P_2, \tag{21}$$

$$\frac{1}{2}v_1^2 + \frac{\gamma}{\gamma - 1}\frac{P_1}{\rho_1} = \frac{1}{2}v_2^2 + \frac{\gamma}{\gamma - 1}\frac{P_2}{\rho_2}. \tag{22}$$

These are the well-known Rankine-Hugoniot jump conditions. They allow us to find downstream quantities, provided that upstream quantities are known.

If we denote density jump with X and pressure jump with Y, after some manipulation the last three equations give

$$X = \frac{\rho_2}{\rho_1} = \frac{(\gamma + 1)\mathrm{M}_1^2}{2 + (\gamma - 1)\mathrm{M}_1^2}, \tag{23}$$

$$Y = \frac{P_2}{P_1} = \frac{\gamma + 1 + 2\gamma(\mathrm{M}_1^2 - 1)}{\gamma + 1}. \tag{24}$$

where Mach's number $\mathrm{M}_1 = \frac{v_1}{c_s}$, v_1 is equal to shock speed (by absolute value) and $c_s^2 = \gamma\frac{P_1}{\rho_1}$ is adiabatic sound speed. If $\mathrm{M}_1 = 1$, we have a trivial solution $X = 1$, $Y = 1$. In strong shocks $\mathrm{M}_1 \to \infty$ and $X = \frac{\gamma+1}{\gamma-1} \to 4$ for $\gamma = 5/3$, which is an important result.

Case $\mathbf{B} \perp \mathbf{v}$

In the case $\mathbf{B} \perp \mathbf{v}$ jump conditions are

$$\rho_1 v_1 = \rho_2 v_2 \tag{25}$$

$$\rho_1 v_1^2 + P_1 + \frac{1}{8\pi} B_1^2 = \rho_2 v_2^2 + P_2 + \frac{1}{8\pi} B_2^2 \tag{26}$$

$$\frac{1}{2} v_1^2 + \frac{\gamma}{\gamma - 1} \frac{P_1}{\rho_1} + \frac{1}{4\pi} \frac{B_1^2}{\rho_1} = \frac{1}{2} v_2^2 + \frac{\gamma}{\gamma - 1} \frac{P_2}{\rho_2} + \frac{1}{4\pi} \frac{B_2^2}{\rho_2} \tag{27}$$

$$v_1 B_1 = v_2 B_2. \tag{28}$$

We immediately see that parallel magnetic field (parallel with respect to the shock front) is compressed in the same way as the density. One can check that compression ratio $X = \frac{\rho_2}{\rho_1}$ is now

$$X = \frac{-(1 + \frac{\gamma}{2\beta} + \frac{\gamma-1}{2}\mathrm{M}_1^2) \pm \sqrt{(1 + \frac{\gamma}{2\beta} + \frac{\gamma-1}{2}\mathrm{M}_1^2)^2 + \frac{(\gamma+1)(2-\gamma)}{\beta}\mathrm{M}_1^2}}{\frac{(2-\gamma)}{\beta}}, \tag{29}$$

$$X \approx \frac{(\gamma+1)\mathrm{M}_1^2}{2(1 + \frac{\gamma}{2\beta} + \frac{\gamma-1}{2}\mathrm{M}_1^2)} \to \frac{(\gamma+1)\mathrm{M}_1^2}{2 + (\gamma-1)\mathrm{M}_1^2} \quad \text{if} \quad \beta \to \infty, \tag{30}$$

where plasma beta is $\beta = c_s^2 / v_A^2$ and $v_A^2 = \frac{1}{4\pi}\frac{B_1^2}{\rho_1}$ is the upstream Alfvén speed.

Case $\mathbf{B} \parallel \mathbf{v}$

In the case $\mathbf{B} \parallel \mathbf{v}$ the magnetic field does not play any role since $B_1 = B_2$. The jump conditions are just Rankine-Hugoniot jump conditions.

However, in our analysis we have always assumed that the fluid velocity is perpendicular to a flat discontinuity surface – the shock front, i.e. that the shock is not oblique. An oblique shock wave, unlike a normal shock, is inclined with respect to the incident upstream flow direction. The presence of a magnetic field additionally complicates the situation. For example, it is possible to have magnetic field component parallel to the shock front equal to zero behind the shock (switch-off shock) or ahead of the shock (switch-on shock). The existence of such cases might have some consequences for the shock propagation parallel to the magnetic field. Namely, we can have far upstream and far downstream magnetic fields lying in their original directions, but a switch-on and a switch-off shock in-between (see Shu 1992).

Case $\gamma_1 \neq \gamma_2$

As we shall see in the next subsection, strong shocks are believed to be the sites of particle acceleration up to ultra-relativistic energies. Behind the shock thus we might have a population with different adiabatic index. For the sake of exercise let us consider a shock with different adiabatic index upstream and downstream, with $\mathbf{B} = 0$ or $\mathbf{B} \parallel \mathbf{v}$. Jump conditions are similar to Rankine-Hugoniot jump conditions, except $\gamma_1 \neq \gamma_2$.

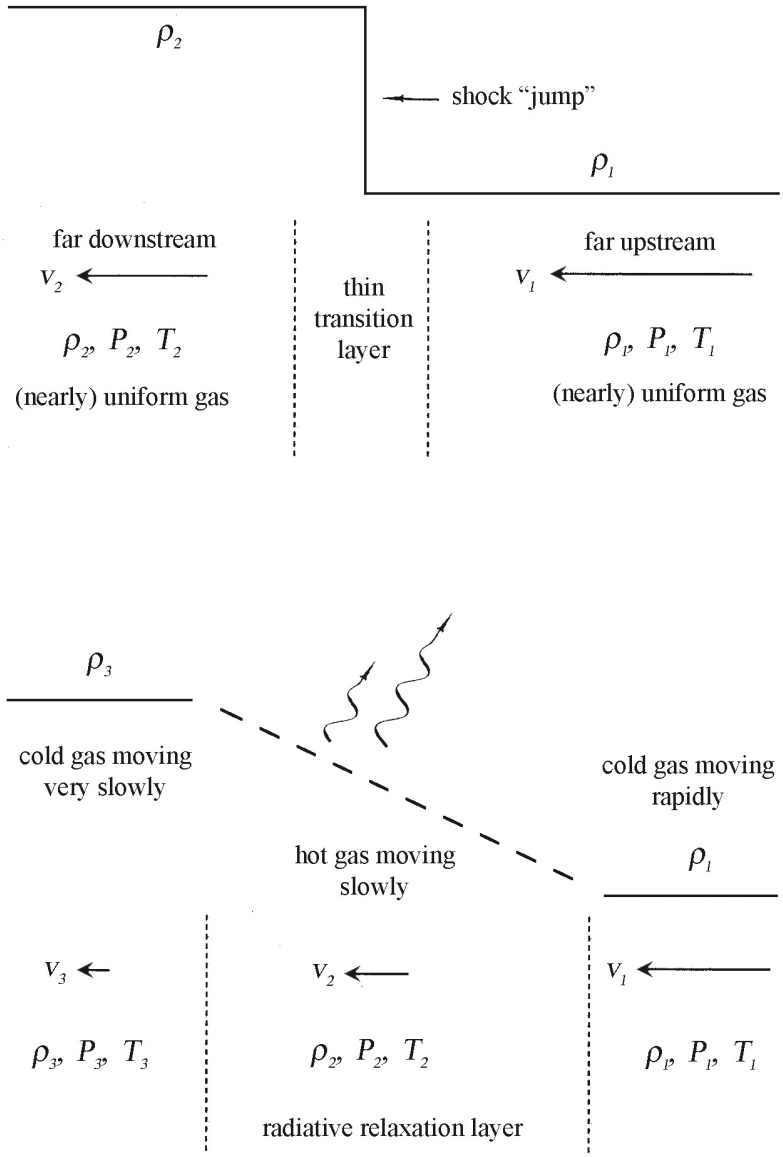

Figure 11: Adiabatic i.e. non-radiative (up) and isothermal i.e. radiative shocks (down). Adapted from Shu (1992).

The jump in density X is

$$X^{-1} = \frac{\gamma_2(\mathrm{M}_1'^{\,2}+1) \pm \sqrt{\mathrm{M}_1'^{\,4} - 2\mathrm{M}_1'^{\,2}(\gamma_2^2-\gamma_1)/(\gamma_1-1)+\gamma_2^2}}{(\gamma_2+1)\mathrm{M}_1'^{\,2}}, \qquad (31)$$

where $\mathrm{M}_1' = v_1/\sqrt{P_1/\rho_1}$. For large M_1'

$$X^{-1} \approx \frac{\mathrm{M}_1'^{\,2}(\gamma_2 \pm 1) + (\gamma_2 \mp \frac{\gamma_2^2-\gamma_1}{\gamma_1-1})}{(\gamma_2+1)\mathrm{M}_1'^{\,2}}, \qquad (32)$$

i.e. for strong shocks (where we should take the square root with minus sign) $X \approx \frac{\gamma_2+1}{\gamma_2-1}$ independent of γ_1. For $\gamma_2 = 5/3$, $X \to 4$, while for $\gamma_2 = 4/3$, $X \to 7$.

2.2.2 Isothermal shocks

Similarly to the term adiabatic shock, isothermal shock is a term that only approximately describes what is actually a radiative shock (or a variant of it). In the case of a radiative shock, between upstream region (1) and downstream region (3) we have not so thin intermediate region – radiative relaxation layer (2) where we have energy loss from the system (Fig. 11). If we are not interested in the structure of this layer, we can assume mass and momentum conservation between upstream and downstream region, and instead of energy conservation, we may assume that the downstream gas has returned to the temperature T_3 not very different from initial equilibrium value, $T_3 \approx T_1$ (hence the term isothermal).

Jump conditions for isothermal shocks are thus

$$\rho_1 v_1 = \rho_3 v_3, \qquad (33)$$

$$\rho_1 v_1^2 + P_1 = \rho_3 v_3^2 + P_3, \qquad (34)$$

$$\frac{P_1}{\rho_1} = \frac{P_3}{\rho_3} \quad (T_1 = T_3). \qquad (35)$$

From Eqs. (33), (34) and (35) follows

$$X = \frac{\rho_3}{\rho_1} = \mathrm{M}_1'^{\,2},$$

$$Y = \frac{P_3}{P_1} = X,$$

where isothermal Mach's number $\mathrm{M}_1' = \frac{v_1}{c_s}$, and $c_s^2 = \frac{P_1}{\rho_1} = \frac{P_3}{\rho_3} = \text{const}$ is now isothermal sound speed. We see that in isothermal shocks density jump is not limited to the value 4, but can be infinitely large, theoretically.

2.3 Cosmic rays and particle acceleration

Strong shock are believed to be the sites of particle acceleration i.e. birthplaces of Galactic cosmic rays (CRs). A mechanism for particle acceleration was first proposed by Fermi (1949). The original Fermi mechanism is called type II (A and B) or the second order Fermi acceleration, because the relative gain in

particle energy is $\Delta E/E \sim (u/c)^2$, where u is the velocity of an interstellar medium cloud which acts as a magnetic mirror that reflect particles. Contrary to this, in type I or the first order Fermi acceleration, $\Delta E/E \sim u/c$, which is why it is expected to be a more efficient process.

Let us consider a particle with initial energy $\mathcal{E} = mc^2 + E$ and velocity v, i.e. $\beta = v/c$ circulating in a low-density medium with a turbulent magnetic field. Consider next a magnetic perturbation of this medium (e.g. a cloud) moving along the x axis with velocity u. When encountering the cloud, a particle is reflected by a magnetic mirror and comes back with the same pitch angle θ and the direction of motion of its guiding center being inverted. Applying the relativistic transformations between a fixed 'laboratory' reference frame and the (primed) reference frame of the cloud, the energy and the momentum of the particle are respectively $\mathcal{E}' = \gamma_u(\mathcal{E} + up_x)$ and $p'_x = \gamma_u(p_x + u\mathcal{E}/c^2)$, with $\gamma_u = 1/\sqrt{1 - u^2/c^2}$. Using the same relations to come back to the fixed frame, after changing p'_x into $-p'_x$ to account for the inversion of the direction of propagation of the particle, we find

$$\mathcal{E}'' = \gamma_u(\mathcal{E}' + up'_x) = \gamma_u^2(\mathcal{E} + 2up_x + u^2\mathcal{E}/c^2), \tag{36}$$

i.e., since $p_x/\mathcal{E} = p\cos\theta/\mathcal{E} = v\cos\theta/c^2$,

$$\frac{\mathcal{E}''}{\mathcal{E}} = \frac{1 + 2(u/c)(v/c)\cos\theta + (u/c)^2}{1 - (u/c)^2} \approx 1 + 2(u/c)(v/c)\cos\theta + 2(u/c)^2. \tag{37}$$

The probabilities of head-on and trailing collisions are proportional to the relative velocities of approach of the particle and the cloud, i.e $v + u\cos\theta$ and $v - u\cos\theta$, respectively (for $\cos\theta > 0$). For $v \approx c$ and $0 < \theta < \pi$ we can write this probability as proportional to $1 + (u/c)\cos\theta$, and average the second term in Eq. (37) to obtain (Longair 2011)

$$\langle \frac{2u}{c}\cos\theta \rangle = \frac{2u}{c}\frac{\int_{-1}^{1}\mu(1 + (u/c)\mu)d\mu}{\int_{-1}^{1}(1 + (u/c)\mu)d\mu} = \frac{2}{3}\Big(\frac{u}{c}\Big)^2, \quad \mu = \cos\theta, \tag{38}$$

i.e.

$$\langle \Delta E/E \rangle = \frac{8}{3}\Big(\frac{u}{c}\Big)^2, \tag{39}$$

where we have not made a distinction between total $\mathcal{E}$ and kinetic energy E.

In the interstellar case, the original mechanism proposed by Fermi (type II) is not very efficient ($\Delta E/E \sim (u/c)^2$) and we would do much better if we had only head-on collisions (type I, $\Delta E/E \sim u/c$). Diffuse shock acceleration (DSA) theory – a modern version of the first order Fermi acceleration was developed independently by Axford et al (1977), Krymsky (1977), Bell (1978a) and Blandford & Ostriker (1978). There are two main approaches to the problem: macroscopic (e.g. Blandford & Ostriker 1978) and microscopic (Bell 1978a). In the rest of this subsection we will follow the derivation by Bell (1978a) because it is more intuitive.

2.3.1 Acceleration of ultra-relativistic particles

Let us consider a strong shock moving through the unperturbed ambient medium with velocity v_s (Fig. 12a). In the frame of the shock (Fig. 12b) the upstream

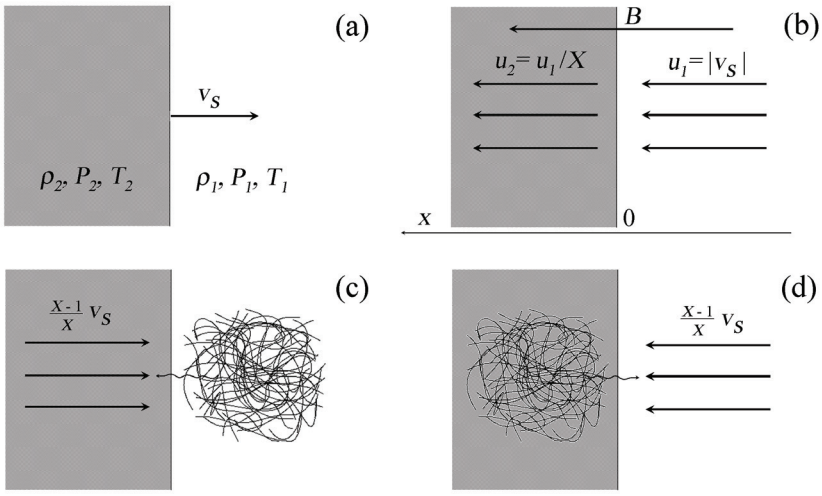

Figure 12: Diffuse shock acceleration of high energy particles in the vicinity of a strong shock wave. Adapted from Longair (2011).

gas flows through the shock with velocity $u_1 = |v_s|$. We shall assume that the shock is parallel i.e. the direction of propagation is along the magnetic field lines B. The equation of continuity requires $\rho_1 u_1 = \rho_2 u_2$ and Rankine-Hugoniot relations give us $\rho_2/\rho_1 = u_1/u_2 = X = (\gamma + 1)/(\gamma - 1)$, where γ is the ratio of specific heats of the gas.

Consider now high-energy particles ahead of the shock (upstream) whose distribution function is isotropic in the frame of reference in which the gas is at rest (Fig. 12c). The particles cross the shock front and encounter gas behind the shock travelling at velocity $\frac{X-1}{X} v_s$. They are scattered by the turbulence in the downstream region, receiving a small amount of energy $\Delta E/E \sim v_s/c$, isotropized and ready to move back upstream. A beauty of the mechanism is that the opposite process of particles diffusing from behind the shock to the upstream region is exactly the same (Fig. 12d) – when particles cross the shock front from downstream they now encounter upstream gas moving at velocity $\frac{X-1}{X} v_s$ and again receive a small increase in energy. In the upstream they are scattered back by Alfvén waves excited by the energetic particles attempting to escape from the shock. As a result, particles can recross the shock front many times, each time receiving a small amount of energy – there are no crossings in which a particle loses energy.

Let us now look at this process in more detail (see Bell 1978a, Longair 2011, Lequeux 2005). We shall consider test particles with phase-space distribution function $f(x, p, t)$ injected isotropically into the planar shock with a velocity v much higher than that of the shock. In order to treat this mechanism analytically we will choose a reference frame in which shock is stationary, the gas flows from upstream, $(x < 0)$ with a velocity $u_1 \approx |v_s|$, to downstream where $u_2 < |v_s|$. The problem here is that of diffusion in a fluid moving with different velocities on either side of the shock described by diffusion-advection equation

near a discontinuity (Drury 1983, Blandford & Eichler 1987)

$$\frac{\partial f}{\partial t} + u\frac{\partial f}{\partial x} = \frac{\partial}{\partial x}\left[D(x,p)\frac{\partial f}{\partial x}\right] + \frac{1}{3}\frac{\partial u}{\partial x}p\frac{\partial f}{\partial p} + Q(x,p). \tag{40}$$

In the first term on the right-hand side

$$D(x,p) = \frac{\lambda v}{3} \tag{41}$$

is the diffusion coefficient in the x direction for particles with velocity v, where for the mean free path of particles one usually assumes $\lambda \sim r_g$,

$$r_g = \frac{p_\perp}{eB}\frac{A}{Z} \tag{42}$$

being gyro-radius of particle with atomic mass number A and charge number Z. Elementary charge is e and perpendicular component of momentum per nucleon $p_\perp$. The last term in Eq. (40) is the injection term (we shall assume δ-function injection at the shock).

In the chosen reference frame, it is natural to search for a stationary solution. Since $\partial f/\partial t = 0$ and $\partial u/\partial t = 0$ outside the shock, and $\partial u/\partial x = 0$ in the downstream

$$u_2\frac{\partial f}{\partial x} - \frac{\partial}{\partial x}\left[D(x,p)\frac{\partial f}{\partial x}\right] = 0, \tag{43}$$

whose general solution, obtained by double integration over x, is

$$f(x,p) = A(p) + B(p)\exp\left(\int \frac{u_2}{D(x',p)}dx'\right), \tag{44}$$

where A and B are the integration constants. $D(x',p)$ being finite but x extending to infinity, the second term diverges, unless $B = 0$. A physical solution therefore requires that $f(x,p) = A(p)$ i.e. is constant in space. The flow of particles away from the shock i.e. the flux density of particles that escape from the shock far downstream is $u_2 n(x,p) - D(x,p)(\partial n/\partial x)$, which is equal to $u_2 n(0,p)$, where the number density of particles, for isotropic distribution, is $n = \int_0^\infty 4\pi p^2 f(p)dp$. The flux density, i.e. the rate at which particles are crossing and recrossing the shock is $\int\int f v_x p'^2 dp' d\Omega = \int_0^\infty 2\pi v(p') f(p') p'^2 dp' \int_0^{\pi/2} \cos\theta \sin\theta d\theta = \frac{1}{2}vn\int_0^1 \mu d\mu = \frac{1}{4}vn(0,p)$, where $\mu = \cos\theta$ and where we assumed $f(p') = \frac{n}{4\pi p^2}\delta(p-p')$, $\delta(p-p')$ being δ-function. The (small) escape probability is thus

$$\eta = \frac{u_2 n(0,p)}{\frac{1}{4}vn(0,p)} = 4\frac{u_2}{v}. \tag{45}$$

For very energetic particles ($v \approx c$), this probability is independent of energy.

When a particle with energy E_k goes from region 1 to region 2, its energy is (according to Eq. (36))

$$E_k' \approx E_k\left[1 + (u_1 - u_2)\frac{v_{k1}\cos\theta_{k1}}{c^2}\right], \tag{46}$$

where $u = u_1 - u_2$. When it comes back to region 1 (after finishing $k+1$ cycle), its energy is

$$\frac{E_{k+1}}{E_k} \approx \left[1 + (u_1 - u_2)\frac{v_{k2}\cos\theta_{k2}}{c^2}\right]\left[1 + (u_1 - u_2)\frac{v_{k1}\cos\theta_{k1}}{c^2}\right]. \tag{47}$$

Particles injected with energy E_0 (such that $v \approx c$) have an energy after l cycles

$$\frac{E_l}{E_0} = \prod_{k=0}^{l-1} \frac{E_{k+1}}{E_k}, \tag{48}$$

i.e.

$$\ln\left(\frac{E_l}{E_0}\right) = \sum_{k=1}^{l-1} \ln\left(1 + \frac{u_1 - u_2}{c}\cos\theta_{k1}\right) + \sum_{k=1}^{l-1} \ln\left(1 + \frac{u_1 - u_2}{c}\cos\theta_{k2}\right). \tag{49}$$

For having a significant energy gain, l must be at least of the order of $c/(u_1 - u_2)$, and the distribution of $\ln(E_l/E_0)$ must be strongly concentrated around the mean (central limit theorem), so we can treat all particles completing l cycles as having their energy increased by the same amount and write

$$\ln\left(\frac{E_l}{E_0}\right) = l\Big[\Big\langle \ln\big(1 + \frac{u_1 - u_2}{c} cos\theta_{k1}\big)\Big\rangle + \Big\langle \ln\big(1 + \frac{u_1 - u_2}{c} cos\theta_{k2}\big)\Big\rangle\Big]. \tag{50}$$

Expanding the logarithm we find

$$\ln\left(\frac{E_l}{E_0}\right) \approx l\frac{u_1 - u_2}{c}[\langle cos\theta_{k1}\rangle + \langle cos\theta_{k2}\rangle]. \tag{51}$$

The number of particles that cross the shock between angles θ and $\theta + d\theta$ is proportional to $2\pi \sin\theta \cos\theta d\theta$ and averaging over angles from 0 to $\pi/2$ results in

$$\langle cos\theta_{k1}\rangle = \langle cos\theta_{k2}\rangle = \frac{\int_0^1 \mu^2 d\mu}{\int_0^1 \mu d\mu} = \frac{2}{3}, \quad \mu = \cos\theta. \tag{52}$$

Finally,

$$\ln\left(\frac{E_l}{E_0}\right) = \frac{4}{3} l \frac{u_1 - u_2}{c}. \tag{53}$$

The probability of completing at least l cycles and reaching energy $E \geq E_l$ is given by

$$P_l = \frac{N(E \geq E_l)}{N_o} = \zeta^l, \quad \zeta = 1 - \eta, \tag{54}$$

$$\ln P_l = l \ln\left(1 - \frac{4u_2}{c}\right) \approx -l\frac{4u_2}{c} = -\frac{3u_2}{u_1 - u_2} \ln\left(\frac{E_l}{E_0}\right), \tag{55}$$

where ζ is the probability of staying in acceleration process after one cycle, N_0 is the initial number of particles and $N(E \geq E_l)$ the number of particles that reached $E \geq E_l$. By combining Eqs. (53) and (55) we have

$$N(E \geq E_l) = N_o \left(\frac{E_l}{E_0}\right)^{1-\Gamma} = \int_{E_l}^{\infty} N(E) dE, \quad \Gamma = \frac{X+2}{X-1}, \quad X = \frac{u_1}{u_2}, \tag{56}$$

i.e. differential energy spectrum

$$N(E)dE = KE^{-\Gamma} dE, \tag{57}$$

where K is constant. In the case of strong shocks, $X = 4$ so $\Gamma = 2$.

2.3.2 Acceleration of supra-thermal particles

The calculation presented in the previous subsection is, in principle, valid for ultra-relativistic particles only. It is possible to lift this restriction, but in any case the initial velocity of the particles must be larger than that of the shock i.e. the particles must be supra-thermal.

We shall now make a distinction between kinetic E and total energy $\mathcal{E} = E + mc^2 = \sqrt{p^2c^2 + m^2c^4}$ and transform Eq. (46) into

$$\mathcal{E}'_k \approx \mathcal{E}_k + (u_1 - u_2)p_k cos\theta_{k1} = \mathcal{E}_k\left[1 + (u_1 - u_2)\frac{p_k \cos\theta_{k1}}{\mathcal{E}_k}\right], \tag{58}$$

$$p'^2_k \approx p^2_k\left[1 + 2(u_1 - u_2)\frac{\mathcal{E}_k \cos\theta_{k1}}{p_k c^2}\right] = p^2_k\left[1 + 2(u_1 - u_2)\frac{cos\theta_{k1}}{v_{k1}}\right]. \tag{59}$$

Instead of Eq. (47) we then have

$$\frac{p_{k+1}}{p_k} \approx \left[1 + (u_1 - u_2)\frac{\cos\theta_{k2}}{v_{k2}}\right]\left[1 + (u_1 - u_2)\frac{\cos\theta_{k1}}{v_{k1}}\right]. \tag{60}$$

and, assuming that the particle velocity is large enough i.e. always larger than the velocity of the shock $v_k \gg u_1 = |v_s|$ after following the previous derivation,

$$\ln\left(\frac{p_l}{p_0}\right) = \frac{4}{3}l\frac{u_1 - u_2}{v}. \tag{61}$$

The probability of completing a cycle is $\zeta = 1 - \eta = 1 - 4u_2/v$ and for l cycles, again

$$\ln P_l = \ln\frac{N(p \geq p_l)}{N_o} = l\ln\left(1 - \frac{4u_2}{v}\right) \approx -l\frac{4u_2}{v} = -\frac{3u_2}{u_1 - u_2}\ln\left(\frac{p_l}{p_0}\right), \tag{62}$$

i.e. differential momentum spectrum is

$$n(p)dp \propto p^{-\Gamma}dp, \tag{63}$$

with $\Gamma = \frac{X+2}{X-1}$ and $X = \frac{u_1}{u_2}$.

The CRs distribution function in momentum space is $f(p) = kp^{-(\Gamma+2)}$. Remember that $N(E)dE = 4\pi p^2 f(p)dp$, $N = \int_{p_{\rm inj}}^{\infty} 4\pi p^2 f(p)dp = \int_{E_{\rm inj}}^{\infty} N(E)dE$. We will now show that:

a) for ultra-relativistic particles $N(E)dE = KE^{-\Gamma}dE$ and we will find constant $K = K(N, E_{\rm inj})$, where $N = N_0$ is the total number of particles per unit volume and $E_{\rm inj} = E_0$ the injection energy.

b) Assuming an equal number of protons and electrons and equal injection energy $E_{\rm inj} \ll m_e c^2$ we will find proton to electron number ratio at low ($E_{\rm inj} < E \ll m_e c^2$) and high energies ($E \gg m_p c^2$).

a) The total number of particles per unit volume is

$$N = \int_{p_{\rm inj}}^{\infty} 4\pi p^2 f(p)dp = \int_{p_{\rm inj}}^{\infty} 4\pi k p^{-\Gamma}dp = 4\pi k\frac{p^{1-\Gamma}}{1-\Gamma}\Big|_{p_{\rm inj}}^{\infty} = 4\pi k\frac{p_{\rm inj}^{1-\Gamma}}{\Gamma - 1}. \tag{64}$$

Constant k then can be expressed as

$$k = \frac{N}{4\pi}(\Gamma - 1)p_{\rm inj}^{\Gamma-1}. \tag{65}$$

The relativistic relation $p = p(E)$ is

$$p^2c^2 = E^2 + 2mc^2E, \tag{66}$$

and

$$dp = \frac{E + mc^2}{c\sqrt{E^2 + 2mc^2E}}dE. \tag{67}$$

We finally have

$$N(E)dE = 4\pi p^2 f(p)dp = 4\pi p^2 \frac{N}{4\pi}(\Gamma - 1)p_{\rm inj}^{\Gamma-1}p^{-\Gamma-2}\frac{E + mc^2}{c\sqrt{E^2 + 2mc^2E}}dE \tag{68}$$
$$= N(\Gamma - 1)(E_{\rm inj}^2 + 2mc^2E_{\rm inj})^{(\Gamma-1)/2}(E^2 + 2mc^2E)^{-(\Gamma+1)/2}(E + mc^2)dE,$$

since $p_{\rm inj}^2 = \frac{E_{\rm inj}^2 + 2mc^2E_{\rm inj}}{c^2}$. This is the differential energy spectrum given by Bell (1978b). For $E \gg mc^2$

$$N(E)dE = N(\Gamma - 1)(E_{\rm inj}^2 + 2mc^2E_{\rm inj})^{(\Gamma-1)/2}E^{-\Gamma}dE = KE^{-\Gamma}dE, \tag{69}$$

based on which we see the functional dependence $K = K(N, E_{\rm inj})$.

b) Fig. 13 shows proton and electron energy spectra, assuming an equal total number of protons and electrons and equal injection energy $E_{\rm inj}$. If $E_{\rm inj} \ll m_ec^2$ for $E_{\rm inj} < E \ll m_ec^2$, ratio $\kappa' = N_p(E)/N_e(E) \approx 1$. At high energies ($E \gg m_pc^2$) electron and proton spectra are parallel and

$$\kappa' = N_p(E)/N_e(E) = \Big(\frac{m_p}{m_e}\Big)^{(\Gamma-1)/2} = \Big(\frac{m_p}{m_e}\Big)^{\alpha}, \tag{70}$$

where $\alpha = (\Gamma - 1)/2$ is the so-called spectral index. For $\Gamma = 2$, $\kappa' \sim 40$, while for $\Gamma = 2.7$, $\kappa' \sim 600$. The observed ratio for Galactic CRs is $\kappa' \sim 100$. One can also check that, given $E_{\rm inj} \ll m_ec^2$, the ratio of proton to electron energy densities is $\epsilon_p/\epsilon_e \approx (m_p/m_e)^{(3-\Gamma)/2}$. In young SNRs shock velocity v_s can be larger than $v_s \sim 10000$ km s^{-1}, so the injection energy, which is estimated to be $E_{\rm inj} \sim m_pv_s$, is $E_{\rm inj} > m_ec^2$ (Fig. 14).

What would exactly be the energy of supra-thermal particles $E_{\rm inj}$? Although most of the particles will go through the shock front, we may assume, for example, that a small fraction of them η will be reflected by the shock.[5] If we treat the approaching shock as a "wall" of particles with mass $M \gg m$ and consider only head-on collisions, the conservation of energy and momentum give

$$\frac{1}{2}MV_1^2 + \frac{1}{2}mv_1^2 = \frac{1}{2}MV_2^2 + \frac{1}{2}mv_2^2, \tag{71}$$

$$MV_1 - mv_1 = MV_2 + mv_2, \tag{72}$$

[5]It is also possible that particles with sufficient energy i.e. momentum (e.g. from the tail of Maxwell distribution) can escape from downstream back to upstream region and thus become seed particles for acceleration.

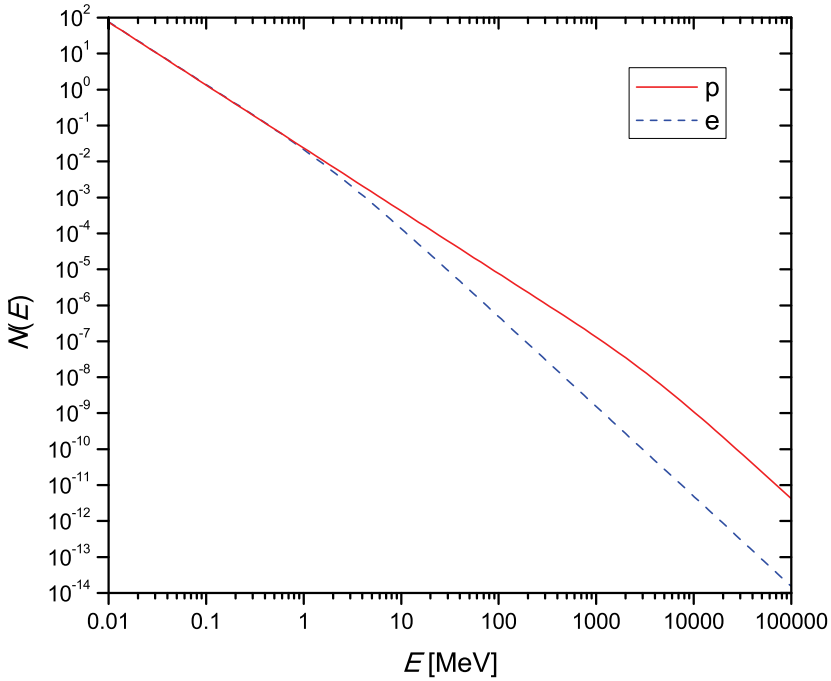

Figure 13: Proton and electron energy spectra, assuming an equal total number of protons and electrons and equal injection energy $E_{\rm inj} \ll m_e c^2$.

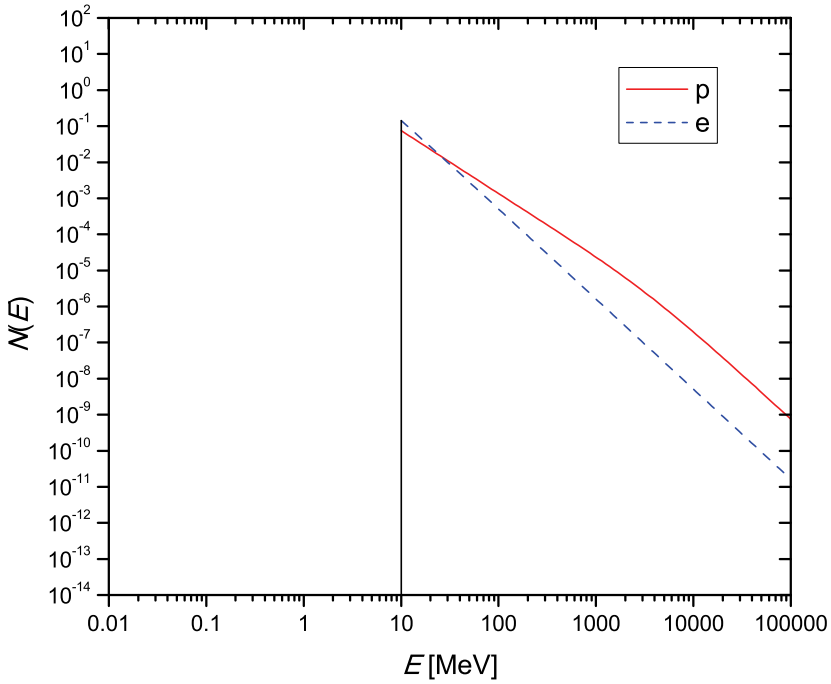

Figure 14: Proton and electron energy spectra, assuming an equal total number of protons and electrons and equal injection energy $E_{\rm inj} > m_e c^2$.

and with $v_1 \to 0$ and $V_1 = v_s$, we obtain for reflected particles

$$v_2 = \frac{2V_1}{1 + m/M} \approx 2v_s, \tag{73}$$

i.e. $E_{\rm inj} = 4\frac{1}{2}mv_s$.

It is, however, questionable whether one can assume equal injection energy for both protons and electrons. If the shock thickness is of the order of magnitude of gyration radius r_g of protons, in order to cross the shock front unaffected, the electrons should have a similar gyro-radius, implying that it is more justified to assume injection momentum for protons and electrons to be the same (Eq. (42)). In this case the ratio of protons to electrons must be $\kappa' = N_p(p)/N_e(p) \approx 10^2$ at high momentum (energy) as well as at injection.

2.3.3 Galactic cosmic rays

In 1912 Victor Hess carried out balloon experiments to measure the ionization of the atmosphere and found an increasing ionization rate with altitude, concluding that there must be an extraterrestrial source of ionizing radiation producing this effect. For the discovery of this cosmic radiation – CRs, he was awarded Nobel prize in physics in 1936.

We can make a distinction between primary CRs coming from above Earth's atmosphere, and secondary CRs i.e. air showers or cascades, produced when primary CRs collide with atoms and molecules in the atmosphere. A distinction is also made between particles originating outside the solar system and energetic particles coming from the Sun. In the following text, by CRs we will assume only primary CRs of non-solar origin. CRs are primarily composed of high-energy protons (∼90%), α-particles (∼10%) and heavier nuclei. The ratio of protons to electrons is approximately 100:1. The all particle spectrum is to a very good approximation a power-law with energy index $\Gamma \approx 2.7$ up to $\sim 10^{15}$ eV. This is the so-called "knee" in the spectrum (Fig. 15) and sources within our Galaxy, such as SNRs, are likely to be able to produce CR particles up to this or even higher energy $\sim 10^{17}$ eV (Morlino 2016). The CRs distribution in this energy range is highly isotropic. Below ∼1 GeV, the spectrum is affected by solar modulation – a diffusive-convective process in which the particles are scattered by the magnetic irregularities in the solar wind (Grupen 2005, Longair 2011).

Above the "knee" the spectrum steepens, up to the energy of around 5×10^{18} eV – the so-called "ankle", after which it slightly flattens again. It is believed that the highest energy CRs are of extragalactic origin. Ultra-high energy CRs would interact with cosmic microwave background radiation and rapidly lose energy, producing a cut-off at 5×10^{19} eV – the Greisen-Zatsepin-Kuzmin (GZK) effect. If the highest energy CRs are protons, the GZK effect limits the volume from which these particles must originate to a radius of few tens of megaparsecs from our Galaxy (Grupen 2005). The observation of several events in excess of 10^{20} eV (the "toe" region), therefore, represents a certain mystery.

The CRs propagate from their sources and fill out the Galaxy. Disregarding interaction and energy losses, CRs propagation may be described with a diffusion-loss equation (Longair 2011)

$$\frac{\partial N}{\partial t} = D\Delta N - \frac{N}{\tau_{\rm e}} + Q, \tag{74}$$

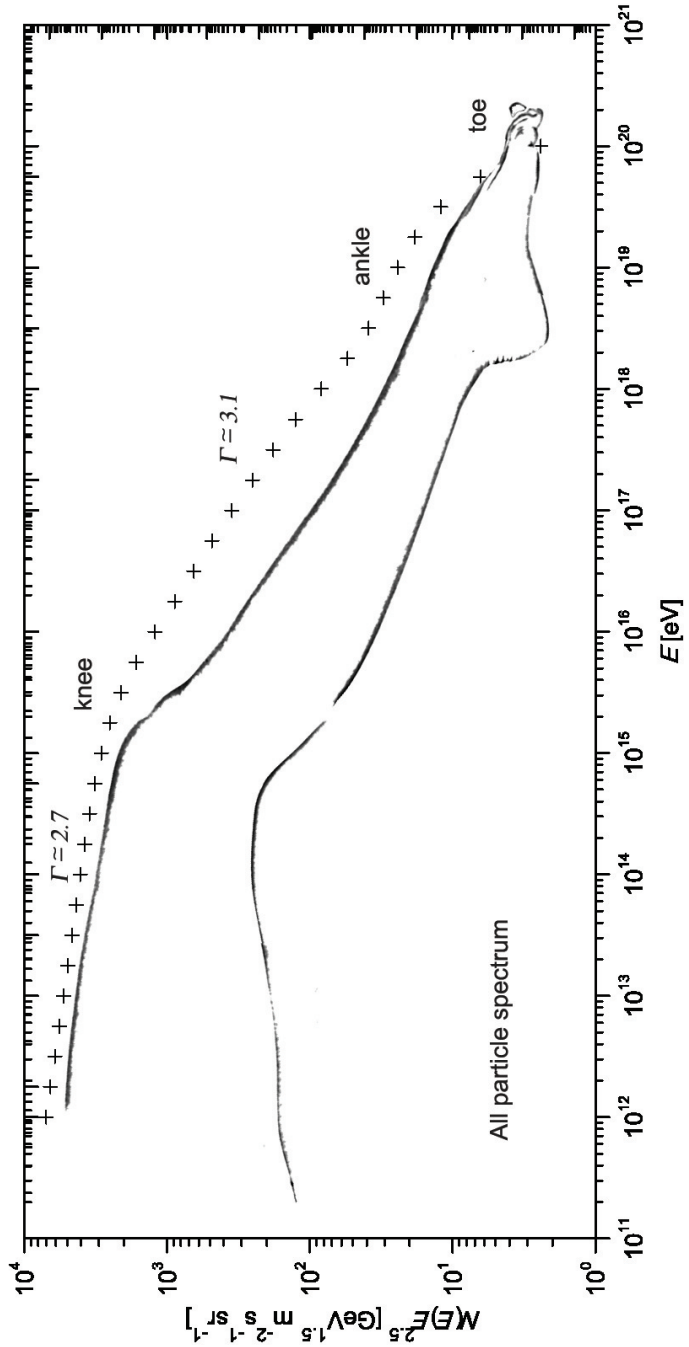

Figure 15: Sketch of the cosmic rays energy spectrum, as in Grupen (2005). Data are from H4a model (Gaisser 2012).

where $\Delta = \nabla^2$ is Laplacian, D is diffusion coefficient, $\tau_{\rm e}$ is the characteristic escape time and Q is the source term. If $\tau_{\rm e} \to \infty$, particles simply diffuse from their sources to the observer – there is practically no escape, and we can think about the Galaxy as a certain "closed box". If $D \to 0$ and $\tau_{\rm e} = \tau_{\rm e}(E) \propto E^{-\delta}$ ($\delta > 0$) there would be an energy-dependent leakage – higher energy CRs are more likely to escape out of the Galaxy. In the stationary case $\frac{\partial N}{\partial t} = 0$, $N(E) = Q(E)\tau_{\rm e}(E)$. The CR particles may still diffuse freely inside some confinement volume, being reflected at its boundaries. However, in each encounter with the boundary, there is some probability of escape. This is the basis for the so-called "leaky-box" model.

2.3.4 Re-acceleration of cosmic rays

Although re-acceleration of CRs is most commonly assumed to be a diffusive process in which galactic CRs are re-accelarated through the second order Fermi acceleration in the interstellar medium (Drury & Strong 2015), we will consider here a re-acceleration of pre-existing CRs by the shock through DSA. In this case pre-existing CRs are simply seed particles that are injected in DSA process and play the role of supra-thermal particles previously discussed. The momentum distribution function is then

$$f(p) = \int_0^\infty f_0(p')Q(p,p')4\pi p'^2 dp' = \int_{p_0}^p f_0(p')Q(p,p')4\pi p'^2 dp', \quad p' < p, \quad (75)$$

where

$$f_0 = \frac{N}{4\pi}(\Gamma - 1)\frac{p'^{-\Gamma-2}}{p_0^{1-\Gamma}} \quad (76)$$

is the distribution function of pre-existing CRs, N their number per unit volume, p_0 some minimum momentum and Γ energy index, while

$$Q(p,p') = \frac{1}{4\pi}\frac{3}{X-1}\frac{p^{-3X/(X-1)}}{p'^{-3/(X-1)}}, \quad p > p', \quad (77)$$

is the resulting DSA spectrum for particles injected monoenergetically with momentum p (for $p < p'$, $Q(p,p') \equiv 0$), into the shock with compression ratio X.

If CRs are reaccelerated by the same shock (or multiple shocks with the same X), then $\Gamma = \frac{X+2}{X-1}$ and

$$f(p) = \frac{N}{4\pi}(\Gamma - 1)^2 \ln\Big(\frac{p}{p_0}\Big)\frac{p^{-\Gamma-2}}{p_0^{1-\Gamma}} \quad (78)$$

(see Bell 1978b). For $\Gamma \neq \frac{X+2}{X-1}$

$$f(p) = \frac{N}{4\pi}\frac{3(\Gamma-1)}{(\Gamma+2)(X-1)-3X}\frac{p^{-\Gamma-2}}{p_0^{1-\Gamma}}\Big(\Big(\frac{p}{p_0}\Big)^{\Gamma+2-3X/(X-1)} - 1\Big). \quad (79)$$

We can see that at high energies (momenta)

$$f(p \to \infty) \propto p^{-3X/(X-1)}, \quad \Gamma > \frac{X+2}{X-1} \quad (80)$$
$$f(p \to \infty) \propto p^{-\Gamma-2}, \quad \Gamma < \frac{X+2}{X-1}.$$

2.3.5 Cosmic rays back-reaction

Derivation of accelerated particle spectrum presented earlier in this subsection, represents the so-called test particle approach or linear DSA which assumes that the pressure or energy density of high-energy particles is small, so that their presence does not modify jump conditions i.e. the shock structure. If this is not the case, then we are talking about CR back-reaction or non-linear DSA (see e.g. Drury 1983, Malkov & Drury 2001, Blasi 2002, Amato & Blasi 2005). The most important CR back-reaction effect on the shock is that high-energy particles diffuse upstream inducing the shock precursor with density, pressure and velocity gradients, while the jump in these quantities is still present at the so-called subshock. The total change in density for a modified shock is larger than the compression ratio at the subshock $X_{\rm tot} > X_{\rm sub}$.

The shock modification in turn changes the distribution of CR particles, producing the concave-up spectrum. This can be qualitatively explained with, conditionally speaking, three CR populations: low-energy, intermediate, and high-energy population (Berezhko & Ellison 1999). Lower-energy CRs will only experience the jump at the subshock and have power-law index $\Gamma \approx (X_{\rm sub} + 2)/(X_{\rm sub} - 1)$, while higher-energy particles sample a broader portion of the precursor velocity profile and experience larger compression ratio, consequently having flatter power-law index. Since for $\Gamma < 2$ the total number of CR particles would diverge, there must be a cut-off in the spectrum at some maximum energy. At highest energies, particles are able to escape from the acceleration region, far upstream.

2.4 Magnetic fields

Magnetic fields in galaxies can be broadly classified into regular and turbulent fields. One of the most promising mechanisms to sustain magnetic field and generate large scale regular field from turbulent field in the ISM of galaxies is the $\alpha - \Omega$ dynamo (Beck et al. 1996). It is based on differential rotation (Ω), expanding gas flows, driven by SN explosions or CRs, carrying magnetic fields that are twisted by the Coriolis force (α-effect), and on magnetic diffusivity driven by turbulence. The typical magnetic field strength assumed for our Galaxy is $\sim 5\mu G$, though galactic fields can be significantly larger (Beck 2016).

Radio polarization studies of SNRs show that in young SNRs, the magnetic field is largely disordered, with a small radial prevalence, while in older, larger SNRs, the field is often disordered but sometimes tangential (to the shock front) (Reynolds et al. 2012). The field strength is at least by an order of magnitude larger than the typical ISM value. Generally, we can distinguish between compressed and amplified fields. As seen previously, in non-radiative shocks the radial (parallel, $\mathbf{B} \parallel \mathbf{v}$) component should be conserved, while the tangential (perpendicular, $\mathbf{B} \perp \mathbf{v}$) component's compression is limited to $X = u_1/u_2$.

The mechanism for additional field amplification is still uncertain. It is assumed that amplified field is turbulent, produced by CRs streaming ahead of the shock. Streaming CRs excite MHD turbulence in the upstream region: resonant Alfvén waves, with a wavelength matching the CR Larmor radius, but also non-resonant instabilities (Bell 2004). One expects different dependence on the shock and Alfvén velocities, for resonantly and non-resonantly amplified magnetic fields (Amato 2011):

$$\left(\frac{\delta B}{B_0}\right)_{\rm res} \approx \sqrt{\eta \frac{v_s}{v_A}}, \tag{81}$$

$$\left(\frac{\delta B}{B_0}\right)_{\rm Bell} \approx \sqrt{\eta \frac{v_s^3}{c v_A^2}}, \tag{82}$$

where $\delta B = B - B_0$, B_0 being the ambient field, and η being the fraction of shock ram pressure that is converted into CR energy. From the latter equation, for $B \gg B_0$, with $v_A = B_0/\sqrt{4\pi\rho}$ one gets the saturated field energy density (Bell 2004)

$$\epsilon_B = \frac{1}{8\pi} B^2 \approx \frac{1}{2} \frac{v_s}{c} \epsilon_{\rm CR}, \tag{83}$$

where CR energy density is assumed to be $\epsilon_{\rm CR} = \eta \rho v_s^2$.

In the following text, we will discuss the equipartition i.e. the minimum energy calculation, a widespread method for estimating magnetic field strength and energy contained in the magnetic field and cosmic-ray particles by using only the radio synchrotron emission. Despite its approximate character, it remains a useful tool, especially when there are no other magnetic field estimates of a source. Although, the physical motivation to assume equipartition in SNRs is questionable (Reynolds et al. 2012), there still exists a possibility of a sort of constant partition between magnetic field and CR energies, and the shock ram pressure in older remnants

$$\epsilon_B \approx \beta \epsilon_{\rm CR} \approx \beta \eta \rho v_s^2. \tag{84}$$

2.4.1 Equipartition calculation

The details of equipartition and revised equipartition calculation for radio sources in general are available in Pacholczyk (1970) and Beck & Krause (2005), respectively. A discussion on whether equipartition of energy is fulfilled in real sources and how reliable magnetic field estimates from equipartition calculation are can be found in Duric (1990).

Pacholczyk (1970) provided the following formulas to estimate magnetic field strength and minimum energy (in magnetic fields and CRs) in a radio synchrotron source:

$$B = (4.5)^{2/7} (1+\kappa)^{2/7} c_{12}(\alpha)^{2/7} f^{-2/7} R^{-6/7} L^{2/7}, \tag{85}$$

$$E_{\rm min} = (1+\kappa)^{4/7} c_{13}(\alpha) f^{3/7} R^{9/7} L^{4/7}, \tag{86}$$

where $\alpha = (\Gamma - 1)/2$ is the spectral index, R is the source radius, f is the volume filling factor, $L = \int_{\nu_1}^{\nu_2} L_\nu d\nu$ is the total radio luminosity, ν_1 and ν_2 define the frequency range (usually $\nu_1 = 10^7$ Hz, $\nu_2 = 10^{11}$ Hz) and κ is the ratio of heavy particles to electrons energy. The constants are

$$c_{12} = \frac{\sqrt{c_1}}{c_2} \cdot \frac{2\alpha - 2}{2\alpha - 1} \cdot \frac{\nu_1^{(1-2\alpha)/2} - \nu_2^{(1-2\alpha)/2}}{\nu_1^{1-\alpha} - \nu_2^{1-\alpha}},$$

$$c_{13} = 0.921 \cdot c_{12}^{4/7}, \quad c_1 = \frac{3e}{4\pi m_e^3 c^5}, \quad c_2 = \frac{2e^4}{3 m_e^4 c^7}, \tag{87}$$

where e and m_e are electron's charge and mass, respectively. All quantities are in cgs units.

We will be relying on Bell's theory of diffusive shock acceleration (Bell 1978a,b) and his assumption concerning the injection of particles into the acceleration process to derive a slightly modified equipartition i.e. minimum-energy calculation applicable to "mature" SNRs ($v_s \ll 6000-7000$ km s^{-1}) with spectral index $0.5 < \alpha < 1$ (energy index $2 < \Gamma < 3$) (Arbutina et al. 2011). Then we will incorporate the dependence $\epsilon = \epsilon(E_{\rm inj})$ which will make formula applicable to the younger i.e. all SNRs (Arbutina et al. 2012).

A simple approach

Following Bell (1978a,b) we will assume that a certain number of particles have been injected into the acceleration process all with the same injection energy $E_{\rm inj} \approx 4\frac{1}{2} m_p v_s^2$.[6] If we assume that the shock velocity is low enough so that $E_{\rm inj} \ll m_e c^2$ (and $p^e_{\rm inj} \ll m_e c$), for energy density of a CR species (assuming power-law momentum distribution) we have[7]

$$\begin{aligned}
\epsilon &= \int_{p_{\rm inj}}^{p_\infty} 4\pi k p^{-\Gamma}(\sqrt{p^2c^2+m^2c^4}-mc^2)dp \\
&\approx \int_0^{\infty} 4\pi k p^{-\Gamma}(\sqrt{p^2c^2+m^2c^4}-mc^2)dp \\
&= 4\pi k c (mc)^{2-\Gamma}\int_0^{\infty} x^{-\Gamma}(\sqrt{x^2+1}-1)dx, \quad x=\frac{p}{mc} \\
&= K(mc^2)^{2-\Gamma}\frac{\Gamma(\frac{3-\Gamma}{2})\Gamma(\frac{\Gamma-2}{2})}{2\sqrt{\pi}(\Gamma-1)}.
\end{aligned} \tag{88}$$

The total CR energy density is then

$$\begin{aligned}
\epsilon_{\rm CR} &= \frac{\Gamma(\frac{3-\Gamma}{2})\Gamma(\frac{\Gamma-2}{2})}{2\sqrt{\pi}(\Gamma-1)}\left(K_e(m_ec^2)^{2-\Gamma}+\sum_i K_i(m_ic^2)^{2-\Gamma}\right) \\
&= \frac{\Gamma(\frac{3-\Gamma}{2})\Gamma(\frac{\Gamma-2}{2})}{2\sqrt{\pi}(\Gamma-1)}\left(K_e(m_ec^2)^{2-\Gamma}+K_p(m_pc^2)^{2-\Gamma}\sum_i \frac{n_i}{n_p}\Big(\frac{m_i}{m_p}\Big)^{(3-\Gamma)/2}\right) \\
&= \frac{\Gamma(\frac{3-\Gamma}{2})\Gamma(\frac{\Gamma-2}{2})}{2\sqrt{\pi}(\Gamma-1)}K_e(m_ec^2)^{2-\Gamma}\cdot \\
&\cdot \left(1+\frac{n}{n_e}\Big(\frac{m_p}{m_e}\Big)^{(3-\Gamma)/2}\sum_i \frac{n_i}{n}\Big(\frac{m_i}{m_p}\Big)^{(3-\Gamma)/2}\right) \\
&= K_e(m_ec^2)^{2-\Gamma}\frac{\Gamma(\frac{3-\Gamma}{2})\Gamma(\frac{\Gamma-2}{2})}{2\sqrt{\pi}(\Gamma-1)}(1+\kappa),
\end{aligned} \tag{89}$$

where

$$\kappa = \Big(\frac{m_p}{m_e}\Big)^{(3-\Gamma)/2}\frac{\sum_i A_i^{(3-\Gamma)/2}\nu_i}{\sum_i Z_i\nu_i}, \tag{90}$$

[6] We assume fully ionized, globally electro-neutral plasma.

[7] One should not confuse energy index Γ with the Gamma function $\Gamma(z)$.

$n_e = \sum_i Z_i n_i$, $\nu_i = n_i/n$ are ion abundances ($\sum_i \nu_i = 1$), A_i and Z_i are mass and charge numbers of elements and we assumed that at high energies $K_p/K_e \approx (n_p/n_e)\cdot (m_p/m_e)^{(\Gamma-1)/2}$. Note that we have neglected energy losses.

Emission coefficient for synchrotron radiation is, on the other hand (see the next subsection),

$$\varepsilon_\nu = c_5 K_e (B\sin\Theta)^{(\Gamma+1)/2}\Big(\frac{\nu}{2c_1}\Big)^{(1-\Gamma)/2}, \tag{91}$$

where c_1, c_3 and $c_5 = c_3\Gamma(\frac{3\Gamma-1}{12})\Gamma(\frac{3\Gamma+19}{12})/(\Gamma+1)$ are defined in Pacholczyk (1970).[8] We will use the flux density which is defined as

$$S_\nu = \frac{L_\nu}{4\pi d^2} = \frac{\frac{4\pi}{3}R^3 f\mathcal{E}_\nu}{4\pi d^2} = \frac{4\pi}{3}\varepsilon_\nu f\theta^3 d, \tag{92}$$

where f is volume filling factor, $\theta = R/d$ is angular radius and d is the distance.

If we assume isotropic distribution for the orientation of pitch angles (Longair 2011), we can take for the average $\langle(\sin\Theta)^{(\Gamma+1)/2}\rangle$

$$\frac{1}{2}\int_0^\pi (\sin\Theta)^{(\Gamma+3)/2} d\Theta = \frac{\sqrt{\pi}}{2}\frac{\Gamma(\frac{\Gamma+5}{4})}{\Gamma(\frac{\Gamma+7}{4})}. \tag{93}$$

For the total energy we have

$$E = \frac{4\pi}{3}R^3 f(\epsilon_{\rm CR} + \epsilon_B), \quad \epsilon_B = \frac{1}{8\pi}B^2, \tag{94}$$

$$E = \frac{4\pi}{3}R^3 f\left(K_e(m_e c^2)^{2-\Gamma}\frac{\Gamma(\frac{3-\Gamma}{2})\Gamma(\frac{\Gamma-2}{2})}{2\sqrt{\pi}(\Gamma-1)}(1+\kappa) + \frac{1}{8\pi}B^2\right). \tag{95}$$

Looking for the minimum energy with respect to B, $\frac{dE}{dB} = 0$ gives

$$\frac{dK_e}{dB}(m_e c^2)^{2-\Gamma}\frac{\Gamma(\frac{3-\Gamma}{2})\Gamma(\frac{\Gamma-2}{2})}{2\sqrt{\pi}(\Gamma-1)}(1+\kappa) + \frac{1}{4\pi}B = 0, \tag{96}$$

where (by using Eqs. (91), (92) and (93))

$$\frac{dK_e}{dB} = -\frac{3}{4\pi}\frac{S_\nu}{f\theta^3 d}\frac{1}{c_5}\Big(\frac{\nu}{2c_1}\Big)^{-(1-\Gamma)/2}\frac{(\Gamma+1)\Gamma(\frac{\Gamma+7}{4})}{\sqrt{\pi}\Gamma(\frac{\Gamma+5}{4})}B^{-(\Gamma+3)/2}, \tag{97}$$

i.e. the magnetic field for the minimum energy is

$$B = \Big(\frac{3}{2\pi}\frac{(\Gamma+1)\Gamma(\frac{3-\Gamma}{2})\Gamma(\frac{\Gamma-2}{2})\Gamma(\frac{\Gamma+7}{4})}{(\Gamma-1)\Gamma(\frac{\Gamma+5}{4})}\frac{S_\nu}{f d\theta^3}$$
$$\cdot(m_e c^2)^{2-\Gamma}\frac{(2c_1)^{(1-\Gamma)/2}}{c_5}(1+\kappa)\nu^{(\Gamma-1)/2}\Big)^{2/(\Gamma+5)}, \tag{98}$$

or

$$B\ [\mathrm{Ga}] \approx \Big(6.286\cdot 10^{(9\Gamma-79)/2}\frac{\Gamma+1}{\Gamma-1}\frac{\Gamma(\frac{3-\Gamma}{2})\Gamma(\frac{\Gamma-2}{2})\Gamma(\frac{\Gamma+7}{4})}{\Gamma(\frac{\Gamma+5}{4})}(m_e c^2)^{2-\Gamma} \tag{99}$$
$$\times\ \frac{(2c_1)^{(1-\Gamma)/2}}{c_5}(1+\kappa)\frac{S_\nu[\mathrm{Jy}]}{f\ d[\mathrm{kpc}]\ \theta[\mathrm{arcmin}]^3}\nu[\mathrm{GHz}]^{(\Gamma-1)/2}\Big)^{2/(\Gamma+5)},$$

[8] Namely, $c_1 = 6.264\cdot 10^{18}$ and $c_3 = 1.866\cdot 10^{-23}$ in cgs units.

where $m_e c^2 \approx 8.187 \cdot 10^{-7}$ ergs. We also have

$$E_B = \frac{\Gamma+1}{4} E_{\rm CR}, \quad E_{\rm min} = \frac{\Gamma+5}{\Gamma+1} E_B. \tag{100}$$

A more general derivation

We shall now provide a more general formula for κ. Let us start again with equation (88)

$$\begin{aligned} \epsilon &\approx \int_{p_{\rm inj}}^{\infty} 4\pi k p^{-\Gamma} (\sqrt{p^2c^2 + m^2c^4} - mc^2) dp \\ &= 4\pi k c (mc)^{2-\Gamma} \int_{\frac{p_{\rm inj}}{mc}}^{\infty} x^{-\Gamma} (\sqrt{x^2+1} - 1) dx, \quad x = \frac{p}{mc} \\ &= 4\pi k c (mc)^{2-\Gamma} I\Big(\frac{p_{\rm inj}}{mc}\Big). \end{aligned} \tag{101}$$

Integral $I(x)$ can be expressed through Gauss hypergeometric function ${}_2F_1$ (for $\Gamma > 2$)

$$I(x) = \frac{\Gamma(\frac{3-\Gamma}{2})\Gamma(\frac{\Gamma-2}{2})}{2\sqrt{\pi}(\Gamma-1)} - \frac{x^{1-\Gamma}(1 - {}_2F_1(-\frac{1}{2}, \frac{1-\Gamma}{2}, \frac{3-\Gamma}{2}; -x^2))}{\Gamma-1}, \tag{102}$$

but we will try to find a more simple approximation. Note first that

$$I(x) \approx \frac{\Gamma(\frac{3-\Gamma}{2})\Gamma(\frac{\Gamma-2}{2})}{2\sqrt{\pi}(\Gamma-1)} - \frac{x^{3-\Gamma}}{2(3-\Gamma)} + \frac{x^{5-\Gamma}}{8(5-\Gamma)} - \ldots, \quad x \to 0, \tag{103}$$

$$I(x) \approx \frac{x^{2-\Gamma}}{\Gamma-2}, \quad x \to \infty. \tag{104}$$

So we can try an approximation ($2 < \Gamma < 3$)

$$I(x)_{\rm approx} = \frac{\frac{\Gamma(\frac{3-\Gamma}{2})\Gamma(\frac{\Gamma-2}{2})}{2\sqrt{\pi}(\Gamma-1)} - \frac{x^{3-\Gamma}}{2(3-\Gamma)} + F(\Gamma)x^{5-\Gamma}}{1 + F(\Gamma)(\Gamma-2)x^3} \tag{105}$$

which has correct limits when $x \to 0$ and $x \to \infty$. We shall find $F(\Gamma)$ from matching condition $I(1) = I(1)_{\rm approx}$:

$$F(\Gamma) = \frac{\frac{1}{2(3-\Gamma)} - \frac{1 - {}_2F_1(-\frac{1}{2}, \frac{1-\Gamma}{2}, \frac{3-\Gamma}{2}; -1)}{\Gamma-1}}{1 - (\Gamma-2)(\frac{\Gamma(\frac{3-\Gamma}{2})\Gamma(\frac{\Gamma-2}{2})}{2\sqrt{\pi}(\Gamma-1)} - \frac{1 - {}_2F_1(-\frac{1}{2}, \frac{1-\Gamma}{2}, \frac{3-\Gamma}{2}; -1)}{\Gamma-1})}. \tag{106}$$

Since the last expression also involves a hypergeometric function, by trial and error we found an approximation

$$F(\Gamma)_{\rm approx} = \frac{17}{1250} \frac{(2\Gamma+1)\Gamma}{(\Gamma-2)(5-\Gamma)}. \tag{107}$$

From now on we will assume $I(x) = I(x)_{\rm approx}$ and $F(\Gamma) = F(\Gamma)_{\rm approx}$ (relative error is less than 3.5%).

Total CRs energy density is then

$$\epsilon_{\rm CR} = \epsilon_e + \epsilon_{\rm ion} = K_e (m_e c^2)^{2-\Gamma} I\Big(\frac{p^e_{\rm inj}}{m_e c}\Big) + \sum_i K_i (m_i c^2)^{2-\Gamma} I\Big(\frac{p^i_{\rm inj}}{m_i c}\Big), \tag{108}$$

where (because $\frac{p^i_{\rm inj}}{m_i c} \ll 1$)

$$\begin{aligned}
\epsilon_{\rm ion} &\approx \sum_i K_i (m_i c^2)^{2-\Gamma} \\
&\times \left(\frac{\Gamma(\frac{3-\Gamma}{2})\Gamma(\frac{\Gamma-2}{2})}{2\sqrt{\pi}(\Gamma-1)} - \frac{1}{2(3-\Gamma)} \left(\frac{\sqrt{E^2_{\rm inj} + 2 m_i c^2 E_{\rm inj}}}{m_i c^2} \right)^{3-\Gamma} \right) \\
&\approx K_p (m_p c^2)^{2-\Gamma} \sum_i \frac{n_i}{n_p} \Big(\frac{p^i_{\rm inj}}{p^p_{\rm inj}} \Big)^{\Gamma-1} \Big(\frac{m_i}{m_p} \Big)^{2-\Gamma} \\
&\times \left(\frac{\Gamma(\frac{3-\Gamma}{2})\Gamma(\frac{\Gamma-2}{2})}{2\sqrt{\pi}(\Gamma-1)} - \frac{1}{2(3-\Gamma)} \left(\frac{2E_{\rm inj}}{m_i c^2} \right)^{\frac{3-\Gamma}{2}} \right) \\
&\approx K_p (m_p c^2)^{2-\Gamma} \sum_i \left[\frac{n_i}{n_p} \Big(\frac{m_i}{m_p} \Big)^{\frac{3-\Gamma}{2}} \frac{\Gamma(\frac{3-\Gamma}{2})\Gamma(\frac{\Gamma-2}{2})}{2\sqrt{\pi}(\Gamma-1)} \right. \\
&- \left. \frac{1}{2(3-\Gamma)} \left(\frac{2E_{\rm inj}}{m_p c^2} \right)^{\frac{3-\Gamma}{2}} \frac{n_i}{n_p} \right] \\
&\approx K_p (m_p c^2)^{2-\Gamma} \frac{n}{n_p} \left[\frac{\Gamma(\frac{3-\Gamma}{2})\Gamma(\frac{\Gamma-2}{2})}{2\sqrt{\pi}(\Gamma-1)} \sum_i A_i^{\frac{3-\Gamma}{2}} \nu_i \right. \\
&- \left. \frac{1}{2(3-\Gamma)} \left(\frac{2E_{\rm inj}}{m_p c^2} \right)^{\frac{3-\Gamma}{2}} \right]. \qquad (109)
\end{aligned}$$

Finally,

$$\begin{aligned}
\epsilon_{\rm CR} &= K_e (m_e c^2)^{2-\Gamma} \left[I \left(\frac{\sqrt{E^2_{\rm inj} + 2 m_e c^2 E_{\rm inj}}}{m_e c^2} \right) \right. \\
&+ \frac{1}{\sum_i Z_i \nu_i} \Big(\frac{m_p}{m_e} \Big)^{2-\Gamma} \Big(\frac{2 m_p c^2 E_{\rm inj}}{E^2_{\rm inj} + 2 m_e c^2 E_{\rm inj}} \Big)^{\frac{\Gamma-1}{2}} \\
&\times \left. \left(\frac{\Gamma(\frac{3-\Gamma}{2})\Gamma(\frac{\Gamma-2}{2})}{2\sqrt{\pi}(\Gamma-1)} \sum_i A_i^{\frac{3-\Gamma}{2}} \nu_i - \frac{1}{2(3-\Gamma)} \left(\frac{2E_{\rm inj}}{m_p c^2} \right)^{\frac{3-\Gamma}{2}} \right) \right] \\
&= K_e (m_e c^2)^{2-\Gamma} \frac{\Gamma(\frac{3-\Gamma}{2})\Gamma(\frac{\Gamma-2}{2})}{2\sqrt{\pi}(\Gamma-1)} (1+\kappa), \qquad (110)
\end{aligned}$$

where

$$\begin{aligned}
\kappa &= I \left(\frac{\sqrt{E^2_{\rm inj} + 2 m_e c^2 E_{\rm inj}}}{m_e c^2} \right) \left(\frac{\Gamma(\frac{3-\Gamma}{2})\Gamma(\frac{\Gamma-2}{2})}{2\sqrt{\pi}(\Gamma-1)} \right)^{-1} \\
&+ \frac{1}{\sum_i Z_i \nu_i} \Big(\frac{m_p}{m_e} \Big)^{2-\Gamma} \Big(\frac{2 m_p c^2 E_{\rm inj}}{E^2_{\rm inj} + 2 m_e c^2 E_{\rm inj}} \Big)^{\frac{\Gamma-1}{2}} \qquad (111) \\
&\times \left(\sum_i A_i^{\frac{3-\Gamma}{2}} \nu_i - \frac{1}{2(3-\Gamma)} \left(\frac{2E_{\rm inj}}{m_p c^2} \right)^{\frac{3-\Gamma}{2}} \left(\frac{2\sqrt{\pi}(\Gamma-1)}{\Gamma(\frac{3-\Gamma}{2})\Gamma(\frac{\Gamma-2}{2})} \right) \right) - 1.
\end{aligned}$$

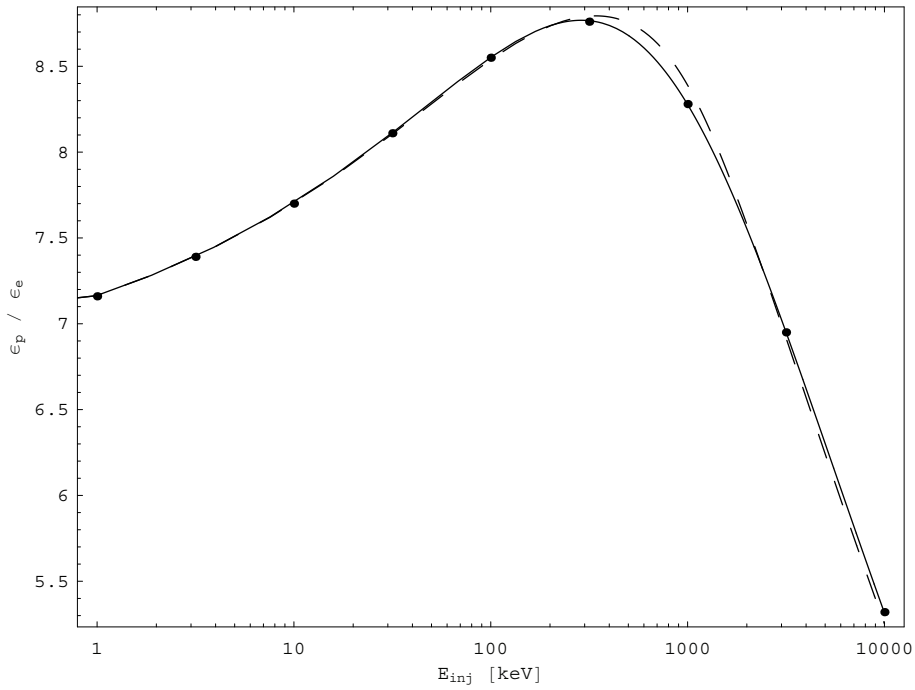

Figure 16: Proton to electron energy density ratio as a function of injection energy in our approximation (dashed line) and exact ratio (solid line) for $\Gamma = 2.5$. Data points are from Bell (1978b).

In the above derivation we used the fact that (Bell 1978b):

$$K_i/K_p = \frac{n_i}{n_p}\Big(\frac{p^i_{\rm inj}}{p^p_{\rm inj}}\Big)^{\Gamma-1} \approx (n_i/n_p)\cdot(m_i/m_p)^{(\Gamma-1)/2} \tag{112}$$

and

$$K_p/K_e = (n_p/n_e)\Big(\frac{E^2_{\rm inj}+2m_pc^2E_{\rm inj}}{E^2_{\rm inj}+2m_ec^2E_{\rm inj}}\Big)^{\frac{\Gamma-1}{2}} \approx (n_p/n_e)\cdot\Big(\frac{2m_pc^2E_{\rm inj}}{E^2_{\rm inj}+2m_ec^2E_{\rm inj}}\Big)^{\frac{\Gamma-1}{2}}. \tag{113}$$

Eq. (111) has the correct limit (90) when $E_{\rm inj} \ll m_ec^2 \ll m_pc^2$. It can be shown that for low $E_{\rm inj}$ CR energy density is almost constant (independent of $E_{\rm inj}$) and the use of Eq. (90) is justified. When shock velocity can be estimated, one should calculate injection energy $E_{\rm inj} \approx 4\frac{1}{2}m_pv_s^2$ and use Eq. (111). Formulae (99) and (100) for magnetic field and minimum energy remain the same.[9] In Fig. 16 we give proton to electron energy density ratio as a function of injection energy in our approximation compared to the same data from Bell (1978b). Agreement is quite good despite the approximative character of our formulae.

Even if strict equipartition does not apply, but $\epsilon_B/\epsilon_{\rm CR} = \beta =$ constant is somehow known (independent information about CR electrons can come from

[9]Note that κ is no longer ions to electrons energy ratio but a suitable parameter introduced to make new formulae same as the old ones.

X-ray data – inverse Compton scattering, or about CRs from gamma rays – bremsstrahlung or pion decay), the magnetic field may be recalculated as

$$B' = \Big(\frac{4\beta}{\Gamma+1}\Big)^{2/(\Gamma+5)} B, \tag{114}$$

where B is the field corresponding to the minimum energy.

Cases $\alpha = 0.5$ *and* $\alpha = 1$

Generalization to cases $\alpha = 0.5$ and $\alpha = 1$ (energy indices $\Gamma = 2$ and $\Gamma = 3$) can be found in Arbutina et al. (2013). If Γ is exactly 2, the integral for CR energy density diverges and one has to set an upper limit for particle energy. A similar situation arises in the case $\alpha = 1$ – the integral for CR energy density diverges unless a lower limit for particle energy, i.e. $E_{\rm inj}$, is set.

Let us start with the energy density of a CR species with $\Gamma = 2$ ($\alpha = 0.5$)

$$\begin{aligned}
\epsilon &= \int_{p_{\rm inj}}^{p_\infty} 4\pi k p^{-2}(\sqrt{p^2c^2+m^2c^4} - mc^2)dp \qquad (115)\\
&= K\int_{x_{\rm inj}}^{x_\infty} x^{-2}(\sqrt{x^2+1}-1)dx, \quad x = \frac{p}{mc},\ K = 4\pi kc,\\
&= K\ I_2(x)|_{x_{\rm inj}}^{x_\infty} = K\ \Big(\frac{1}{x} - \frac{\sqrt{x^2+1}}{x} + \operatorname{arcsinh} x\Big)\Big|_{x_{\rm inj}}^{x_\infty},
\end{aligned}$$

where k and K are constants in the momentum and energy distribution functions, respectively. When $x \to 0$, $I_2(x) \approx x/2$ while for $x \to \infty$, $I_2(x) \approx \ln x$. Total CR energy density $\epsilon_{\rm CR} = \epsilon_{\rm e} + \epsilon_{\rm ion}$ is then

$$\begin{aligned}
\epsilon_{\rm CR} &= K_e\Big(I_2\big(\tfrac{p^e_\infty}{m_e c}\big) - I_2\big(\tfrac{p^e_{\rm inj}}{m_e c}\big)\Big)\\
&+ \sum_i K_i\Big(I_2\big(\tfrac{p^i_\infty}{m_i c}\big) - I_2\big(\tfrac{p^i_{\rm inj}}{m_i c}\big)\Big)\\
&\approx K_e\Bigg\{\ln\big(\frac{E^e_\infty}{m_e c^2}\big) - I_2\big(\tfrac{\sqrt{E^2_{\rm inj}+2m_ec^2E_{\rm inj}}}{m_ec^2}\big) + \frac{1}{\sum_i Z_i\nu_i}\\
&\cdot \sqrt{\tfrac{2m_pc^2E_{\rm inj}}{E^2_{\rm inj}+2m_ec^2E_{\rm inj}}}\Big(\sum_i \sqrt{A_i}\nu_i \ln\big(\frac{E^p_\infty}{m_pc^2}\big) - \sqrt{\frac{E_{\rm inj}}{2m_pc^2}}\\
&+ \sum_i \sqrt{A_i}\ln\big(\tfrac{Z_i}{A_i}\big)\nu_i\Big)\Bigg\}. \qquad (116)
\end{aligned}$$

where we used Eqs. (112) and (113) and assumed $E_{\rm inj} \ll m_pc^2$, $p_\infty \approx E_\infty/c$ for all CR species. A_i and Z_i are mass and charge numbers, respectively, and ν_i represent ion abundances. Assuming Bohm diffusion and synchrotron losses for electrons, for maximum electron energy we use $E^e_\infty = \frac{3}{8}\frac{m_e^2c^3v_s}{\sqrt{\frac{2}{3}e^3B}}$ (Zirakashvili & Aharonian 2007) and for ions $E^i_\infty = \frac{3}{8}\frac{v_s}{c}Z_ieBR$ (see Bell et al. 2013 and references therein), where R is SNR radius. Both formulae are in cgs units. In reality, of course, we do not expect a sharp break in the energy spectra, but rather some steepening, especially in the case of electrons (Blasi 2010).

For the total energy we have $E = \frac{4\pi}{3} R^3 f(\epsilon_{\rm CR} + \epsilon_B)$, $\epsilon_B = \frac{1}{8\pi} B^2$. Looking for the minimum energy with respect to B, $\frac{dE}{dB} = 0$ gives

$$\begin{aligned} & \frac{dK_e}{dB}\Bigg[\ln\big(\frac{E^e_\infty}{m_e c^2}\big) - I\big(\tfrac{\sqrt{E^2_{\rm inj} + 2 m_e c^2 E_{\rm inj}}}{m_e c^2}\big) + \frac{1}{3} + \frac{1}{\sum_i Z_i \nu_i} \\ \cdot \quad & \sqrt{\tfrac{2 m_p c^2 E_{\rm inj}}{E^2_{\rm inj} + 2 m_e c^2 E_{\rm inj}}} \Big(\sum_i \sqrt{A_i} \nu_i \ln\big(\frac{E^p_\infty}{m_p c^2}\big) - \sqrt{\frac{E_{\rm inj}}{2 m_p c^2}} \\ + \quad & \sum_i \sqrt{A_i} \ln\big(\tfrac{Z_i}{A_i}\big) \nu_i - \frac{2}{3} \sum_i \sqrt{A_i} \nu_i \Big) \Bigg] + \frac{1}{4\pi} B = 0. \end{aligned} \tag{117}$$

where (by using Eqs. (91), (92) and (93))

$$\frac{dK_e}{dB} = -\frac{3}{2}\frac{K_e}{B} = -\frac{9}{4\pi}\frac{S_\nu}{f \theta^3 d}\frac{1}{c_5}\Big(\frac{\nu}{2c_1}\Big)^{1/2} \frac{\Gamma(\frac{9}{4})}{\sqrt{\pi}\Gamma(\frac{7}{4})} B^{-5/2}. \tag{118}$$

In order to find magnetic field, Eq. (117) has to be solved numerically. When one finds B, minimum energy can be obtained from

$$E_{\rm min} = \Big(1 + \frac{4}{3}\frac{\{\ldots\}}{[\ldots]}\Big) E_B, \quad E_B = \frac{4\pi}{3} R^3 f\ \epsilon_B, \tag{119}$$

where $\{\ldots\}$ and $[\ldots]$ are expressions in the corresponding brackets in Eqs. (116) and (117), respectively.

In the situations when $\Gamma = 3$ ($\alpha = 1$), the energy density of a CR species is

$$\begin{aligned} \epsilon &= \int_{p_{\rm inj}}^{p_\infty} 4\pi k p^{-3} (\sqrt{p^2 c^2 + m^2 c^4} - m c^2) dp \\ &= \frac{K}{mc^2}\ I_3(x)\big|^{x_\infty}_{x_{\rm inj}}, \quad x = \frac{p}{mc},\ K = 4\pi k c^2, \\ &= \frac{K}{mc^2}\ \Big(\frac{1 - \sqrt{x^2+1}}{2x^2} - \frac{1}{2}\ln\Big(\frac{1+\sqrt{x^2+1}}{x}\Big)\Big)\Big|^{x_\infty}_{x_{\rm inj}}. \end{aligned} \tag{120}$$

When $x \to 0$, $I_3(x) \approx \frac{1}{2}\ln x$, while when $x \to \infty$, $I_3(x) \approx -\frac{1}{2x}$. Total CR energy density is then

$$\begin{aligned} \epsilon_{\rm CR} &= \frac{K_e}{m_e c^2}\Big(I_3\big(\tfrac{p^e_\infty}{m_e c}\big) - I_3\big(\tfrac{p^e_{\rm inj}}{m_e c}\big)\Big) \\ &+ \sum_i \frac{K_i}{m_i c^2}\Big(I_3\big(\tfrac{p^i_\infty}{m_i c}\big) - I_3\big(\tfrac{p^i_{\rm inj}}{m_i c}\big)\Big) \\ &\approx \frac{K_e}{m_e c^2}\Bigg\{ -\frac{m_e c^2}{2E^e_\infty} - I_3\big(\tfrac{\sqrt{E^2_{\rm inj} + 2 m_e c^2 E_{\rm inj}}}{m_e c^2}\big) - \frac{1}{\sum_i Z_i \nu_i} \\ &\cdot \quad \tfrac{m_e c^2 E_{\rm inj}}{E^2_{\rm inj} + 2 m_e c^2 E_{\rm inj}} \Big(\sum_i \frac{A_i}{Z_i}\frac{m_p c^2}{E^p_\infty}\nu_i + \frac{1}{2}\ln\big(\frac{2E_{\rm inj}}{m_p c^2}\big) \\ &- \frac{1}{2}\sum_i \ln(A_i)\nu_i\Big)\Bigg\}, \end{aligned} \tag{121}$$

where we have used the same assumptions as in the derivation of Eq. (116).

Derivative of the total energy with respect to B gives

$$\frac{1}{m_e c^2}\frac{dK_e}{dB}\Bigg[-\frac{3m_e c^2}{8E_\infty^e}-I_3\big(\tfrac{\sqrt{E_{\rm inj}^2+2m_e c^2 E_{\rm inj}}}{m_e c^2}\big)-\frac{1}{\sum_i Z_i\nu_i}$$
$$\cdot\quad \tfrac{m_e c^2 E_{\rm inj}}{E_{\rm inj}^2+2m_e c^2 E_{\rm inj}}\Big(\frac{3}{2}\sum_i\frac{A_i}{Z_i}\frac{m_p c^2}{E_\infty^p}\nu_i+\frac{1}{2}\ln\big(\frac{2E_{\rm inj}}{m_p c^2}\big)$$
$$-\quad \frac{1}{2}\sum_i\ln(A_i)\nu_i\Big)\Bigg]+\frac{1}{4\pi}B=0. \tag{122}$$

where (see Eqs. (91), (92) and (93))

$$\frac{dK_e}{dB}=-2\frac{K_e}{B}=-\frac{9}{8\pi}\frac{S_\nu}{f\theta^3 d}\frac{1}{c_5}\frac{\nu}{c_1}B^{-3}. \tag{123}$$

To find magnetic field more precisely, Eq. (122) has to be solved numerically. Nevertheless, unlike the case $\alpha = 0.5$, the solution will only weakly depend on the upper limits for energy, so the terms containing E_∞^e and E_∞^p could, in principle, be neglected. When one finds B, minimum energy can be obtained from

$$E_{\rm min}=\Big(1+\frac{\{\ldots\}}{[\ldots]}\Big)E_B,\quad E_B=\frac{4\pi}{3}R^3 f\,\epsilon_B, \tag{124}$$

where now $\{\ldots\}$ and $[\ldots]$ are expressions in the corresponding brackets in Eqs. (121) and (122), respectively.

We have implemented our modified equipartition calculation by developing a PHP calculator available at `http://poincare.matf.bg.ac.rs/~arbo/eqp/`.

2.5 Synchrotron radiation

Whenever we have ultra-relativistic electrons in a strong magnetic field, we also expect the synchrotron radiation or magneto-bremsstrahlung (as opposed to thermal or non-thermal bremsstrahlung or "breaking" radiation). Synchrotron radiation is thus evidence of particle acceleration in strong shocks (electrons, at least) and magnetic field amplification. As we will soon see, for a power-law electron distribution $N(E) \propto E^{-\Gamma}$, the resulting radio spectrum will also be a power law $I_\nu \propto \nu^{-\alpha}$, where spectral index is $\alpha = (\Gamma - 1)/2$. For $\Gamma = 2$ one obtains a typical spectral index for strong shocks $\alpha = 0.5$. Let us first find specific intensity I_ν and flux density S_ν of a thin shell and then we will move on to emission coefficient for synchrotron radiation.

2.5.1 Radiation from a thin shell

Let us consider an infinitely thin homogenous shell (or, in other words, homogenous optically thin sphere). Flux of radiation energy (power) is by definition

$$dF_\nu = B_\nu \cos\theta' d\Omega' d\sigma' d\nu, \tag{125}$$

where $B_\nu \neq B_\nu(\Theta, \varphi)$ is the surface brightness of the sphere,

$$d\sigma' = R^2 \sin\Theta d\Theta d\varphi \tag{126}$$

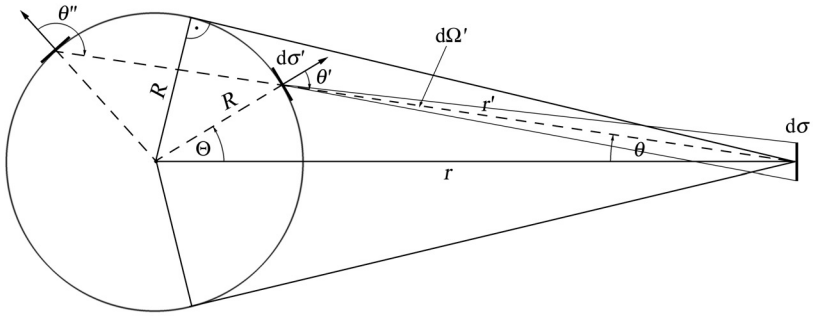

Figure 17: Radiation from an infinitely thin homogenous shell.

is elementary surface and

$$d\Omega' = \frac{d\sigma \cos\theta}{r'^2} \tag{127}$$

is the corresponding solid angle in which radiation is emitted by this surface and received by the collector of the surface area $d\sigma$. Radius of the sphere is R, distance to the observer is $d = r$, for the definition of r', θ', θ, θ_s and Θ see Fig. 17.

Flux density is now

$$dS_\nu = \frac{dF_\nu}{d\sigma d\nu} = \frac{B_\nu \cos\theta' \cos\theta}{r'^2} R^2 \sin\Theta d\Theta d\varphi. \tag{128}$$

Let us first consider radiation from the front side ($0 \leq \Theta \leq \Theta_s$). We shall prove the familiar result

$$dS_\nu = B_\nu \cos\theta d\Omega, \quad d\Omega = \sin\theta d\theta d\varphi, \tag{129}$$

which comes from the fact that specific intensity of radiation $I_\nu = B_\nu$ is constant (independent of distance) if there are no sources or sinks along the path of the "ray of light" (one consequence of this is the reversibility theorem).

We will start with the trivial equality

$$z = r - Z, \tag{130}$$

where z is measured from observer towards the source, while Z is measured from the center of the sphere (source) towards the observer. From Eq. (130) we have

$$r' \cos\theta = r - R\cos\Theta. \tag{131}$$

On the other hand, from cosine theorem

$$r'^2 = r^2 + R^2 - 2rR\cos\Theta \tag{132}$$

we have

$$\begin{aligned} r'^2 &= r^2 + R^2 - 2r(r - r'\cos\theta) \\ &= R^2 - r^2 + 2rr'\cos\theta, \end{aligned} \tag{133}$$

$$\begin{aligned} r'dr' &= rdr'\cos\theta - rr'\sin\theta d\theta \\ &= -\frac{rr'\sin\theta d\theta}{1-\frac{r}{r'}\cos\theta}. \end{aligned} \tag{134}$$

Directly from (132), however,

$$r'dr' = rR\sin\Theta d\Theta. \tag{135}$$

Combination of the last two equations gives

$$R^2\sin\Theta d\Theta = \frac{r'R\sin\theta d\theta}{\frac{r}{r'}\cos\theta - 1}. \tag{136}$$

Two other cosine theorems

$$r^2 = R^2 + r'^2 + 2Rr'\cos\theta', \tag{137}$$

$$R^2 = r^2 + r'^2 - 2rr'\cos\theta, \tag{138}$$

added together give

$$\cos\theta' = \frac{r\cos\theta - r'}{R}. \tag{139}$$

From (136) and (139) we have:

$$dS_\nu^+ = B_\nu\cos\theta\sin\theta d\theta d\varphi, \quad (0 \le \theta \le \theta_s). \tag{140}$$

For the rear side ($\Theta_s \le \Theta \le \pi$) we have, similarly,

$$\begin{aligned} dS_\nu = \frac{dF_\nu}{d\sigma d\nu} &= \frac{B_\nu\cos(180^\circ - \theta'')\cos\theta}{r'^2}R^2\sin\Theta d\Theta d\varphi \\ &= -\frac{B_\nu\cos\theta''\cos\theta}{r'^2}R^2\sin\Theta d\Theta d\varphi, \end{aligned} \tag{141}$$

i.e. (after following the same procedure with θ' replaced by θ'')

$$\begin{aligned} dS_\nu^- &= -B_\nu\cos\theta\sin\theta d\theta d\varphi, \quad (\theta_s \le \theta \le 0), \\ &= B_\nu\cos\theta\sin\theta d\theta d\varphi, \quad (0 \le \theta \le \theta_s). \end{aligned} \tag{142}$$

The contribution from the front and the rear side is thus equal and

$$dS_\nu = dS_\nu^+ + dS_\nu^- = 2B_\nu\cos\theta\sin\theta d\theta d\varphi. \tag{143}$$

For the total flux density we have

$$\begin{aligned} S_\nu &= \int_0^{2\pi}\int_0^{\theta_s} 2B_\nu\cos\theta\sin\theta d\theta d\varphi \\ &= 2\pi\sin^2\theta_s B_\nu = 2\pi(1-\cos\theta_s)(1+\cos\theta_s)B_\nu \\ &= 2B_\nu\Omega_s\Big(1-\frac{\Omega_s}{4\pi}\Big), \end{aligned} \tag{144}$$

where $\Omega_s = 2\pi(1-\cos\theta_s)$.

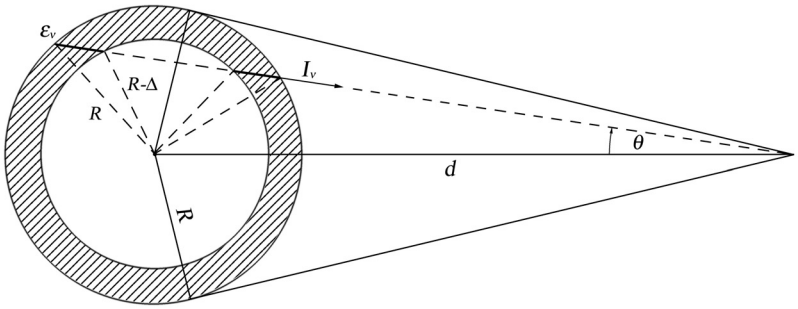

Figure 18: Radiation from an optically thin homogenous shell with thickness Δ and radius R, at the distance d from the observer.

Now, let us consider a homogenous emitting shell with emissivity $\varepsilon_\nu = \text{const}$ and thickness Δ. For specific intensity, if the medium is optically thin, we have

$$I_\nu = \int \varepsilon_\nu ds = \begin{cases} \varepsilon_\nu(r'_{2+} - r'_{1+}) + \varepsilon_\nu(r'_{1-} - r'_{2-}), & 0 < \sin\theta < \frac{R-\Delta}{d} \\ \varepsilon_\nu(r'_{2+} - r'_{2-}), & \frac{R-\Delta}{d} \le \sin\theta \le \frac{R}{d}, \end{cases} \tag{145}$$

where $ds = dr'$. Cosine theorems (see Fig. 18)

$$(R-\Delta)^2 = d^2 + r_1'^2 - 2dr'_1\cos\theta, \tag{146}$$

$$R^2 = d^2 + r_2'^2 - 2dr'_2\cos\theta, \tag{147}$$

give us

$$r'_{1\pm} = d\cos\theta \pm \sqrt{(R-\Delta)^2 - d^2\sin^2\theta}, \tag{148}$$

$$r'_{2\pm} = d\cos\theta \pm \sqrt{R^2 - d^2\sin^2\theta}. \tag{149}$$

Finally, we have

$$I_\nu = \begin{cases} 2\varepsilon_\nu\Big(\sqrt{R^2 - d^2\sin^2\theta} - \sqrt{(R-\Delta)^2 - d^2\sin^2\theta}\Big), & 0 < \sin\theta < \frac{R-\Delta}{d} \\ 2\varepsilon_\nu\sqrt{R^2 - d^2\sin^2\theta}, & \frac{R-\Delta}{d} \le \sin\theta \le \frac{R}{d}. \end{cases} \tag{150}$$

From the last equation one can see that $I_\nu^0 = 2\varepsilon_\nu R\delta$ and $I_\nu^{\max} = 2\varepsilon_\nu R\sqrt{\delta(2-\delta)}$, where $\delta = \Delta/R$. Therefore, for an optically thin homogenous shell we have a sort of "limb-brightening" (Fig. 19).

For the total flux density we have

$$\begin{aligned} S_\nu &= \int_0^{2\pi}\int_0^{\theta_s} I_\nu\cos\theta\sin\theta d\theta d\varphi \\ &= 4\pi\varepsilon_\nu\int_0^{\theta_1}\Big(\sqrt{R^2 - d^2\sin^2\theta} - \sqrt{(R-\Delta)^2 - d^2\sin^2\theta}\Big)\cos\theta\sin\theta d\theta \\ &+ 4\pi\varepsilon_\nu\int_{\theta_1}^{\theta_2}\sqrt{R^2 - d^2\sin^2\theta}\cos\theta\sin\theta d\theta, \end{aligned} \tag{151}$$

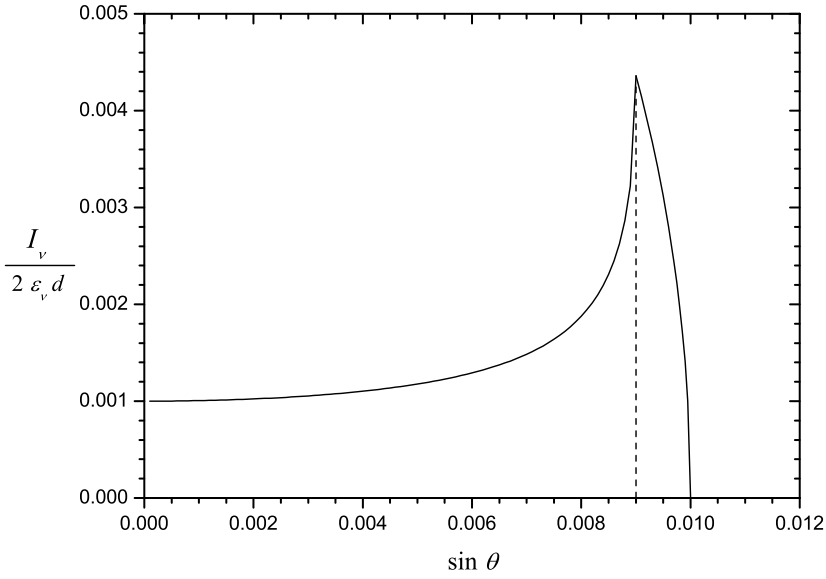

Figure 19: Brightness distribution for an optically thin homogenous shell-like source with $\delta = \Delta/R = 0.1$ and $R/d = 0.01$.

where $\theta_1 = \arcsin\frac{R-\Delta}{d}$ and $\theta_2 = \theta_s = \arcsin\frac{R}{d}$. After integration we obtain the expected result

$$S_\nu = \frac{4\pi}{3}\varepsilon_\nu d\Big[\Big(\frac{R}{d}\Big)^3 - \Big(\frac{R-\Delta}{d}\Big)^3\Big] = \frac{\varepsilon_\nu V}{d^2} = \frac{\mathcal{E}_\nu V}{4\pi d^2} = \frac{L_\nu}{4\pi d^2}, \tag{152}$$

where the shell volume is $V = \frac{4\pi}{3} f R^3$, $f = 1-(1-\delta)^3$ is the volume filling factor, $\mathcal{E}_\nu = 4\pi\varepsilon_\nu$ is total volume emissivity (ε_ν is emissivity per unit solid angle) and L_ν is luminosity.

If we had a source with uniform surface brightness $\Sigma_\nu = I_\nu = \text{const.}$ we would have

$$S_\nu \;=\; \int_0^{2\pi}\int_0^{\theta_s} \Sigma_\nu \cos\theta \sin\theta d\theta d\varphi = \Sigma_\nu \pi \sin^2\theta_s = \Sigma_\nu \frac{R^2\pi}{d^2}, \tag{153}$$

i.e. average surface brightness of the shell-like source is $\Sigma_\nu = \frac{4}{3} R f \varepsilon_\nu$.

If all the swept-up ISM in the shell were compressed to a value $X = \rho/\rho_0 = 4$, then

$$\rho = \frac{M}{V} = \frac{\rho_0}{f}, \quad \text{since } M = \frac{4\pi\rho_0 R^3}{3},\ V = \frac{4\pi R^3 f}{3} \tag{154}$$

and the volume filling factor $f = 1/X = 0.25$, i.e. relative thickness is $\delta = \Delta/R \approx 10\%$. In this case $f = \text{const}$, during the evolution. If, on the other hand, $\Delta = \text{const}$, $f = 1-(1-\Delta/R)^3 \approx 3\Delta/R$ for large R.

If we have a synchrotron shell source with a radial magnetic field, the emission coefficient is $\varepsilon_\nu \propto (B\sin\theta')^{\alpha+1}\nu^{-\alpha}$ (see the following text) i.e.

$$\varepsilon_\nu = \tilde{\varepsilon}_\nu (\sin\theta')^{\alpha+1}. \tag{155}$$

Of course, the field cannot extend all the way to the center, since $\nabla \cdot \mathbf{B} = 0$. Sine theorem (see Fig. 17) gives us

$$\frac{r'}{d} = \frac{\sin\Theta}{\sin\theta'}, \quad \Theta = \theta' - \theta, \tag{156}$$

i.e.

$$r' = d(\cos\theta - \sin\theta\ \cot\theta') \tag{157}$$

and

$$ds = dr' = d\sin\theta\frac{d\theta'}{\sin^2\theta'}. \tag{158}$$

Intensity is then

$$I_\nu = \int \varepsilon_\nu ds = \tilde{\varepsilon}_\nu d\sin\theta \int (\sin\theta')^{\alpha-1} d\theta', \tag{159}$$

i.e.

$$I_\nu = \begin{cases} \tilde{\varepsilon}_\nu d\sin\theta\Big(\int_{\mu_{2+}}^{\mu_{1+}}(1-\mu^2)^{(\alpha-2)/2}d\mu + \int_{\mu_{1-}}^{\mu_{2-}}(1-\mu^2)^{(\alpha-2)/2}d\mu\Big) \\ \quad = 2\tilde{\varepsilon}_\nu d\sin\theta\int_{\mu_{1-}}^{\mu_{2-}}(1-\mu^2)^{(\alpha-2)/2}d\mu, & 0 < \sin\theta < \frac{R-\Delta}{d} \\ \tilde{\varepsilon}_\nu d\sin\theta\int_{\mu_{2+}}^{\mu_{2-}}(1-\mu^2)^{(\alpha-2)/2}d\mu, & \frac{R-\Delta}{d} \le \sin\theta \le \frac{R}{d}, \end{cases} \tag{160}$$

where $\mu = \cos\theta'$ and

$$\mu_{1\pm} = \frac{d^2 - (R-\Delta)^2 - r_{1\pm}'^2}{2(R-\Delta)r_{1\pm}'} = \mp\frac{\sqrt{(R-\Delta)^2 - d^2\sin^2\theta}}{R-\Delta} = \mp\frac{\sqrt{\sin^2\theta_1 - \sin^2\theta}}{\sin\theta_1}, \tag{161}$$

$$\mu_{2\pm} = \frac{d^2 - R^2 - r_{2\pm}'^2}{2Rr_{2\pm}'} = \mp\frac{\sqrt{R^2 - d^2\sin^2\theta}}{R} = \mp\frac{\sqrt{\sin^2\theta_2 - \sin^2\theta}}{\sin\theta_2}. \tag{162}$$

We immediately see from (160) that unlike the case $\varepsilon_\nu = \text{const}$, here $I_\nu = 0$ when $\theta = 0$.

Rather than by direct integration we will find flux density through

$$S_\nu = \frac{L_\nu}{4\pi d^2} = \frac{\mathcal{E}_\nu V}{4\pi d^2}, \tag{163}$$

where

$$\mathcal{E}_\nu = \int_{4\pi}\varepsilon_\nu d\omega' = \int_0^{2\pi}\int_0^{\pi}\tilde{\varepsilon}_\nu(\sin\theta')^{\alpha+1}\sin\theta' d\theta' d\varphi = 2\pi\tilde{\varepsilon}_\nu\int_0^{\pi}(\sin\theta')^{\alpha+2}d\theta' \tag{164}$$

i.e. $\mathcal{E}_\nu = 2\pi\sqrt{\pi}\frac{\Gamma(\frac{\alpha+3}{2})}{\Gamma(\frac{\alpha+4}{2})}\tilde{\varepsilon}_\nu$ and the shell volume is as before $V = \frac{4\pi}{3}fR^3$, $f = 1-(1-\delta)^3$.

2.5.2 Synchrotron emissivity

In the following paragraphs we will present a detailed derivation of the emission coefficient for synchrotron radiation. For even more details, consult Shu (1991), Rybicki & Lightman (2004) or Longair (2011).

Let us start by finding the motion of an electron of mass m_e and charge e in a magnetic field using the correct relativistic equations[10]

$$\frac{d}{dt}(\gamma m_e \mathbf{v}) = \frac{e}{c}\mathbf{v}\times\mathbf{B} \tag{165}$$

$$\frac{d}{dt}(\gamma m_e c^2) = e\mathbf{v}\cdot\mathbf{E} = 0. \tag{166}$$

This last equation implies that γ = const or that $|\mathbf{v}|$= const. Therefore, it follows that

$$m_e\gamma\frac{d\mathbf{v}}{dt} = \frac{e}{c}\mathbf{v}\times\mathbf{B}. \tag{167}$$

Separating the velocity components along the field $\mathbf{v}_\parallel$ and in a plane normal to the field $\mathbf{v}_\perp$ we have

$$\frac{d\mathbf{v}_\parallel}{dt} = 0, \qquad \frac{d\mathbf{v}_\perp}{dt} = \frac{e}{\gamma m_e c}\mathbf{v}_\perp\times\mathbf{B}. \tag{168}$$

It follows that $\mathbf{v}_\parallel$ = const, and, since the total $|\mathbf{v}|$ = const, also $|\mathbf{v}_\perp|$ = const, so the particle has a helical motion with frequency of the gyration

$$\omega_B = \frac{eB}{\gamma m_e c} = \frac{\omega_o}{\gamma}, \tag{169}$$

and gyro-radius $r_g = v\sin\Theta/\omega_B$, Θ being the pitch angle.

To obtain emissivity of synchrotron radiation we shall start from Liénard-Wiechert potentials

$$\phi = \Big[\frac{e}{\kappa R}\Big], \tag{170}$$

$$\mathbf{A} = \Big[\frac{e\mathbf{v}}{c\kappa R}\Big], \tag{171}$$

where brackets denote retarded times t' ($t = t' + R(t')/c$), $\kappa = 1 - \mathbf{n}\cdot\boldsymbol{\beta}$, $\boldsymbol{\beta} = \mathbf{v}/c$, $\mathbf{n} = \mathbf{R}/R$, $\mathbf{R} = \mathbf{r} - \mathbf{r}_0$ (vector $\mathbf{r}_o$ marks position of the particle).

The fields are

$$\begin{aligned}\mathbf{E}(\mathbf{r},t) &= e\Big[\frac{(\mathbf{n}-\boldsymbol{\beta})(1-\beta^2)}{\kappa^3 R^2}\Big] + \frac{e}{c}\Big[\frac{\mathbf{n}}{\kappa^3 R}\times\big((\mathbf{n}-\boldsymbol{\beta})\times\dot{\boldsymbol{\beta}}\big)\Big] \\ &\approx \frac{e}{c}\Big[\frac{\mathbf{n}}{\kappa^3 R}\times\big((\mathbf{n}-\boldsymbol{\beta})\times\dot{\boldsymbol{\beta}}\big)\Big],\end{aligned} \tag{172}$$

$$\mathbf{B}(\mathbf{r},t) = \big[\mathbf{n}\times\mathbf{E}(\mathbf{r},t)\big], \tag{173}$$

in the radiative zone.

Energy per unit frequency per unit solid angle corresponding to radiation field of a single particle is

$$\begin{aligned}\frac{dW}{d\omega d\Omega} &= \frac{c}{4\pi^2}\Big|\int\big[R\mathbf{E}(\mathbf{r},t)\big]e^{i\omega t}dt\Big|^2 \\ &= \frac{e^2}{4\pi^2 c}\Big|\int\Big[\frac{\mathbf{n}}{\kappa^3}\times\big((\mathbf{n}-\boldsymbol{\beta})\times\dot{\boldsymbol{\beta}}\big)\Big]e^{i\omega t}dt\Big|^2 \\ &= \frac{e^2}{4\pi^2 c}\Big|\int\Big[\frac{\mathbf{n}}{\kappa^2}\times\big((\mathbf{n}-\boldsymbol{\beta})\times\dot{\boldsymbol{\beta}}\big)\Big]e^{i\omega t}dt'\Big|^2\end{aligned}$$

[10] Do not confuse adiabatic index γ with $\gamma = (1-\beta^2)^{-1/2}$.

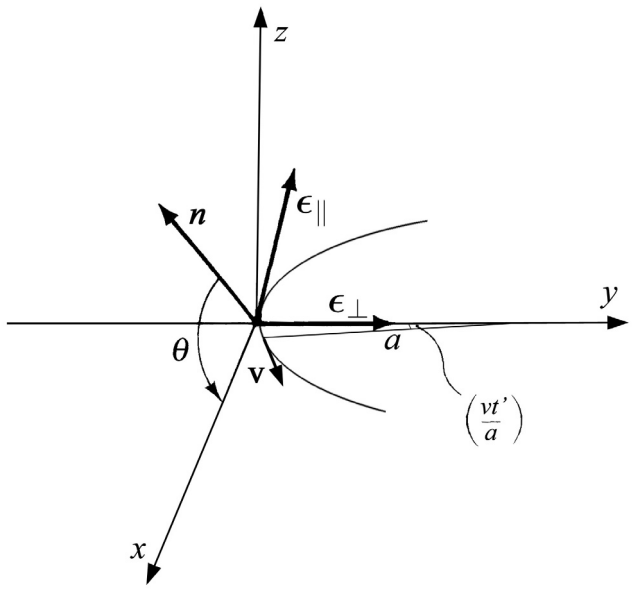

Figure 20: Coordinate system adopted for calculating electron's synchrotron emission. (Rybicki & Lightman 2004)

$$
\begin{aligned}
&= \frac{e^2}{4\pi^2 c}\Big|\int d\Big(\Big[\frac{\mathbf{n}}{\kappa}\times\big(\mathbf{n}\times\boldsymbol{\beta}\big)\Big]\Big)e^{i\omega t}\Big|^2 \\
&= \frac{e^2\omega^2}{4\pi^2 c}\Big|\int\Big[\mathbf{n}\times\big(\mathbf{n}\times\boldsymbol{\beta}\big)\Big]e^{i\omega(t'-\mathbf{n}\cdot\mathbf{r}_0(t')/c)}dt'\Big|^2, \qquad (174)
\end{aligned}
$$

where we used identities $dt=\kappa dt'$, $d/dt'\big(\kappa^{-1}\mathbf{n}\times(\mathbf{n}\times\boldsymbol{\beta})\big)=\kappa^{-2}\mathbf{n}\times\big((\mathbf{n}-\boldsymbol{\beta})\times\dot{\boldsymbol{\beta}}\big)$, $R(t')\approx r-\mathbf{n}\cdot\mathbf{r}_0(t')$ $(r_0\ll r)$ and integrated by parts to obtain an expression involving only $\boldsymbol{\beta}$ (and not $\dot{\boldsymbol{\beta}}$).

Consider the orbital trajectory in Fig. 20 where the origin of the coordinates is the location of the particle at the origin of retarded time $t'=0$, and $a=v/(\omega_B\sin\Theta)$ is the radius of curvature of the trajectory. The coordinate system has been chosen so that the particle has velocity $\mathbf{v}$ along the x axis at time $t'=0$; $\boldsymbol{\epsilon}_\perp$ is a unit vector along the y axis in the orbital xy–plane, and $\boldsymbol{\epsilon}_\parallel=\mathbf{n}\times\boldsymbol{\epsilon}_\perp$. We have

$$
\begin{aligned}
\mathbf{v} &= v\cos\left(\frac{vt'}{a}\right)\boldsymbol{\epsilon}_x + v\sin\left(\frac{vt'}{a}\right)\boldsymbol{\epsilon}_\perp \\
&= v\cos\theta\cos\left(\frac{vt'}{a}\right)\mathbf{n} - v\sin\ \theta\cos\left(\frac{vt'}{a}\right)\boldsymbol{\epsilon}_\parallel + v\sin\left(\frac{vt'}{a}\right)\boldsymbol{\epsilon}_\perp, \qquad (175)
\end{aligned}
$$

i.e.

$$
\mathbf{n}\times(\mathbf{n}\times\boldsymbol{\beta}) = -\boldsymbol{\epsilon}_\perp\ \sin\left(\frac{vt'}{a}\right) + \boldsymbol{\epsilon}_\parallel\ \cos\left(\frac{vt'}{a}\right)\sin\ \theta, \qquad (176)
$$

where we have set $\beta = 1$, and

$$\begin{aligned} t' - \frac{\mathbf{n}\cdot\mathbf{r}(t')}{c} &= t' - \frac{a}{c}\cos\theta \sin\left(\frac{vt'}{a}\right) \\ &\approx t'(1-\frac{v}{c}) + \frac{v}{c}\frac{\theta^2}{2}t' + \frac{v^3}{6ca^2}t'^3 \\ &\approx (2\gamma^2)^{-1}\left[(1+\gamma^2\theta^2)t' + \frac{c^2\gamma^2 t'^3}{3a^2}\right], \end{aligned} \tag{177}$$

where we have expanded the sine and cosine functions for small arguments, used the approximation $(1-\beta) \approx 1/2\gamma^2$, and set $\beta = 1$ ($v = c$) elsewhere.

Expanding the sine and cosine functions again, we obtain an expression for the spectrum in the two polarizations states,

$$\frac{dW}{d\omega d\Omega} \equiv \frac{dW_\parallel}{d\omega d\Omega} + \frac{dW_\perp}{d\omega d\Omega} \tag{178}$$

$$\frac{dW_\perp}{d\omega d\Omega} = \frac{e^2\omega^2}{4\pi^2 c}\left|\int \frac{ct'}{a}\,\exp\left[\frac{i\omega}{2\gamma^2}\left(\theta_\gamma^2 t' + \frac{c^2\gamma^2 t'^3}{3a^2}\right)\right]dt'\right|^2, \tag{179}$$

$$\frac{dW_\parallel}{d\omega d\Omega} = \frac{e^2\omega^2\theta^2}{4\pi^2 c}\left|\int \exp\left[\frac{i\omega}{2\gamma^2}\left(\theta_\gamma^2 t' + \frac{c^2\gamma^2 t'^3}{3a^2}\right)\right]dt'\right|^2, \tag{180}$$

where

$$\theta_\gamma^2 \equiv 1 + \gamma^2\theta^2. \tag{181}$$

Now, making the changes of variables

$$y \equiv \gamma\frac{ct'}{a\theta_\gamma}, \tag{182}$$

$$\eta \equiv \frac{\omega a\theta_\gamma^3}{3c\gamma^3}, \tag{183}$$

Eqs. (179) and (180) become

$$\frac{dW_\perp}{d\omega d\Omega} = \frac{e^2\omega^2}{4\pi^2 c}\left(\frac{a\theta_\gamma^2}{\gamma^2 c}\right)^2\left|\int_{-\infty}^{\infty} y\,\exp\left[\frac{3}{2}\,i\eta\left(y + \frac{1}{3}y^3\right)\right]dy\right|^2, \tag{184}$$

$$\frac{dW_\parallel}{d\omega d\Omega} = \frac{e^2\omega^2\theta^2}{4\pi^2 c}\left(\frac{a\theta_\gamma}{\gamma_c}\right)^2\left|\int_{-\infty}^{\infty} \exp\left[\frac{3}{2}\,i\eta\left(y + \frac{1}{3}y^3\right)\right]dy\right|^2, \tag{185}$$

where little error is made in extending the limits of integration from $-\infty$ to ∞. The last integrals may be expressed in terms of the modified Bessel functions of order 1/3 and 2/3 (Abramovitz & Stegun 1972):

$$K_{\frac{1}{3}}(\eta) = \sqrt{3}\int_0^\infty \cos\left[\frac{3}{2}\,\eta\left(y + \frac{1}{3}y^3\right)\right]dy, \tag{186}$$

$$K_{\frac{2}{3}}(\eta) = \sqrt{3}\int_0^\infty y\sin\left[\frac{3}{2}\,\eta\left(y + \frac{1}{3}y^3\right)\right]dy. \tag{187}$$

Therefore we can write

$$\frac{dW_\perp}{d\omega d\Omega} = \frac{e^2\omega^2}{3\pi^2 c}\left(\frac{a\theta_\gamma^2}{\gamma^2 c}\right)^2 K_{\frac{2}{3}}^2(\eta), \tag{188}$$

$$\frac{dW_\parallel}{d\omega d\Omega} = \frac{e^2\omega^2\theta^2}{3\pi^2 c}\left(\frac{a\theta_\gamma}{\gamma c}\right)^2 K_{\frac{1}{3}}^2(\eta). \tag{189}$$

These formulas can now be integrated over solid angle to give the energy per frequency range radiated by the particle per complete orbit in the projected normal plane. During one such orbit the emitted radiation is almost completely confined to the solid angle shown shaded in Fig. 21, which lies within an angle of $1/\gamma$ of a cone of half-angle Θ. Thus it is permissible to take the element of the solid angle to be $d\Omega = 2\pi \sin\Theta\, d\theta$, and we can write

$$\frac{dW_\perp}{d\omega} = \frac{2e^2\omega^2 a^2 \sin\Theta}{3\pi c^3\gamma^4}\int_{-\infty}^{\infty} \theta_\gamma^4 K_{\frac{2}{3}}^2(\eta)\, d\theta, \tag{190}$$

$$\frac{dW_\parallel}{d\omega} = \frac{2e^2\omega^2 a^2 \sin\Theta}{3\pi c^3\gamma^2}\int_{-\infty}^{\infty} \theta_\gamma^2\theta^2 K_{\frac{1}{3}}^2(\eta)\, d\theta. \tag{191}$$

The above integrals have been evaluated by Westfold (1959):

$$\frac{dW_\perp}{d\omega} = \frac{\sqrt{3}\, e^2\gamma \sin\Theta}{2c}\left[F(x) + G(x)\right], \tag{192}$$

$$\frac{dW_\parallel}{d\omega} = \frac{\sqrt{3}\, e^2\gamma \sin\Theta}{2c}\left[F(x) - G(x)\right], \tag{193}$$

where

$$F(x) = x\int_x^\infty K_{\frac{5}{3}}(\xi)\, d\xi, \qquad K_{\frac{5}{3}}(\xi) = -K_{\frac{1}{3}}(\xi) - 2K'_{\frac{2}{3}}(\xi), \tag{194}$$

$$G(x) = xK_{\frac{2}{3}}(x),$$

and, again $x \equiv \omega/\omega_c$ where

$$\omega_c = \frac{3\gamma^2 eB\sin\Theta}{2mc}. \tag{195}$$

To convert this to emitted power per frequency, we divide by the orbital period of the charge, $T = 2\pi/\omega_B$,

$$P_\perp(\omega) = \frac{\sqrt{3}e^3 B\sin\Theta}{4\pi m_e c^2}[F(x) + G(x)], \tag{196}$$

$$P_\parallel(\omega) = \frac{\sqrt{3}e^3 B\sin\Theta}{4\pi m_e c^2}[F(x) - G(x)], \tag{197}$$

The total emitted power per frequency is the sum of these:

$$P(\omega) = \frac{\sqrt{3}e^3 B\sin\Theta}{2\pi m_e c^2}F(x), \tag{198}$$

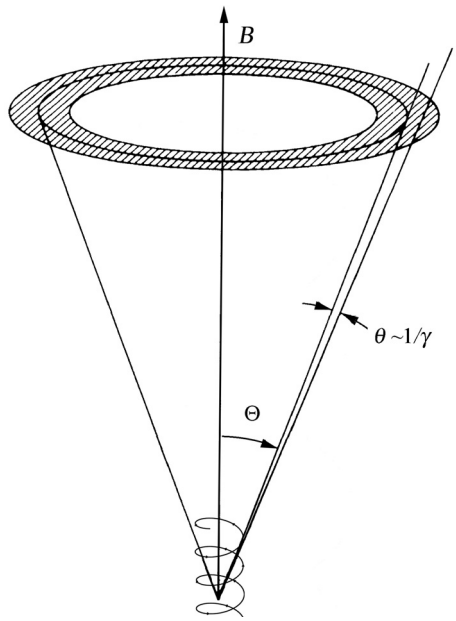

Figure 21: Confinement of emitted radiation of an electron with pitch angle Θ to a small solid angle with $\theta \sim 1/\gamma$ during one orbit (Rybicki & Lightman 2004)

Asymptotic forms for small and large values of x are:

$$F(x) \approx \frac{4\pi}{\sqrt{3}\Gamma\left(\frac{1}{3}\right)}\left(\frac{x}{2}\right)^{1/3}, \qquad x \ll 1, \tag{199}$$

$$F(x) \approx \left(\frac{\pi}{2}\right)^{1/2} e^{-x} x^{1/2}, \qquad x \gg 1. \tag{200}$$

To obtain frequency-integrated emission, or emission from a power-law distribution of electrons, it is useful to have expressions for integrals over the functions $F(x)$ and $G(x)$ (Abramowitz and Stegun 1972):

$$\int_0^\infty x^n F(x)dx = \frac{2^{n+1}}{n+2}\Gamma\left(\frac{n}{2}+\frac{7}{3}\right)\Gamma\left(\frac{n}{2}+\frac{2}{3}\right), \tag{201}$$

$$\int_0^\infty x^n G(x)dx = 2^n\Gamma\left(\frac{n}{2}+\frac{4}{3}\right)\Gamma\left(\frac{n}{2}+\frac{2}{3}\right). \tag{202}$$

The total frequency-integrated power is then

$$\begin{aligned} P &= \frac{\sqrt{3}e^3 B\sin\Theta}{2\pi m_e c^2}\omega_c \int_0^\infty F(x)dx \\ &= \frac{\sqrt{3}e^3 B\sin\Theta}{2\pi m_e c^2}\omega_c \Gamma(2/3)\Gamma(7/3) \\ &= \frac{2}{3}\frac{e^4 B^2}{m_e^2 c^3}\gamma^2\beta^2\sin^2\Theta, \end{aligned} \tag{203}$$

since $\Gamma(2/3) = \frac{2\pi}{\sqrt{3}\Gamma(1/3)}$ and $\Gamma(z+1) = z\Gamma(z)$ and we have taken into account that β may not be exactly 1.

For a power-law distribution of electrons $N(E)dE = KE^{-\Gamma}dE$, the total power per unit volume per unit frequency, $P_{\rm tot}(\omega)$, is

$$\begin{aligned} P_{\rm tot}(\omega) &= \int_0^\infty N(E)P(\omega)dE \propto \int_0^\infty x^{(\Gamma-3)/2}F(x)dx \qquad (204)\\ &= \frac{\sqrt{3}e^3K(B\sin\Theta)^{\frac{\Gamma+1}{2}}}{2\pi m_e c^2(\Gamma+1)}\Gamma\left(\frac{\Gamma}{4}+\frac{19}{12}\right)\Gamma\left(\frac{\Gamma}{4}-\frac{1}{12}\right)\left(\frac{m_e^3c^5\,\omega}{3e}\right)^{-\frac{\Gamma-1}{2}}, \end{aligned}$$

where we switched from $E = \left(\frac{2m_e^3c^5\,\omega}{3eB\sin\Theta}\right)^{1/2} x^{-1/2}$ to x to perform integration. Since $\omega = 2\pi\nu$, $P(\omega) \sim \frac{dW}{d\omega} = \frac{1}{2\pi}\frac{dW}{d\nu}$, total volume emissivity is $\mathcal{E}_\nu = 2\pi P_{\rm tot}(\nu)$, while the emission coefficient $\varepsilon_\nu = \frac{\mathcal{E}_\nu}{4\pi}$ is

$$\varepsilon_\nu = c_5 K(B\sin\Theta)^{(\Gamma+1)/2}\left(\frac{\nu}{2c_1}\right)^{(1-\Gamma)/2}, \qquad (205)$$

where c_1, c_3 and c_5 are defined in Pacholczyk (1970). Finally, we can integrate the last expression over the pitch angle Θ, assuming isotropic distribution, to obtain

$$\frac{1}{2}\int_0^\pi (\sin\Theta)^{(\Gamma+3)/2}d\Theta = \frac{\sqrt{\pi}}{2}\frac{\Gamma(\frac{\Gamma+5}{4})}{\Gamma(\frac{\Gamma+7}{4})}, \qquad (206)$$

which then replaces $(\sin\Theta)^{(\Gamma+1)/2}$ in Eq. (205).

We can also compute the polarization for synchrotron radiation. The degree of linear polarization for particles of a single energy is

$$\Pi(\omega) = \frac{P_\perp(\omega) - P_\parallel(\omega)}{P_\perp(\omega) + P_\parallel(\omega)} = \frac{G(x)}{F(x)}. \qquad (207)$$

For particles with a power-law distribution of energies, the degree of polarization is

$$\begin{aligned} \Pi &= \frac{\int_0^\infty G(x)x^{(\Gamma-3)/2}dx}{\int_0^\infty F(x)x^{(\Gamma-3)/2}dx}\\ &= \frac{\Gamma+1}{4}\frac{\Gamma(\frac{\Gamma}{4}+\frac{7}{12})}{\Gamma(\frac{\Gamma}{4}+\frac{19}{12})}\\ &= \frac{\Gamma+1}{\Gamma+\frac{7}{3}}. \qquad (208) \end{aligned}$$

Thus, for $\Gamma = 2$ the degree of polarization would be 69%.

2.6 Hydrodynamic evolution of supernova remnants

The hydrodynamic evolution of SNRs has already been discussed in some detail in the Introduction to this section. A recent overview of dynamical evolution and radiative processes can be found in Reynolds (2016). Here we will just make a brief recapitulation before proceeding to hydrodynamical solutions. The evolution can be conditionally divided into four different phases:

(i) free expansion, $v_s^2 = (dR/dt)^2 \propto E_o/\mathcal{M}_o = \text{const}$;

(ii) adiabatic or Sedov phase, $R = 1.15\ (E_o/\rho_o)^{1/5} t^{2/5}$,

(iii) isothermal or radiative phase, $R \propto t^{2/7}$ (or possibly $R \propto t^{1/4}$), and

(iv) dissipation, $v_s \approx c_s$.

The evolution during the first two phases can be combined in an approximative formula (Arbutina 2005)

$$\frac{1}{2} v_s^2 = \frac{k_1 E_o}{k_2 \mathcal{M}_o + 4\pi R^3 \rho_o / 3}, \quad v_s = \frac{dR}{dt}, \tag{209}$$

where E_o is the explosion energy, M_o mass of the ejecta and ρ_o ISM density. Constants k_1 and k_2 may be interpreted as the fractions of SN energy and mass in the shell and are determined in such a way so that when $R = 0$, the velocity equals some initial velocity, e.g. $v_s \approx 20000$ km/s, and when $R \gg 0$, the velocity tends toward the Sedov's solution.

In the later phases, after the thin shell formation, the evolution is expected to be governed by the internal pressure of the hot interior (Bandiera & Petruk 2004)

$$\frac{d}{dt}\left(\mathcal{M}\frac{dR}{dt}\right) = 4\pi R^2 (P - P_o), \quad \frac{d\mathcal{M}}{dR} = 4\pi R^2 \rho_o, \tag{210}$$

where P_o is the external pressure, while the internal pressure is assumed to follow the adiabatic law $PV^\gamma = \text{const}$. One can check that the solution of the above equation will have the asymptotic behaviour at large radii, $R \propto t^{2/(2+3\gamma)} \propto t^{2/7}$, for $\gamma = 5/3$. When the right hand side of Eq. (210) is zero, we will have momentum conservation $4\pi R^3 \rho_o v_s / 3 = \text{const}$, i.e. $R \propto t^{1/4}$.

It is important to keep in mind that the division into phases is somewhat artificial – the transition between the phases is, of course, smooth, i.e the real evolution of the shock $R = R(t)$ is a continuous function of time.

2.6.1 Chevalier's solutions

As we already said, there may be significant shock declaration even during the so-called free expansion phase. An intermediate phase between the free expansion and the subsequent Sedov phase is sometimes described by the solutions of Chevalier (1982). Young SNR is assumed to be made of two shells (compressed SN material and swept-up ISM) separated by the contact discontinuity, with forward and reverse shocks. The outer part of the ejecta has a density profile

$$\rho = t^{-3} (r/tg)^{-n}, \tag{211}$$

the ambient density profile is

$$\rho = q r^{-s}. \tag{212}$$

and contact discontinuity advances with time as

$$R_c = (Ag^n/q)^{1/(n-s)} t^{(n-3)/(n-s)}, \tag{213}$$

where n is integer ($n > 5$), $s \in \{0, 2\}$ – for $s = 0$, $q = \rho_o$, while case $s = 2$ corresponds to steady circumstellar wind (e.g. in radio SNe) i.e. $q = \frac{\dot{\mathcal{M}}}{4\pi v_{\rm W}}$, $\dot{\mathcal{M}}$ is the mass loss rate and $v_{\rm W}$ is the wind velocity.

Table 3: R_o/R_c, R_i/R_c and A for $s = 0$ and different n from Chevalier (1982).

n	6	7	8	9	10	12	14
R_o/R_c	1.256	1.181	1.154	1.140	1.131	1.121	1.116
R_i/R_c	0.906	0.935	0.950	0.960	0.966	0.974	0.979
A	2.4	1.2	0.71	0.47	0.33	0.19	0.12

Constant g depends on E_o and $\mathcal{M}_o$. It can be found by considering two parts of the freely expanding ejecta ($v = r/t$) with density profiles $\rho_\delta = t^{-3}(r/th)^{-\delta}$ and $\rho_n = t^{-3}(r/tg)^{-n}$. Integrating to obtain the total mass and energy gives:

$$\begin{aligned}\mathcal{M}_o &= \int_0^{R(u_t)} 4\pi r^2 \rho_\delta dr + \int_{R(u_t)}^{\infty} 4\pi r^2 \rho_n dr \\ &= \int_0^{u_t} 4\pi v^{2-\delta} h^\delta dv + \int_{u_t}^{\infty} 4\pi v^{2-n} g^n dv, \end{aligned} \tag{214}$$

$$\begin{aligned}E_o &= \int_0^{R(u_t)} 4\pi r^2 \frac{1}{2}\rho_\delta v^2 dr + \int_{R(u_t)}^{\infty} 4\pi r^2 \frac{1}{2}\rho_n v^2 dr \\ &= \int_0^{u_t} 2\pi v^{4-\delta} h^\delta dv + \int_{u_t}^{\infty} 2\pi v^{4-n} g^n dv, \end{aligned} \tag{215}$$

i.e.

$$\mathcal{M}_o = \frac{4\pi h^\delta}{3-\delta} u_t^{3-\delta} + \frac{4\pi g^n}{n-3} u_t^{3-n}, \tag{216}$$

$$E_o = \frac{2\pi h^\delta}{5-\delta} u_t^{5-\delta} + \frac{2\pi g^n}{n-5} u_t^{5-n}. \tag{217}$$

At the transition point $v = u_t$, $\rho_\delta = \rho_n$ so

$$\left(\frac{u_t}{h}\right)^{-\delta} = \left(\frac{u_t}{g}\right)^{-n}. \tag{218}$$

From the last three equations we find

$$g^n = \frac{1}{4\pi(n-\delta)} \frac{\big(2(5-\delta)(n-5)\big)^{(n-3)/2}}{\big((3-\delta)(n-3)\big)^{(n-5)/2}} \frac{(E_o)^{(n-3)/2}}{(\mathcal{M}_o)^{(n-5)/2}}. \tag{219}$$

It is often assumed that the inner part of the ejecta is flat, $\delta = 0$, and that $n = 7$ is typical for SNe Ia, while SN II are more likely to have $n \approx 12$. The real profiles are much more complicated and can sometimes, as we have seen, be better approximated by exponential functions than by power-laws. Nevertheless, if $\delta = 0$ and $n = 7$ then from Eq. (219) $g^7 = \frac{25}{21\pi}\frac{E_o^2}{\mathcal{M}_o}$.

We can also find the transition velocity u_t between flat and power-law region of the ejecta. In the case $\delta = 0$, instead of h^δ we should introduce another constant h_0, and by eliminating g^n and h_0 between Eqs. (216) – (218) we find

$$u_t^2 = \frac{10(n-5)}{3(n-3)} \frac{E_o}{\mathcal{M}_o}. \tag{220}$$

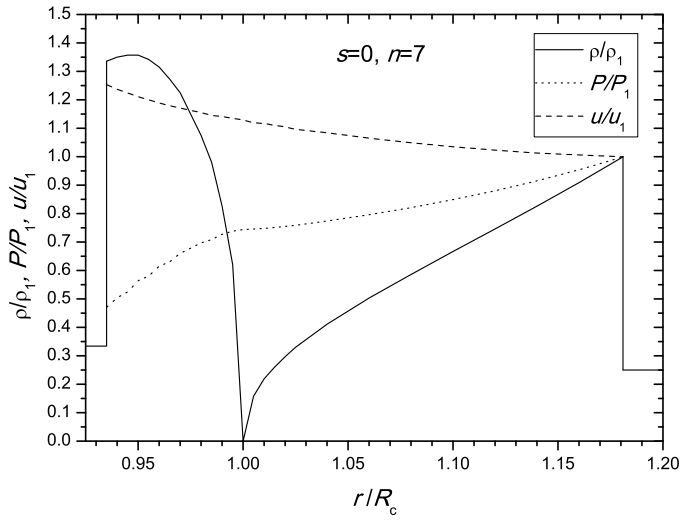

Figure 22: The complete hydrodynamic solution for the case $s = 0$, $n = 7$ from Chevalier (1982).

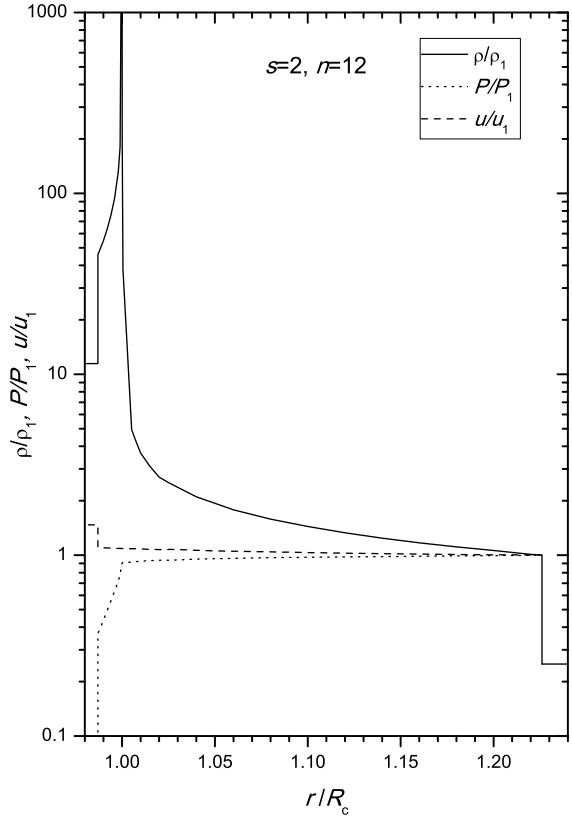

Figure 23: The complete hydrodynamic solution for the case $s = 2$, $n = 12$ from Chevalier (1982).

Table 4: R_o/R_c, R_i/R_c and A for $s = 2$ and different n from Chevalier (1982).

n	6	7	8	9	10	12	14
R_o/R_c	1.377	1.299	1.267	1.250	1.239	1.226	1.218
R_i/R_c	0.958	0.970	0.976	0.981	0.984	0.987	0.990
A	0.62	0.27	0.15	0.096	0.067	0.038	0.025

The complete solutions are obtained by solving Euler equations and are given in Figs. 22 and 23 for cases $s = 0$, $n = 7$, and $s = 2$, $n = 12$ (see Chevalier 1982). Table 3 and Table 4 list the parameter A and position of the outer, forward shock $R = R_o$ and the inner, reverse shock R_i, with respect to the contact discontinuity, for different n, and $s = 0$ and $s = 2$, respectively. The solution for the radius of the forward shock $R = R(t)$ for $s = 0$ and $n = 7$ is

$$R = 1.06\ (E_o^2/(\mathcal{M}_o\rho_o))^{1/7}t^{4/7}. \tag{221}$$

Both, forward and reverse shocks are assumed to be strong, i.e. the compression at the shocks is $X = 4$. The pressure at the contact discontinuity is continuous and there is no mixing between fluids in this model. In reality, because the compressed ejecta is enriched with heavier elements and it has larger specific weight compared to compressed ISM (mostly hydrogen and helium), the contact discontinuity is subjected to Rayleigh-Taylor instability.

2.6.2 Sedov solution

When the shock wave sweeps-up enough space so that the ISM mass many times exceeds the mass of the SN ejecta, a SNR enters the second phase of evolution described by the analytical solution of Sedov (1959) for a point-like explosion in the uniform medium, the so-called blast wave. Euler equations allow similarity solutions with variable $\xi = crt^{-\lambda}$ introduced, from where $R \propto t^{\lambda}$. We can use dimensional analysis to guess the solution for $R = R(t)$ i.e. the constant c and parameter λ. Let us assume that the SNR has "forgotten" the exact initial conditions of SN explosion, so that only parameters E_o and ρ_o are important. Dimensionally $E_o = [\mathrm{erg}] = [\mathrm{g}][\mathrm{cm}^2][\mathrm{s}^{-2}]$, while $\rho_o = [\mathrm{g}][\mathrm{cm}^{-3}]$. Eliminating [g] we have $E_o \times [\mathrm{cm}^{-2}][\mathrm{s}^2] = \rho_o \times [\mathrm{cm}^3]$, i.e. $[\mathrm{cm}^5] = (E_o/\rho_o)\ [\mathrm{s}^2]$, so $R \propto (E_o/\rho_o)^{1/5}t^{2/5}$ and $\lambda = 2/5$.

To find the complete solution, we will write a similarity variable in the form (Landau & Lifshitz 1987):

$$\xi = r/R(t), \quad R(t) = \beta(E_o/\rho_o)^{1/5}t^{2/5}, \tag{222}$$

where we have to solve Euler equations to find β.

Self-similar form of Euler equations

Let us assume that we can express density, pressure and velocity as:

$$\begin{aligned} \rho &= A(t)F(\xi), \\ P &= B(t)G(\xi), \\ v &= C(t)U(\xi). \end{aligned} \tag{223}$$

At the shock front ($\xi = 1$) we shall set boundary conditions $F(1) = G(1) = U(1) = 1$ so that from the Rankine-Hugoniot jump conditions for strong shocks

$$\rho_2 = \frac{\gamma+1}{\gamma-1}\rho_1, \tag{224}$$

$$P_2 = \frac{2}{\gamma+1}\rho_1(v_1 - v_s)^2, \tag{225}$$

$$v_2 = v_s + \frac{\gamma-1}{\gamma+1}(v_1 - v_s), \tag{226}$$

we have (with $\rho_1 = \rho_o$, $R_s = R$, $v_s = \dot{R}$ and $v_1 \equiv 0$ in laboratory frame)

$$A(t) = \frac{\gamma+1}{\gamma-1}\rho_o, \tag{227}$$

$$B(t) = \frac{2}{\gamma+1}\rho_o\dot{R}^2, \tag{228}$$

$$C(t) = \frac{2}{\gamma+1}\dot{R}. \tag{229}$$

Since all dependent variables depend on ξ and R ($R = R(t)$, $\dot{R} = \dot{R}(R)$) we can rewrite partial derivatives as

$$\frac{\partial}{\partial t} = \dot{R}\Big(\frac{\partial}{\partial R} - \frac{\xi}{R}\frac{\partial}{\partial \xi}\Big), \tag{230}$$

$$\frac{\partial}{\partial r} = \frac{1}{R}\frac{\partial}{\partial \xi}. \tag{231}$$

We are now ready to move on to Euler equations in spherical symmetry

$$\frac{\partial \rho}{\partial t} + \frac{1}{r^2}\frac{\partial}{\partial r}\Big(r^2\rho v\Big) = 0, \tag{232}$$

$$\rho\frac{Dv}{Dt} = \rho\frac{\partial v}{\partial t} + \rho v\frac{\partial v}{\partial r} = -\frac{\partial P}{\partial r}, \tag{233}$$

$$\frac{D(P\rho^{-\gamma})}{Dt} = \frac{\partial}{\partial t}\Big(P\rho^{-\gamma}\Big) + v\frac{\partial}{\partial r}\Big(P\rho^{-\gamma}\Big) = 0. \tag{234}$$

Continuity equation (232) can be rewritten as

$$\frac{\partial \rho}{\partial t} + v\frac{\partial \rho}{\partial r} + \rho\frac{\partial v}{\partial r} + \frac{2}{r}\rho v = 0. \tag{235}$$

With the help of Eqs. (230) and (231) we have

$$-(\gamma+1)\xi F' + 2UF' + 2FU' + \frac{4}{\xi}FU = 0, \tag{236}$$

where $f' = \frac{df}{d\xi}$, $f = \{F, G, U\}$. The last equation can be transformed to

$$\Big(\frac{U}{\xi} - \frac{\gamma+1}{2}\Big)\xi\frac{F'}{F} + U' + \frac{2}{\xi}U = 0, \tag{237}$$

$$\Big(V-\frac{\gamma+1}{2}\Big)\frac{d\ln F}{d\ln\xi}+\frac{dV}{d\ln\xi}+3V=0, \tag{238}$$

where we used $U'=\frac{d(\xi V)}{d\xi}=\frac{dV}{d\ln\xi}+V$ and $V=U/\xi$.

Let us move to momentum equation. By using

$$\dot R\frac{\partial\dot R}{\partial R}=\ddot R \quad\text{and}\quad 2R\ddot R=-3\dot R^2 \tag{239}$$

from Eq. (233) we obtain

$$-3U-2\xi U'+\frac{4}{\gamma+1}UU'+2\frac{\gamma-1}{\gamma+1}\frac{G'}{F}=0, \tag{240}$$

$$\xi\Big[\Big(\frac{4}{\gamma+1}\frac{U}{\xi}-2\Big)U'-3\frac{U}{\xi}\Big]+2\frac{\gamma-1}{\gamma+1}\frac{G'}{F}=0, \tag{241}$$

$$\Big[\Big(\frac{4}{\gamma+1}V-2\Big)\Big(\frac{dV}{d\ln\xi}+V\Big)-3V\Big]+2\frac{\gamma-1}{\gamma+1}\frac{1}{F\xi}\frac{dG}{d\xi}=0, \tag{242}$$

$$\Big(V-\frac{\gamma+1}{2}\Big)\frac{dV}{d\ln\xi}+V\Big(V-5\frac{\gamma+1}{4}\Big)+\frac{\gamma-1}{2}\frac{1}{F\xi}\frac{dG}{d\xi}=0. \tag{243}$$

Finally, the entropy equation (234) can be rewritten as

$$\frac{\partial P}{\partial t}-\gamma\frac{P}{\rho}\frac{\partial\rho}{\partial t}+v\Big(\frac{\partial P}{\partial r}-\gamma\frac{P}{\rho}\frac{\partial\rho}{\partial r}\Big)=0. \tag{244}$$

From Eqs. (230), (231), (239) and (244) we have

$$-3-\frac{d\ln G}{d\ln\xi}+\gamma\frac{d\ln F}{d\ln\xi}+\frac{2}{\gamma+1}\frac{U}{\xi}\Big(\frac{d\ln G}{d\ln\xi}-\gamma\frac{d\ln F}{d\ln\xi}\Big)=0, \tag{245}$$

i.e.

$$\frac{d\ln(GF^{-\gamma})}{d\ln\xi}=\frac{3}{2}\frac{\gamma+1}{V-\frac{\gamma+1}{2}}. \tag{246}$$

On the other hand, Eq. (238) can be rewritten as

$$\Big(V-\frac{\gamma+1}{2}\Big)\frac{d\ln F}{d\ln\xi}+\frac{d(V-\frac{\gamma+1}{2})}{d\ln\xi}+3\Big(V-\frac{\gamma+1}{2}\Big)+\frac{3}{2}(\gamma+1)=0, \tag{247}$$

$$\frac{d\ln F}{d\ln\xi}+\frac{d\ln(V-\frac{\gamma+1}{2})}{d\ln\xi}+\frac{3}{2}\frac{\gamma+1}{V-\frac{\gamma+1}{2}}+3=0, \tag{248}$$

which in combination with Eq. (246) gives

$$\frac{d\ln F}{d\ln\xi}+\frac{d\ln(V-\frac{\gamma+1}{2})}{d\ln\xi}+\frac{d\ln(GF^{-\gamma})}{d\ln\xi}+3=0, \tag{249}$$

or

$$GF^{1-\gamma}\Big(V-\frac{\gamma+1}{2}\Big)=\text{const}\cdot\xi^{-3}. \tag{250}$$

From boundary conditions we have const $= 1 - \frac{\gamma+1}{2} = \frac{1-\gamma}{2}$ so, finally,

$$GF^{1-\gamma}\Big(V - \frac{\gamma+1}{2}\Big) = \frac{1-\gamma}{2\xi^3}. \tag{251}$$

Instead of any of the Eqs. (232)–(234) we could use the energy equation[11]

$$\frac{\partial}{\partial t}\Big(\rho(\frac{1}{2}v^2 + \mathcal{E})\Big) + \frac{1}{r^2}\frac{\partial}{\partial r}\Big(r^2\rho v(\frac{1}{2}v^2 + \mathcal{E} + \frac{P}{\rho})\Big) = 0. \tag{252}$$

With $\mathcal{E} = \frac{u}{\rho}$, $u = \frac{1}{\gamma-1}P$ and using Eq. (239) we obtain

$$-3(FU^2+G) - \xi\frac{d}{d\xi}\Big(FU^2+G\Big) + \frac{2}{\gamma+1}\frac{1}{\xi^2}\frac{d}{d\xi}\Big(\xi^2U(FU^2+\gamma G)\Big) = 0, \tag{253}$$

$$-\frac{d}{d\xi}\Big(\xi^3(FU^2+G)\Big) + \frac{d}{d\xi}\Big(\xi^2\frac{2U}{\gamma+1}(FU^2+\gamma G)\Big) = 0, \tag{254}$$

$$-\xi^3(FU^2+G) + \frac{2\xi^2U}{\gamma+1}(FU^2+\gamma G) = \text{const}. \tag{255}$$

From boundary conditions const $= 0$ and

$$\frac{U}{\xi}\Big(U^2 + \gamma\frac{G}{F}\Big) = \frac{\gamma+1}{2}\Big(U^2 + \frac{G}{F}\Big). \tag{256}$$

The last equation can also be written as

$$V\Big(V^2 + \gamma\frac{G}{F\xi^2}\Big) = \frac{\gamma+1}{2}\Big(V^2 + \frac{G}{F\xi^2}\Big). \tag{257}$$

In the subsequent derivation we will replace the momentum equation in self-similar form (243), as it appears to be the most complicated, with Eq. (257).

First integral via energy conservation

Eq. (252) (and Eq. (232)) is in the form of the generic conservation law corresponding to conservation of quantity with density f and flux density $\mathbf{F}$:

$$\frac{\partial f}{\partial t} + \nabla\cdot\mathbf{F} = 0. \tag{258}$$

If the surface enclosing a given volume is static, we can apply the Gauss theorem and obtain the integral form of the conservation law (258):

$$\frac{\partial}{\partial t}\int_V f dV + \oint_S \mathbf{F}\cdot\mathbf{n}\, dS = 0, \tag{259}$$

[11] In fact, we can treat internal energy equation (under adiabatic conditions)

$$\frac{D\mathcal{E}}{Dt} + P\frac{D}{Dt}\Big(\frac{1}{\rho}\Big) = 0,$$

as a combination of continuity, momentum and energy equations, which then, if $u = \frac{1}{\gamma-1}P$, produce Eq. (234).

where $\mathbf{n}$ is the unit vector orthogonal to the surface.

If, however, the surface S is moving (expanding) with velocity $\mathbf{u}$, it "sweeps up" f and the additional flux into S is $f\mathbf{u}\cdot\mathbf{n}$. Hence, the conservation law is now

$$\frac{\partial}{\partial t}\int_V f dV + \oint_S \mathbf{F}\cdot\mathbf{n}\; dS = \oint_S f\mathbf{u}\cdot\mathbf{n}\; dS, \tag{260}$$

i.e.

$$\frac{\partial}{\partial t}\int_V f dV + \oint_S (\mathbf{F} - f\mathbf{u})\cdot\mathbf{n}\; dS = 0. \tag{261}$$

Let us now consider a moving surface with $\xi = \text{const}$. Energy within this surface is

$$\begin{aligned} E(\xi) &= \int_0^{r(\xi)} \rho\Big(\frac{1}{2}v^2 + \mathcal{E}\Big)\; 4\pi r^2 dr \\ &= \frac{8\pi}{\gamma^2-1}\rho_o \dot{R}^2 R^3 \int_0^{\xi} \Big(FU^2 + G\Big)\; \xi^2 d\xi \\ &= \frac{32\pi}{25(\gamma^2-1)}\beta^5 E_o \int_0^{\xi} \Big(FU^2 + G\Big)\; \xi^2 d\xi, \end{aligned} \tag{262}$$

where we used the fact that $\dot{R}^2R^3 = \frac{4E_o}{25\rho_o}\beta^5$.

Since this energy is independent of time, it follows from Eq. (261) that it must be $\mathbf{F} = f\mathbf{u}$, i.e.

$$\rho v\big(\frac{1}{2}v^2 + \mathcal{E} + \frac{P}{\rho}\big) = \Big(\rho\big(\frac{1}{2}v^2 + \mathcal{E}\big)\Big)\dot{R}\xi, \tag{263}$$

or after some simplifications

$$\frac{U}{\xi}\Big(U^2 + \gamma\frac{G}{F}\Big) = \frac{\gamma+1}{2}\Big(U^2 + \frac{G}{F}\Big), \tag{264}$$

which is identical to Eq. (256).

Final solution

Finally, we have three equations for three unknowns (Eqs. (238), (251) and (257)):

$$\Big(V - \frac{\gamma+1}{2}\Big)\frac{d\ln F}{d\ln\xi} + \frac{dV}{d\ln\xi} + 3V = 0, \tag{265}$$

$$GF^{1-\gamma}\Big(V - \frac{\gamma+1}{2}\Big) = \frac{1-\gamma}{2\xi^3}, \tag{266}$$

$$V\Big(V^2 + \gamma\frac{G}{F\xi^2}\Big) = \frac{\gamma+1}{2}\Big(V^2 + \frac{G}{F\xi^2}\Big). \tag{267}$$

From the last two equations we have

$$\frac{G}{F\xi^2} = \frac{1-\gamma}{2}\frac{1}{\xi^5 F^{2-\gamma}(V - \frac{\gamma+1}{2})} = \frac{V^2(1 - \frac{2}{\gamma+1}V)}{\frac{2\gamma V}{\gamma+1} - 1}, \tag{268}$$

i.e.

$$F^{2-\gamma} = \frac{\gamma^2-1}{4}\frac{1}{\xi^5 V^2}\frac{\frac{2\gamma V}{\gamma+1}-1}{(V-\frac{\gamma+1}{2})^2}, \tag{269}$$

and

$$(2-\gamma)\frac{d\ln F}{d\ln\xi} = -5-2\frac{d\ln V}{d\ln\xi}+\frac{\frac{2\gamma}{\gamma+1}}{\frac{2\gamma V}{\gamma+1}-1}\frac{dV}{d\ln\xi}+\frac{2}{\frac{\gamma+1}{2}-V}\frac{dV}{d\ln\xi}. \tag{270}$$

The last equation, in combination with Eq. (265), gives

$$(2-\gamma)\Big(\frac{dV}{d\ln\xi}+3V\Big)+\Big(\frac{\gamma+1}{2}-V\Big)\Big[5+\Big(\frac{2}{V}-\frac{\frac{2\gamma}{\gamma+1}}{\frac{2\gamma V}{\gamma+1}-1}-\frac{2}{\frac{\gamma+1}{2}-V}\Big)\frac{dV}{d\ln\xi}\Big]=0. \tag{271}$$

After somewhat long but straightforward algebra, one can show that Eq. (271) simplifies to

$$\frac{V^2-\frac{\gamma+1}{\gamma}V+\frac{\gamma+1}{2\gamma}}{V(V-\frac{\gamma+1}{2\gamma})(\frac{5}{2}-\frac{3\gamma-1}{\gamma+1}V)}\frac{dV}{d\ln\xi}=1. \tag{272}$$

To integrate the last expression we will first separate the left-hand side into three terms

$$\Big(\frac{C_3}{V}+\frac{C_2}{V-\frac{\gamma+1}{2\gamma}}+\frac{C_1}{\frac{5}{2}-\frac{3\gamma-1}{\gamma+1}V}\Big)\frac{dV}{d\ln\xi}=1, \tag{273}$$

where constants are found to be

$$\begin{aligned} C_3 &= -\frac{2}{5}, \\ C_2 &= \frac{\gamma-1}{2\gamma+1}, \\ C_1 &= \frac{13\gamma^2-7\gamma+12}{5(\gamma+1)(2\gamma+1)}. \end{aligned} \tag{274}$$

Integration is now trivial

$$\ln\xi = \frac{1}{5}\ln C-\frac{2}{5}\ln V+\frac{\nu_2}{5}\ln\Big(V-\frac{\gamma+1}{2\gamma}\Big)+\frac{\nu_1}{5}\ln\Big(\frac{5}{2}-\frac{3\gamma-1}{\gamma+1}V\Big), \tag{275}$$

where constant of integration (from boundary condition at $\xi=1$) is

$$C=\Big(\frac{2\gamma}{\gamma-1}\Big)^{\nu_2}\Big(\frac{2(\gamma+1)}{7-\gamma}\Big)^{\nu_1}, \tag{276}$$

and

$$\nu_2 = \frac{5(\gamma-1)}{2\gamma+1}, \tag{277}$$

$$\nu_1 = -\frac{13\gamma^2-7\gamma+12}{(3\gamma-1)(2\gamma+1)}. \tag{278}$$

The final solution, given implicitly through V, is (see Eqs. (268), (269) and (275)):

$$\xi^5 = \frac{1}{V^2}\Big[\frac{\gamma+1}{\gamma-1}\Big(\frac{2\gamma}{\gamma+1}V-1\Big)\Big]^{\nu_2}\Big[\frac{\gamma+1}{7-\gamma}\Big(5-2\frac{3\gamma-1}{\gamma+1}V\Big)\Big]^{\nu_1}, \tag{279}$$

$$F = \left[\frac{\gamma^2-1}{4}\frac{1}{\xi^5V^2}\frac{\frac{2\gamma V}{\gamma+1}-1}{(\frac{\gamma+1}{2}-V)^2}\right]^{\frac{1}{2-\gamma}}, \tag{280}$$

$$G = \frac{\gamma-1}{2}\frac{F^{\gamma-1}}{\xi^3(\frac{\gamma+1}{2}-V)}, \tag{281}$$

$$U = \xi\, V. \tag{282}$$

Since $\nu_4 < 0$ and $\nu_2 > 0$ (for $\gamma > 1$) when $\xi \to 0$, $V \to \frac{\gamma+1}{2\gamma}$, and we have approximately

$$F \approx \left[\frac{4\gamma^4}{(\gamma+1)^4}\Big[\Big(\frac{\gamma+1}{2\gamma}\Big)^2\Big(\frac{(7-\gamma)\gamma}{(\gamma+1)(2\gamma+1)}\Big)^{\nu_1}\Big]^{\frac{1}{\nu_2}}\right]^{\frac{1}{2-\gamma}}\xi^{\frac{3}{\gamma-1}}, \tag{283}$$

$$G \approx \frac{\gamma}{\gamma+1}\left[\frac{4\gamma^4}{(\gamma+1)^4}\Big[\Big(\frac{\gamma+1}{2\gamma}\Big)^2\Big(\frac{(7-\gamma)\gamma}{(\gamma+1)(2\gamma+1)}\Big)^{\nu_1}\Big]^{\frac{1}{\nu_2}}\right]^{\frac{\gamma-1}{2-\gamma}}, \tag{284}$$

$$U \approx \frac{\gamma+1}{2\gamma}\xi. \tag{285}$$

Parameters of the solution

If we take for the moving surface $\xi = 1$ (shock front), Eq. (262) will give us the total energy of explosion E_o as the sum of the kinetic and internal energy:

$$\begin{aligned} E_o &= T_o + U_o \\ &= \int_0^R \rho\Big(\frac{1}{2}v^2+\mathcal{E}\Big)\,4\pi r^2 dr \\ &= \frac{32\pi}{25(\gamma^2-1)}\beta^5 E_o\int_0^1\Big(FU^2+G\Big)\,\xi^2 d\xi, \end{aligned} \tag{286}$$

This enables us to find β:

$$\beta^{-5} = \frac{32\pi}{25(\gamma^2-1)}\int_0^1\Big(FU^2+G\Big)\,\xi^2 d\xi = \frac{32\pi}{125(\gamma^2-1)}\int_{\frac{\gamma+1}{2\gamma}}^1\Big(FV^2+\frac{G}{\xi^2}\Big)\,\frac{d\xi^5}{dV}dV. \tag{287}$$

The last integral can be integrated numerically. However, since it contains a removable singularity at $V = \frac{\gamma+1}{2\gamma}$, we can proceed by separating it into two integrals (with arbitrary $\xi_0 \ll 1$)

$$\beta^{-5} = \frac{32\pi}{25(\gamma^2-1)}\Big[\int_0^{\xi_0}\Big(FU^2+G\Big)\,\xi^2 d\xi + \frac{1}{5}\int_{V(\xi_0)}^1\Big(FV^2+\frac{G}{\xi^2}\Big)\,\frac{d\xi^5}{dV}dV\Big], \tag{288}$$

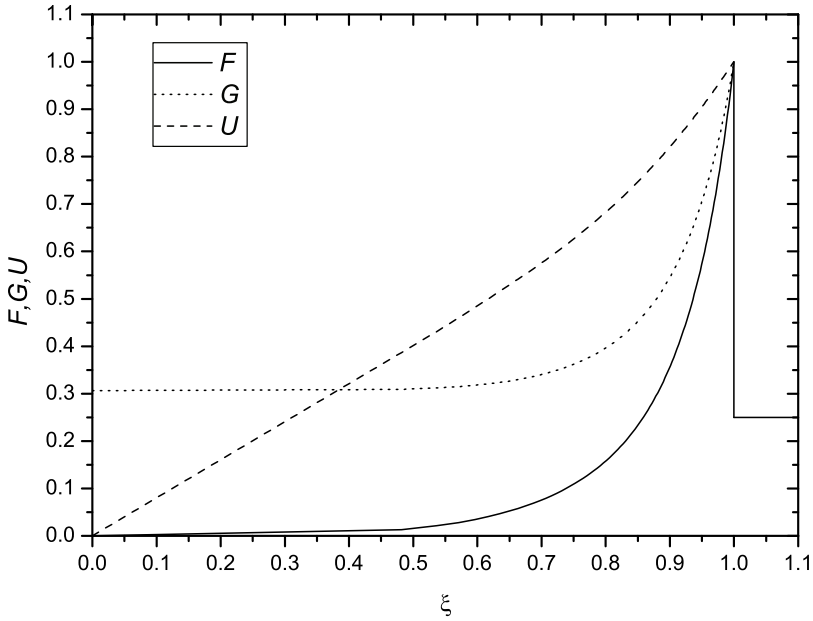

Figure 24: Complete solution for $\gamma = 5/3$.

Table 5: Some parameters of the solutions for different gammas.

γ	β	T_o/E_o	U_o/E_o	P_c/P_2
5/3	1.152	0.283	0.717	0.306
7/5	1.033	0.219	0.781	0.365
4/3	0.995	0.197	0.803	0.383

and use approximate expressions (283)–(285) for the first one. We see that density and velocity drop to zero at the center of explosion ($F(0) = U(0) = 0$), while Eq. (284) gives us the ratio of central to shock pressure $G(0) = P_c/P_2$.

Some parameters of the solutions for different gammas are given in Table 5, while the complete solution for $\gamma = 5/3$ is shown in Fig. 24.

2.6.3 Blast waves with cosmic rays

Blast waves with CRs i.e. with an additional component with power-law number density distribution function $N(p) \propto p^{-\Gamma}$, were already discussed by Chevalier (1983a,b), Toptygin (2000), Petukhov et al. (2006) and more recently by Bell (2015). As in Chevalier's papers, we will assume that CRs are accelerated at the shock front and that they adiabatically cool in the downstream region. However, we will extend the analysis by using slightly modified jump conditions and analyze solutions with different energy indices (Arbutina 2015).

Equation of state

Let us assume that CRs have a power-law number density distribution $N(p) \propto p^{-\Gamma}$, i.e. that the distribution function in momentum space is $f = kp^{-\Gamma-2}$, where k is a constant. By definition, pressure and internal energy density per unit volume are

$$P = \int_{p_0}^{p_\infty} 4\pi p^3 \frac{\partial \mathcal{E}}{\partial p} f dp, \tag{289}$$

$$u = \int_{p_0}^{p_\infty} 4\pi p^2 (\mathcal{E} - mc^2) f dp, \tag{290}$$

where energy is given by the relativistic expression $\mathcal{E}^2 = p^2c^2 + m^2c^4$, m is particle mass, c speed of light, and p_0 and p_∞ are lower and upper limits for momentum, respectively.

For pressure we then have

$$P = \int_{p_0}^{p_\infty} \frac{4\pi k}{3} p^{2-\Gamma} c^2 \frac{1}{\sqrt{p^2c^2 + m^2c^4}} dp. \tag{291}$$

By performing integration by parts, internal energy density is

$$\begin{aligned} u &= \int_{p_0}^{p_\infty} 4\pi k p^{-\Gamma} (\sqrt{p^2c^2 + m^2c^4} - mc^2) dp \\ &= \frac{3}{\Gamma - 1} P + \frac{4\pi k}{\Gamma - 1} \Big[p_0^{1-\Gamma} (\sqrt{p_0^2c^2 + m^2c^4} - mc^2) - \\ &- p_\infty^{1-\Gamma} (\sqrt{p_\infty^2 c^2 + m^2c^4} - mc^2) \Big]. \end{aligned} \tag{292}$$

If $p_0 \ll mc$ and $p_\infty \to \infty$, for $2 < \Gamma < 3$, we have

$$u \approx \frac{3}{\Gamma - 1} P. \tag{293}$$

Since $u = \frac{1}{\gamma - 1} P$,

$$\gamma = \gamma_{\rm CR} = \frac{\Gamma + 2}{3}. \tag{294}$$

We see that CRs with $\Gamma \to 2$ behave like ultra-relativistic gas ($\gamma = 4/3$), while those with $\Gamma \to 3$ behave like ordinary gas with $\gamma = 5/3$.

Jump conditions

The jump conditions are probably the most problematic part of this analysis. For the sake of simplicity, we separate the shock into three regions:

(o) far upstream,

(i) near upstream (precursor),

(ii) downstream.

Conservation of mass, momentum and energy yield Rankine-Hugoniot relations for strong shocks

$$\rho_2 v_2 = \rho_1 v_1 = \rho_0 v_0, \tag{295}$$

$$\rho_2 v_2^2 + P_{g2} + P_{\rm CR2} = \rho_1 v_1^2 + P_{\rm CR1} = \rho_0 v_0^2, \tag{296}$$

$$\frac{1}{2} v_2 + \frac{\gamma_g}{\gamma_g - 1} \frac{P_{g2}}{\rho_2} + \frac{\gamma_{\rm CR}}{\gamma_{\rm CR} - 1} \frac{P_{\rm CR2}}{\rho_2} = \frac{1}{2} v_0^2. \tag{297}$$

We have not assumed conservation of energy at the subshock (between regions (ii) and (i)) and we shall set $P_{\rm CR2} = P_{\rm CR1}$, i.e. assume that CR pressure is continuous – high-energy particles do not see the subshock, but we have neglected the CRs diffusion and escape.

Conservation of energy can also be written as

$$\frac{1}{2} v_2 + \frac{\gamma}{\gamma - 1} \frac{P_2}{\rho_2} = \frac{1}{2} v_0^2, \tag{298}$$

where we have defined effective γ, so that

$$\frac{\gamma}{\gamma - 1} = \frac{\gamma_g}{\gamma_g - 1} \beta + \frac{\gamma_{\rm CR}}{\gamma_{\rm CR} - 1} (1 - \beta), \tag{299}$$

where $\beta = P_{g2}/P_2$, $P_2 = P_{g2} + P_{\rm CR2}$. For total jump in density we then have

$$X_{\rm tot} = \frac{\rho_2}{\rho_0} = \frac{\gamma + 1}{\gamma - 1} \tag{300}$$

and

$$P_{g2} = \frac{2\beta}{\gamma + 1} \rho_0 v_s^2, \tag{301}$$

$$P_{\rm CR2} = \frac{2(1 - \beta)}{\gamma + 1} \rho_0 v_s^2, \tag{302}$$

$$v_2 = \frac{2}{\gamma + 1} v_s, \tag{303}$$

where $v_s = \dot{R} = -v_0$ is shock velocity. We also know from diffuse shock acceleration theory that (see Eq. (294))

$$X = \frac{\rho_2}{\rho_1} = \frac{\Gamma + 2}{\Gamma - 1} = \frac{\gamma_{\rm CR}}{\gamma_{\rm CR} - 1}. \tag{304}$$

and from momentum conservation we can obtain the relation:

$$X - 1 = \beta (X_{\rm tot} - 1). \tag{305}$$

By combining Eqs. (293), (294), (298) and (299) we finally have:

$$\beta = \frac{1 - \sqrt{1 - 2 \frac{\gamma_g - \gamma_{\rm CR}}{\gamma_g - 1}}}{2 \frac{\gamma_g - \gamma_{\rm CR}}{\gamma_g - 1}}, \tag{306}$$

$$\gamma = 1 + 2\beta (\gamma_{\rm CR} - 1). \tag{307}$$

The solution of Euler equations

To find the complete solution, we will again write a similarity variable in the form:

$$\xi = r/R(t), \quad R(t) = B(E_o/\rho_o)^{1/5}t^{2/5}, \tag{308}$$

where we have to solve Euler equations to find B. If we are dealing just with an ordinary gas with $\gamma_g = 5/3$, we shall obtain the Sedov solution with $R = 1.15(E_o/\rho_o)^{1/5}t^{2/5}$. If similarity is maintained, the introduction of a new, CR component would not change $R = R(t)$ dependence but only the B value.

By using Eqs. (301)–(304) we can define dimensionless density F, gas pressure G, CR pressure H and velocity U as:

$$\rho = \frac{\gamma+1}{\gamma-1}\rho_0 F(\xi) \tag{309}$$

$$P_g = \frac{2\beta}{\gamma+1}\rho_0\dot{R}^2 G(\xi) \tag{310}$$

$$P_{\rm CR} = \frac{2(1-\beta)}{\gamma+1}\rho_0\dot{R}^2 H(\xi) \tag{311}$$

$$v = \frac{2}{\gamma+1}\dot{R}U(\xi). \tag{312}$$

At the shock front ($\xi = 1$) the boundary conditions are $F(1) = G(1) = U(1) = 1$. With these last expressions and partial derivatives

$$\frac{\partial}{\partial t} = \dot{R}\Big(\frac{\partial}{\partial R} - \frac{\xi}{R}\frac{\partial}{\partial \xi}\Big), \tag{313}$$

$$\frac{\partial}{\partial r} = \frac{1}{R}\frac{\partial}{\partial \xi}, \tag{314}$$

we are ready to move to Euler equations in spherical symmetry

$$\frac{\partial \rho}{\partial t} + \frac{1}{r^2}\frac{\partial}{\partial r}\Big(r^2\rho v\Big) = 0, \tag{315}$$

$$\rho\frac{Dv}{Dt} = \rho\frac{\partial v}{\partial t} + \rho v\frac{\partial v}{\partial r} = -\frac{\partial P_g}{\partial r} - \frac{\partial P_{\rm CR}}{\partial r}, \tag{316}$$

$$\frac{D(P_g\rho^{-\gamma_g})}{Dt} = \frac{\partial}{\partial t}\Big(P_g\rho^{-\gamma_g}\Big) + v\frac{\partial}{\partial r}\Big(P_g\rho^{-\gamma_g}\Big) = 0, \tag{317}$$

$$\frac{D(P_{\rm CR}\rho^{-\gamma_{\rm CR}})}{Dt} = \frac{\partial}{\partial t}\Big(P_{\rm CR}\rho^{-\gamma_{\rm CR}}\Big) + v\frac{\partial}{\partial r}\Big(P_{\rm CR}\rho^{-\gamma_{\rm CR}}\Big) = 0, \tag{318}$$

where $\frac{D}{Dt}$ is Lagrange or substantial derivative.

Continuity equation (315) gives us

$$\Big(\frac{U}{\xi} - \frac{\gamma+1}{2}\Big)\xi\frac{F'}{F} + U' + \frac{2}{\xi}U = 0, \tag{319}$$

while the entropy equations (317) and (318), with the help of Eq. (315), can be integrated to give:

$$GF^{1-\gamma_g}\Big(\frac{U}{\xi} - \frac{\gamma+1}{2}\Big) = \frac{1-\gamma}{2\xi^3}, \tag{320}$$

$$HF^{1-\gamma_{\rm CR}}\Big(\frac{U}{\xi}-\frac{\gamma+1}{2}\Big)=\frac{1-\gamma}{2\xi^3}. \tag{321}$$

In all the expressions we have used notation $f'=\frac{df}{d\xi}$, $f=\{F,G,H,U\}$, as earlier.

Finally, a self-similar form of momentum equation (316) is

$$\xi\Big[\Big(\frac{2}{\gamma+1}\frac{U}{\xi}-1\Big)U'-\frac{3}{2}\frac{U}{\xi}\Big]+\frac{\gamma-1}{\gamma+1}\frac{1}{F}\Big[\beta G'+(1-\beta)H'\Big]=0. \tag{322}$$

If we use Eqs. (320) and (321) to find G' and H', and insert them into Eq. (322), with little transformation Eqs. (322) and (319) become

$$\begin{aligned}\frac{dU}{d\xi} &= \frac{(\gamma-1)^2}{\xi} \qquad (323)\\ &\times \Bigg\{\frac{\beta F^{\gamma_g-2}(\frac{3}{2}(\gamma+1)\xi-2\gamma_g U)+(1-\beta)F^{\gamma_{\rm CR}-2}(\frac{3}{2}(\gamma+1)\xi-2\gamma_{\rm CR}U)}{(\gamma-1)^2\Big[\beta\gamma_g F^{\gamma_g-2}+(1-\beta)\gamma_{\rm CR}F^{\gamma_{\rm CR}-2}\Big]+4\xi^2\Big[U-\frac{\gamma+1}{2}\xi\Big]^3}\\ &+ \frac{3(\gamma+1)\xi^3U\Big[U-\frac{\gamma+1}{2}\xi\Big]^2}{(\gamma-1)^4\Big[\beta\gamma_g F^{\gamma_g-2}+(1-\beta)\gamma_{\rm CR}F^{\gamma_{\rm CR}-2}\Big]+4\xi^2\Big[U-\frac{\gamma+1}{2}\xi\Big]^3}\Bigg\},\end{aligned}$$

$$\begin{aligned}\frac{dF}{d\xi} &= -\frac{F}{U-\frac{\gamma+1}{2}\xi} \qquad (324)\\ &\times \Bigg\{\frac{\frac{3}{2}(\gamma+1)(\gamma-1)^2\Big[\beta F^{\gamma_g-2}+(1-\beta)F^{\gamma_{\rm CR}-2}\Big]}{(\gamma-1)^2\Big[\beta\gamma_g F^{\gamma_g-2}+(1-\beta)\gamma_{\rm CR}F^{\gamma_{\rm CR}-2}\Big]+4\xi^2\Big[U-\frac{\gamma+1}{2}\xi\Big]^3}\\ &+ \frac{\xi U\Big[8U-(\gamma+1)\xi\Big]\Big[U-\frac{\gamma+1}{2}\xi\Big]^2}{(\gamma-1)^2\Big[\beta\gamma_g F^{\gamma_g-2}+(1-\beta)\gamma_{\rm CR}F^{\gamma_{\rm CR}-2}\Big]+4\xi^2\Big[U-\frac{\gamma+1}{2}\xi\Big]^3}\Bigg\}.\end{aligned}$$

These last two equations ought to be solved numerically. The results are shown in Fig. 25. As we approach the center $\xi\to 0$, if $\beta\neq 1$, the velocity becomes approximately $U\approx\frac{\gamma+1}{2\gamma_{\rm CR}}\xi$ and $F\propto\xi^{3/(\gamma_{\rm CR}-1)}$, $G\propto\xi^{3(\gamma_g-\gamma_{\rm CR})/(\gamma_{\rm CR}-1)}$, $H\propto$ const. If $\beta=1$, we get the Sedov solution results: $U\approx\frac{\gamma_g+1}{2\gamma_g}\xi$, $F\propto\xi^{3/(\gamma_g-1)}$ and $G\approx$ const.

Energy integral

Let us now consider a moving surface with $\xi=$ const. Energy within this surface is

$$\begin{aligned}E(\xi) &= \int_0^{r(\xi)}\Big(\frac{1}{2}\rho v^2+\frac{1}{\gamma_g-1}P_g+\frac{1}{\gamma_{\rm CR}-1}P_{\rm CR}\Big)\,4\pi r^2dr\\ &= \frac{8\pi\rho_o}{\gamma+1}\dot R^2R^3\int_0^{\xi}\Big(\frac{1}{\gamma-1}FU^2+\frac{\beta}{\gamma_g-1}G+\frac{1-\beta}{\gamma_{\rm CR}-1}H\Big)\,\xi^2d\xi \qquad (325)\\ &= \frac{32\pi E_o}{25(\gamma+1)}B^5\int_0^{\xi}\Big(\frac{1}{\gamma-1}FU^2+\frac{\beta}{\gamma_g-1}G+\frac{1-\beta}{\gamma_{\rm CR}-1}H\Big)\,\xi^2d\xi,\end{aligned}$$

where we used the fact that $\dot R^2R^3=\frac{4E_o}{25\rho_o}B^5$.

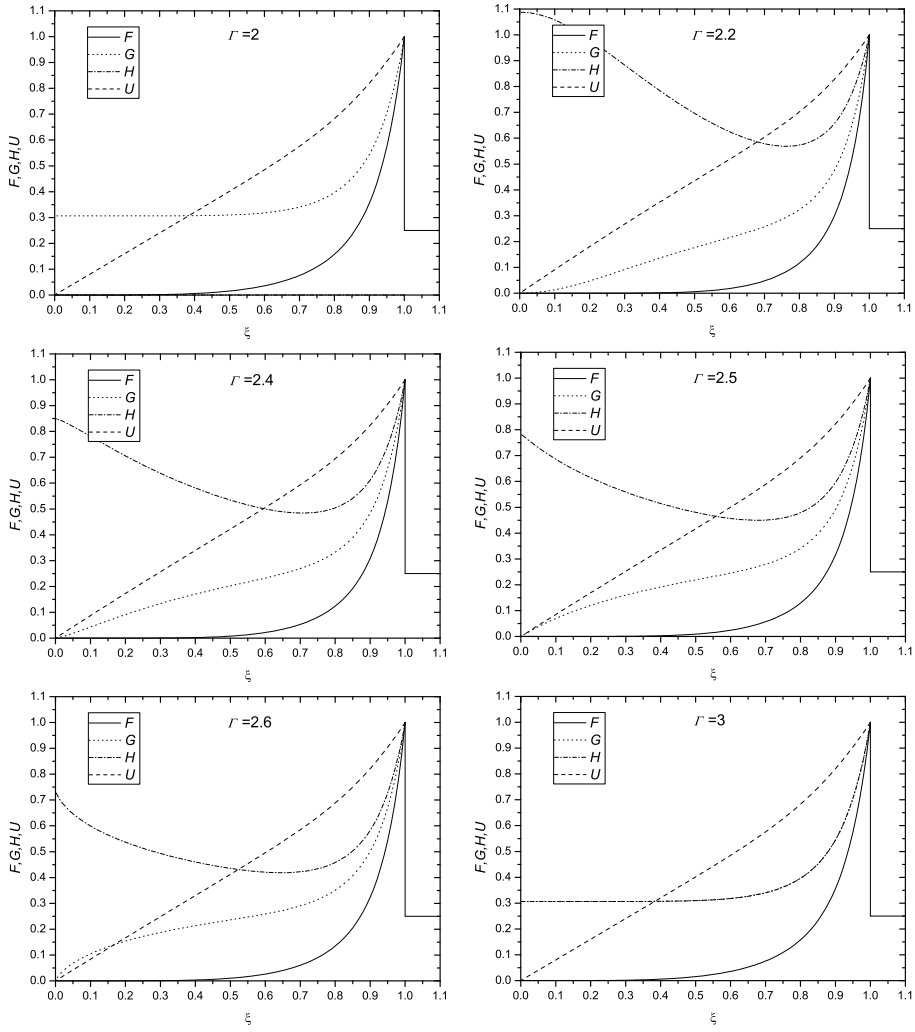

Figure 25: Complete solutions for different energy indices Γ.

Table 6: Parameters of solutions for different energy indices Γ. E_o is the explosion energy, T_o – the total kinetic energy, $U_{o,g}$ – the total thermal energy and $U_{o,CR}$ – the total CR energy. The last two columns represent center to shock gas and CR pressure ratios, P_{g0}/P_{g2} and $P_{\rm CR0}/P_{\rm CR2}$, respectively. For other parameters see the text.

Γ	γ_g	$\gamma_{\rm CR}$	β	γ	X	$X_{\rm tot}$	B	T_o/E_o	$U_{o,g}/E_o$	$U_{o,{\rm CR}}/E_o$	P_{g0}/P_{g2}	$P_{\rm CR0}/P_{\rm CR2}$
2	5/3	4/3	1	1.67	4	4	1.152	0.283	0.717	0	0.306	0
2.1	5/3	1.37	0.76	1.56	3.73	4.59	1.090	0.245	0.356	0.399	0	1.401
2.2	5/3	7/5	0.69	1.55	3.5	4.62	1.092	0.247	0.324	0.429	0	1.088
2.3	5/3	1.43	0.65	1.56	3.31	4.57	1.099	0.252	0.315	0.433	0	0.941
2.4	5/3	1.47	0.61	1.57	3.14	4.5	1.107	0.257	0.315	0.428	0	0.849
2.5	5/3	3/2	0.59	1.59	3	4.41	1.115	0.262	0.319	0.418	0	0.784
2.6	5/3	1.53	0.56	1.60	2.88	4.33	1.123	0.267	0.325	0.407	0	0.733
2.7	5/3	1.57	0.54	1.62	2.76	4.24	1.131	0.272	0.333	0.395	0	0.687
2.8	5/3	8/5	0.53	1.63	2.67	4.16	1.138	0.276	0.341	0.383	0	0.623
2.9	5/3	1.63	0.51	1.65	2.58	4.08	1.145	0.279	0.350	0.371	0	0.501
3	5/3	5/3	0.5	1.67	2.5	4	1.152	0.283	0.359	0.359	0.306	0.306

If for the moving surface we take $\xi = 1$ (shock front), Eq. (325) will give us the total energy of explosion E_o as the sum of the kinetic, internal gas energy and CR energy:

$$\begin{aligned} E_o &= T_o + U_{o,g} + U_{o,\mathrm{CR}} \\ &= \int_0^R \left(\frac{1}{2}\rho v^2 + \frac{1}{\gamma_g - 1}P_g + \frac{1}{\gamma_{\mathrm{CR}} - 1}P_{\mathrm{CR}}\right) 4\pi r^2 dr \\ &= \frac{32\pi}{25(\gamma+1)}B^5 E_o \int_0^1 \left(\frac{1}{\gamma - 1}FU^2 + \frac{\beta}{\gamma_g - 1}G + \frac{1-\beta}{\gamma_{\mathrm{CR}} - 1}H\right) \xi^2 d\xi. \end{aligned} \tag{326}$$

This enables us to find B:

$$B^{-5} = \frac{32\pi}{25(\gamma+1)} \int_0^1 \left(\frac{1}{\gamma - 1}FU^2 + \frac{\beta}{\gamma_g - 1}G + \frac{1-\beta}{\gamma_{\mathrm{CR}} - 1}H\right) \xi^2 d\xi, \tag{327}$$

as well as the fractions T_o/E_o, $U_{o,g}/E_o$ and $U_{o,\mathrm{CR}}/E_o$ (see Table 6).

2.7 Radio evolution of supernova remnants

2.7.1 Theoretical $\Sigma - D$ relation

SNRs can be detected at many wavelengths, across the entire electromagnetic spectrum, but they are primarily radio emitters. Investigations in radio domain have provided a deep insight into SNRs properties, physical processes in them and their evolutionary characteristics (see Dubner 2016).

The question of radio evolution of SNRs is closely related to the so-called surface brightness to diameter ($\Sigma - D$) relation. The surface brightness is defined as

$$\Sigma_\nu = \frac{L_\nu}{\pi^2 D^2} = \frac{4\pi d^2 S_\nu}{\pi^2 D^2} = \frac{S_\nu}{\Omega_s}, \tag{328}$$

where L_ν is radio luminosity, S_ν is the flux density, d is the distance, $D \approx \theta d$ is diameter of the source, θ is angular diameter and $\Omega_s \approx \theta^2\pi/4$ is the source's solid angle. As we can see, Σ_ν is the quantity independent of distance and can be calculated directly, since both S_ν and Ω_s are directly measurable.

The $\Sigma - D$ relation is usually assumed to be in the form

$$\Sigma_\nu = AD^{-\beta}, \tag{329}$$

where A and β are approximately constant. As we shall see, this is only fulfilled for certain phases of evolution and if all other variables involved have power-law dependence on diameter. The theoretical $\Sigma - D$ relation was discussed by Shklovsky (1960a), Lequeux (1962), Poveda & Woltjer (1968), Kesteven (1968), Reynolds & Chevalier (1981), Duric & Seaquist (1986), Berezhko & Völk (2004) and others.

Assuming that total number of CR particles $\mathcal{N} = nV$ is conserved and adiabatic conditions apply for CR gas

$$d\mathcal{U} + PdV = 0, \tag{330}$$

where $\mathcal{U} = uV$ is total energy of CRs, $P = (\gamma - 1)u$ CR pressure and V the volume, we can find the $\Sigma - D$ relation for a "spherically expanding nebula" (Shklovsky 1960a).

If we assume a power-law spectrum $N(E)dE = KE^{-\Gamma}dE$, for the total number of particles $\mathcal{N}$ and total energy $\mathcal{U}$ we have:

$$N = \frac{\mathcal{N}}{V} = \int_{E_0}^{\infty} N(E)dE = \int_{E_0}^{\infty} KE^{-\Gamma}dE = K\frac{E_0^{1-\Gamma}}{\Gamma - 1}, \tag{331}$$

$$u = \frac{\mathcal{U}}{V} = \int_{E_0}^{\infty} N(E)EdE = \int_{E_0}^{\infty} KE^{1-\Gamma}dE = K\frac{E_0^{2-\Gamma}}{\Gamma - 2}. \tag{332}$$

Then

$$d\ln\mathcal{N} - d\ln V = d\ln K + (1-\Gamma)d\ln E_0 \tag{333}$$

and

$$d\ln\mathcal{U} - d\ln V = d\ln K + (2-\Gamma)d\ln E_0. \tag{334}$$

Since $d\ln\mathcal{N} = 0$, combining Eqs. (333) and (334) gives us $d\ln\mathcal{U} = d\ln E_0$, i.e.

$$\frac{d\mathcal{U}}{\mathcal{U}} = \frac{dE_0}{E_0}. \tag{335}$$

On the other hand, from Eq. (330) we find

$$d\mathcal{U} + PdV = d\mathcal{U} + (\gamma - 1)udV = d\mathcal{U} + (\gamma - 1)\mathcal{U}d\ln V = 0, \tag{336}$$

$$d\ln\mathcal{U} + (\gamma - 1)d\ln V = 0, \tag{337}$$

which, in combination with Eq. (333) gives

$$d\ln K = -\big(1 + (\Gamma - 1)(\gamma - 1)\big)d\ln V, \tag{338}$$

i.e.

$$K \propto D^{-3(1+(\Gamma-1)(\gamma-1))}. \tag{339}$$

Assuming that the magnetic flux is frozen in plasma (Alfvén's theorem) $\Phi = BS = 4\pi R^2 B = \pi D^2 B =$ const, we have

$$B \propto D^{-2}. \tag{340}$$

If Eq. (339) applies for CR electrons, from Eq. (294) $\gamma = \frac{\Gamma+2}{3}$, and with synchrotron emissivity from Eq. (205), the surface brightness is finally

$$\Sigma_\nu \propto D^{-\beta} \propto \varepsilon_\nu D \propto KB^{1+\alpha}D \propto D^{-[\Gamma+3+(\Gamma-1)^2]}. \tag{341}$$

For $\alpha = 0.5$ ($\Gamma = 2\alpha+1 = 2$), the slope $\beta = 6$ in the first $\Sigma - D$ relation obtained by Skhlovsky (1960a). Of course, SNRs are not simple spherical nebulae whose expansion is driven by CR pressure, so this relation is of historical interest only.

Assuming CRs "energy conservation"

$$d\mathcal{U} = 0, \tag{342}$$

instead of adiabatic conditions (330), since $d\ln\mathcal{N} = 0$ and $d\ln\mathcal{U} = 0$, Eqs. (333) and (334) give $d\ln K = -d\ln V$, i.e.

$$K \propto D^{-3}. \tag{343}$$

Assuming, further, constant partition between magnetic field and CRs energy densities

$$u_B = \frac{1}{8\pi} B^2 \propto u, \tag{344}$$

we obtain $B^2 \propto u = \mathcal{U}/V \propto K \propto D^{-3}$, i.e.

$$B \propto D^{-1.5}. \tag{345}$$

Finally, from Eq. (341)

$$\Sigma \propto D^{-(7+3\alpha)/2}, \tag{346}$$

and if $\alpha = 0.5$, $\beta = 17/4$ which is the slope of the theoretical relations obtained by Reynolds & Chevalier (1981).

By using the same assumptions, we can also derive $S_\nu - t$ relation, assuming for ambient density $\rho \propto R^{-s}$ and that shock propagation as $R \propto t^m$. Flux density for synchrotron radiation is

$$S_\nu \propto \varepsilon_\nu V \propto K B^{1+\alpha} \nu^{-\alpha} V. \tag{347}$$

Assuming again constant partition between magnetic field, CR energy and thermal energy i.e. shock ram pressure, we have:

$$K \propto u \propto u_B = \frac{1}{8\pi} B^2 \propto \rho v_s^2. \tag{348}$$

where v_s is the shock velocity. With $\Gamma = 2\alpha + 1$

$$S_\nu \propto K^{(5+\Gamma)/4} V \propto t^{-\{2(5+\Gamma) - m[(2-s)(5+\Gamma)+12]\}/4}, \tag{349}$$

i.e. for the case $s = 2$ and $m = (n-3)/(n-s) \to 1$ (e.g. radio SNe, Chevalier 1984):

$$S_\nu \propto t^{-(5+\Gamma-6m)/2} \propto t^{-\alpha}. \tag{350}$$

If $s = 0$ and $m = 2/5$ (as in Sedov's solution) we have

$$S_\nu \propto t^{-3(\alpha+1)/5}. \tag{351}$$

Duric & Sequest (1986) based their theory on Bell's (1978a,b) formulation of DSA, evolution of amplified turbulent magnetic field proposed by Gull (1973) and Fedorenko (1983), and the hydrodynamic solution of Sedov (1959).

According to Eq. (69):

$$K \propto n_{\rm H} (\Gamma - 1)(E_{\rm inj}^2 + 2 m_e c^2 E_{\rm inj})^{(\Gamma-1)/2}, \tag{352}$$

where $n_{\rm H}$ is hydrogen number density, $E_{\rm inj} \approx 2 m_p v_s^2$ injection energy, v_s shock velocity, and $m_{\rm e}$ and $m_{\rm p}$ electron and proton mass, respectively. With $B \propto D^{-\delta}$, $\delta = 1.5 - 2$, Duric & Seaquist (1986) find:

$$\beta = \begin{cases} 6\alpha + \delta\alpha + \delta - 1, & v \gg v_o, \\ 3\alpha + \delta\alpha + \delta - 1, & v \ll v_o, \end{cases} \tag{353}$$

where $v_o = \sqrt{m_{\rm e}/m_{\rm p}}\, c \approx 7000$ km/s. To be more specific, in the Sedov phase, when we expect $v_s \ll v_o$,

$$\Sigma_\nu \propto E_o^\alpha \rho_o^{1-\alpha} D^{-(3\alpha+\delta\alpha+\delta-1)}, \tag{354}$$

Table 7: Hydrodynamic and radio evolution of SNRs going through different phases, according to Berezhko & Völk (2004). The parameter β in the last column is given for $\alpha = 0.5$.

Phase	$v_s \propto$	$\Sigma_\nu \propto$	β
Early free expansion	$(E_o/\mathcal{M}_o)^{1/2}$	$(E_o/\mathcal{M}_o)^{(3+\alpha)/4}\rho_o^{(3+\alpha)/2}D$	-1
Late free expansion	$(E_o^2/(\mathcal{M}_o\rho_o))^{1/4}D^{-3/4}$	$(E_o^2/\mathcal{M}_o)^{(3+\alpha)/8}\rho_o^{3(3+\alpha)/8}D^{-(1+3\alpha)/8}$	5/16
Early Sedov's	$(E_o/\rho_o)^{1/2}D^{-3/2}$	$E_o^{(3+\alpha)/2}D^{-(7+3\alpha)/2}$	17/4
Late Sedov's	$(E_o/\rho_o)^{1/2}D^{-3/2}$	$E_o\rho_o^{(1+\alpha)/2}D^{-2}$	2

i.e. for $\alpha = 0.5$ and $\delta = 2$

$$\Sigma_\nu \propto D^{-7/2}. \tag{355}$$

More recent theory of the radio-synchrotron evolution of SNRs was given by Berezhko & Völk (2004). In the Sedov phase, their result is similar to the result of Reynolds & Chevalier (1981), which assumes constant partition of energies $K \propto B^2 \propto E_o D^{-3}$, i. e.

$$\Sigma_\nu \propto D^{-17/4}, \tag{356}$$

for $\alpha = 0.5$. However, Berezhko & Völk (2004) considered SNRs (primarily type Ia) going through different phases of evolution, by adopting semi-analytical hydrodynamical solutions (Chevalier 1982, Sedov 1959), and solved diffusion-advection equation for CRs numerically. Protons and electrons were assumed to be injected in the acceleration process with the same momentum and $N_p/N_e \approx 100$. Approximate analytical results are given in Table 7.

During the free expansion $K \propto \rho_o v_s$, while in the Sedov phase $K \propto \rho_o v_s^2$. The magnetic field evolves as $B \propto K^{1/2}$, except in the late Sedov phase, when it drops to the ISM field value $B_{\rm ISM} \propto \rho_o^{1/2}$. The surface brightness is, standardly, $\Sigma_\nu \propto \varepsilon_\nu D \propto D^{-\beta}$.

The main problem in describing the radio evolution of SNRs is the uncertain physics and a large number of free parameters in the models. In a situation like this it is difficult to establish a firm theoretical basis for the $\Sigma - D$ relation i.e. difficult to decide on a specific model. In the next part we will briefly discuss the history of the empirical $\Sigma - D$ relation.

2.7.2 Empirical $\Sigma - D$ relation

Distance determination is one of the most prominent problems in astronomy. That is why SNe type Ia and other "standard candles" (or "standard rulers") are so important to astronomers. Since Σ_ν for an object can be found independently of its distance, by establishing a reliable empirical $\Sigma_\nu - D$ relation for calibrators whose distances are known by means of other methods, one can obtain the object's diameter and through $d = D/\theta$ find the distance.

Empirical $\Sigma - D$ relations were discussed by Shklovsky (1960b), Poveda & Woltjer (1968), Milne (1970), Berkhuijsen (1973), Mathewson & Clarke (1973), Green (1984), Case & Bhattacharya (1998), Urošević (2002), Arbutina et al. (2004), Arbutina & Urošević (2005), Urošević et al. (2005), Pavlović et al. (2013, 2014) and many others. For a critical overview of the $\Sigma - D$ relation and discussion of the selection effects, see for example Green (1984, 1991, 2014). It

is clear that any survey for SNRs is limited by sensitivity and angular resolution. In addition, the sample of Galactic SNRs suffers from poorly determined distances to known objects. In recent years, more attention is paid to extragalactic samples, since all SNRs in galaxies far away from the Milky Way can be regarded as being practically at the same distance.

Fig. 26 represents a $\Sigma - D$ plot for radio SNRs in the Milky Way (MW, Green 2014, Ferrand & Safi-Harb 2012, Pavlović et al. 2014), Large Magellanic Cloud (LMC, Bozzetto et al. 2017), Small Magellanic Cloud (SMC, Filipović et al. 2005), M31, M33 (Urošević et al. 2005), NGC4449, NGC1569, NGC4214, NGC2366 (Chomiuk & Wilcots 2009) and Arp 220 (Batejat et al. 2011). The data for Galactic SNRs are also available in Green's (2014) catalogue at `http://www.mrao.cam.ac.uk/surveys/snrs/` and in a catalogue by Ferrand & Safi-Harb (2012) at `http://www.physics.umanitoba.ca/snr/SNRcat/`, while an extragalactic SNRs catalogue by Urošević et al. (2005) is available at `http://astro.matf.bg.ac.rs/dejanurosevic/catalogue/`.

Solid, dashed and dash-dotted curves in Fig. 26 represent "equipartition" evolution models $\epsilon_{\rm CR} \approx \frac{4}{\Gamma+1}\epsilon_B \sim \eta\rho v^2$, $\epsilon_B = \frac{1}{8\pi}B^2$, obtained by applying Eq. (209), and assuming CR proton to electron number 100:1. The volume filling factor is $f = 0.25$, while $\eta = 0.33$. The first model is applicable to SNe type Ia, with energy $E_o = 1$ foe $= 10^{51}$ erg, ejecta mass $\mathcal{M}_o = 1.4\ \mathcal{M}_\odot$ and ambient density $n_{\rm H} = 1$ cm^{-3}. The other two models are more applicable to core-collapse SNe with $\mathcal{M}_o \sim 10\ \mathcal{M}_\odot$, $E_o \sim 1$ and 10 foe (in the case of hypernovae) and densities $n_{\rm H} \sim 10$ and 100 cm^{-3}, where the shock first interacts with CSM in the form of steady circumstellar wind with a mass loss rate $\dot{\mathcal{M}} = 10^{-5}\ \mathcal{M}_\odot {\rm yr}^{-1}$ and wind velocity $v_{\rm W} = 10$ km s^{-1}. These toy-models are similar to those of Reynolds & Chevalier (1981) and Berezhko & Völk (2004), in a sense that the slopes during the Sedov's phase are approximately $\beta = \frac{7+3\alpha}{2} = 4.265 - 4.280$.

If luminosity $L_\nu = f(D) = {\rm const}$, during the evolution, the slope of the $\Sigma - D$ relation would be $\beta = 2$. This is the so called "trivial relation". The problem with this relation is that even if $\nexists f : D \rightarrow L_\nu$, i.e. there is no physical relation at all, we can still obtain $\beta = 2$ empirically simply because the inverse square dependence on D is implied by the definition of surface brightness. This seems to be the case with the Milky Way and most extragalactic relations, except perhaps with the M82 galaxy relation, if standard vertical-offset fitting were used (Arbutina et al. 2004). For the discussion on orthogonal fitting procedure see e.g. Urošević et al. (2010) and Pavlović et al. (2013). It is still quite unlikely that any of the relations obtained thus far represents an evolutionary track. The role of the $\Sigma - D$ relation would hence, at best, be similar to the role of the main sequence on the H-R diagram.

Additionally, early studies of the $\Sigma - D$ relation did not make any distinction between different classes of remnants, mainly due to the lack of observational data, leading to the assumption that all properties, or parameters, of the radio (surface brightness) evolution (such as SN energy, mass of the ejecta or density of ISM) are, practically, the same for all remnants. However, later studies have shown that these properties may substantially differ from remnant to remnant. Consequently, it has been generally accepted over the years that no single $\Sigma - D$ relation can be constructed for all SNRs. The question is whether it is still possible to construct the relations for some classes of SNRs.

In Tables A1, A2 and A3 we compiled data for SNRs in the dense environments of Galactic molecular clouds (GMC), oxygen-rich SNRs, sometimes

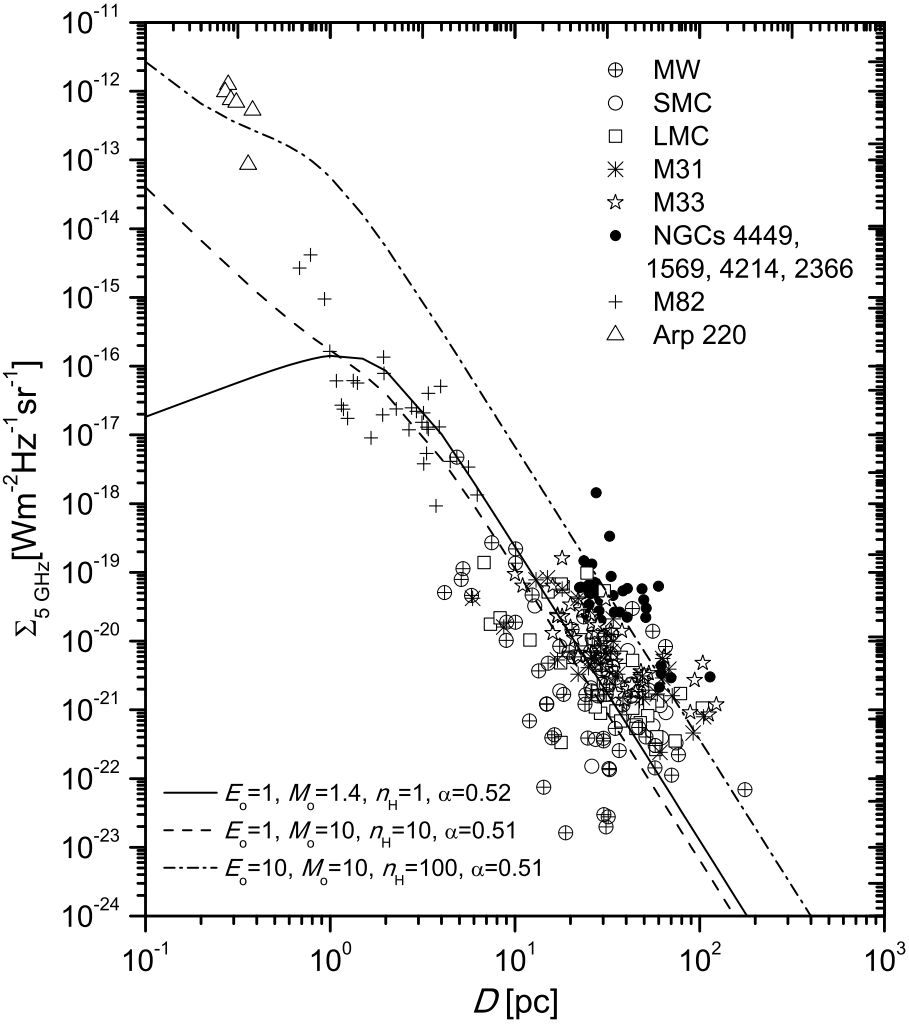

Figure 26: The $\Sigma - D$ plot for radio SNRs in selected galaxies. Solid, dashed and dash-dotted curves represent "equipartition" evolution models $\epsilon_{\rm CR} \approx \frac{4}{\Gamma+1}\epsilon_B \sim \eta\rho v^2$, $\epsilon_B = \frac{1}{8\pi}B^2$, obtained by applying Eq. (209), and assuming CRs proton to electron number 100:1. The volume filling factor is $f = 0.25$, while $\eta = 0.33$ is assumed.

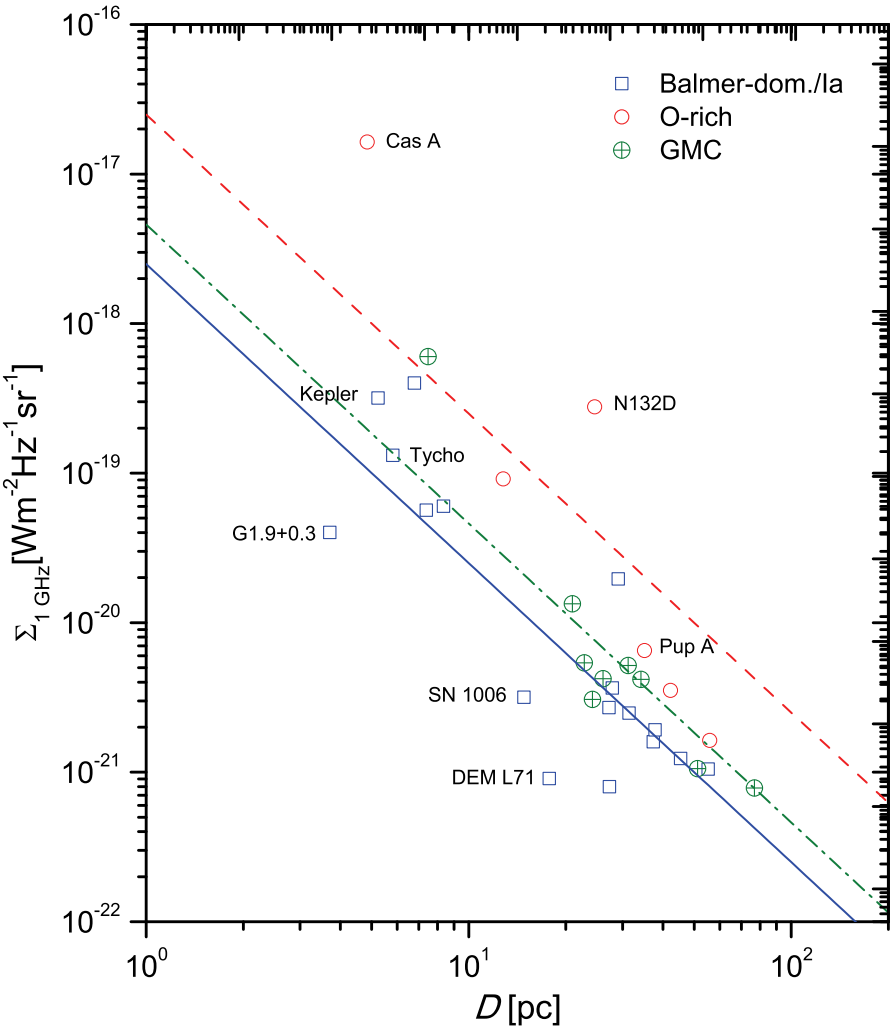

Figure 27: The $\Sigma - D$ plot for SNRs in the Galactic molecular clouds (GMC), oxygen-rich and Balmer-dominated/type Ia SNRs.

linked with SNe Ib/c, and Balmer-dominated/type Ia SNRs. Fig. 27 shows the $\Sigma - D$ plot for these three classes of remnants. We have not included in the figure GMC SNRs G292.0+1.8 and B0540-69.3 that contain pulsars, since pulsar wind nebulae (PWN) introduce additional complications to radio evolution. As with oxygen-rich remnants, some do have PWN and were excluded (G292.0+1.8 and B0540-69.3), but most of them (six of eight) seem to be shell-type SNRs (or with radio-quit neutron stars – Cas A, Pup A). We know from stellar evolution theory that massive stars mainly occur and remain in dense environments (such as molecular clouds) owing to their shorter lifetimes, while the longer lived lower mass stars tend, on average, to be found in less dense environments. SN Ia progenitors thus have enough time to abandon their birthplaces and explode in more dispersed environments, and if the radio luminosity of their remnants is directly proportional to ISM density, they are expected to be, on average, less luminous than the core-collapse SNe.

In Fig. 27 we have shown "trivial" relations with $\beta = 2$, which shows nothing more than that the average luminosities (in erg s^{-1}) for Balmer-dominated/ Ia, GMC and oxygen-rich SNRs are $\langle \log L_{1\mathrm{GHz}} \rangle_{\mathrm{B/Ia}} = 23.38$, $\langle \log L_{1\mathrm{GHz}} \rangle_{\mathrm{GMC}} = 23.63$ and $\langle \log L_{1\mathrm{GHz}} \rangle_{\mathrm{O}} = 24.37$, respectively. For example, it is known that the flux density and thereby luminosity of G1.9+0.3 is actually rising and can be reasonably well modeled by an adapted non-linear DSA theory (Pavlović 2017). It is obvious from Fig. 27 that Balmer-dominated/Ia SNRs lie below other remnants in the $\Sigma - D$ plane, i.e. are indeed less luminous, although the dispersion is quite large. It remains uncertain whether lower ISM density is responsible for their low radio luminosity. This is what is expected based on the theory of Duric & Sequest (1986), for example, but not based on the work of Berezhko & Völk (2004) and similar theories, where the differences in radio luminosities, at least in the early Sedov phase, are mainly due to the dispersion of explosion energy. These questions remain to be answered in the days to come.

Appendix

Tables A1, A2 and A3 present compiled data for SNRs in the dense environments of Galactic molecular clouds (Huang & Thaddeus 1985, Arbutina et al. 2004), oxygen-rich SNRs (Arbutina & Urošević 2005, Vink 2012), and Balmer-dominated/type Ia SNRs (Tuohy et al. 1982, Arbutina & Urošević 2005, Vink 2012). References for adopted distances are given in the footnote of each table.

Table A1: Basic properties of the 11 Galactic SNRs associated with molecular clouds (Huang & Thaddeus 1985, Arbutina et al. 2004). Angular diameters and flux densities are taken from Green's (2014) catalogue. References for adopted distances are given in the footnote. W44 and IC443 are composite type and are only given for completeness.

Catalogue name	Other name	Galaxy	Angular diameter θ (arcmin)	Flux density $S_{1\mathrm{GHz}}$ (Jy)	Surface brightness $\Sigma_{1\mathrm{GHz}}$ $\left(\frac{\mathrm{W}}{\mathrm{m^2 Hz\ sr}}\right)$	Spectral index α	Linear diameter D (pc)	Distance d (kpc)
G34.7-0.4	W44	MW	35×27	250	4.0×10^{-20}	0.37	27.7	3.1[a]
G42.8+0.6		MW	24	3	7.8×10^{-22}	0.5?	76.8	11[b]
G78.2+2.1	DR4, γ Cygni	MW	60	320	1.3×10^{-20}	0.51	20.9	1.2[a]
G84.2-0.8		MW	20×16	11	5.2×10^{-21}	0.5	31.2	6[c]
G89.0+4.7	HB 21	MW	120×90	220	3.1×10^{-21}	0.38	24.2	0.8[a]
G109.1-1.0	CTB 109	MW	28	22	4.2×10^{-21}	0.5	26.1	3.2[d]
G132.7+1.3	HB 3	MW	80	45	1.1×10^{-21}	0.6	51.2	2.2[a]
G189.1+3.0	IC 443, 3C157	MW	45	160	1.2×10^{-20}	0.36	19.6	1.5[a]
G309.8+0.0		MW	25×19	17	5.4×10^{-21}	0.5	22.8	3.6[a]
G315.4-2.3	RCW 86, MSH 14-63	MW	42	49	4.2×10^{-21}	0.6	34.2	2.8[e]
G349.7+0.2		MW	2.5×2	20	6.0×10^{-19}	0.5	7.5	11.5[f]

*References: [a]Huang & Thaddeus (1985); [b]Stanimirović et al. (2003); [c]Leahy & Green (2012); [d]Kothes & Foster (2012); [e]Case & Bhattacharya (1998); [f]Tian & Leahy (2014).

Table A2: Basic properties of eight oxygen-rich remnants (Arbutina & Urošević 2005, Vink 2012). Angular diameters and flux densities and spectral indices for Galactic SNRs are taken from Green's (2014) catalogue, for LMC SNRs from Bozzetto et al. (2017), and for SMC SNRs from Filipović et al. (2005). References for adopted distances are given in the footnote. G292.0+1.8 and B0540-69.3 contain pulsar wind nebulae and are only given for completeness.

Catalogue name	Other name	Galaxy	Angular index θ (arcsec)	Flux density $S_{1\mathrm{GHz}}$ (Jy)	Surface brightness $\Sigma_{1\mathrm{GHz}}$ (W m^{-2}Hz^{-1}sr^{-1})	Spectral α	Linear diameter D (pc)	Distance d (kpc)
G111.7–2.1	Cas A, 3C461	MW	300	2720	1.6×10^{-17}	0.77	4.8	3.33^a
G260.4–3.4	Pup A, MSH 08-44	MW	3600×3000	130	6.5×10^{-21}	0.50	35.1	2.2^b
G292.0+1.8		MW	720×480	15	2.4×10^{-20}	0.40	17.7	6.2^c
B0525–69.6	N132D, LHG 35	LMC	114×90	5.264	2.8×10^{-19}	0.65	24.6	50^d
B0540–69.3	N158A, LHG 79	LMC	67×58	1.027	1.4×10^{-19}	0.63	15.1	50^d
B0049–73.6	IKT 6	SMC	145	0.137	3.5×10^{-21}	0.56	42.2	60^d
B0102–72.3	1E 0102.2-7219, IKT 22	SMC	43×45	0.327	2.2×10^{-20}	0.60	12.8	60^d
B0103–72.6	IKT 23	SMC	192	0.111	1.6×10^{-21}	0.67	55.9	60^d

*References: [a]Alarie et al. (2014); [b]Reynoso et al. (1995); [c]Gaensler & Wallace (2003); [d]Westerlund (1990).

Table A3: Basic properties of 17 Balmer-dominated/type Ia remnants (Tuohy et al. 1982, Arbutina & Urošević 2005, Vink 2012). Angular diameters and flux densities and spectral indices for Galactic SNRs are taken from Green's (2014) catalogue, for LMC SNRs from Bozzetto et al. (2017), and for SMC SNRs from Filipović et al. (2005). References for adopted distances are given in the footnote.

Catalogue name	Other name	Galaxy	Angular diameter θ (arcsec)	Flux density $S_{1\mathrm{GHz}}$ (Jy)	Surface brightness $\Sigma_{1\mathrm{GHz}}$ (W m^{-2}Hz^{-1}sr^{-1})	Spectral index α	Linear diameter D (pc)	Distance d (kpc)
G1.9+0.3		MW	90	0.6	4.0×10^{-20}	0.60	3.7	8.5[a]
G4.5+6.8	Kepler	MW	180	19	3.2×10^{-19}	0.64	5.2	6[b]
G120.1+1.4	Tycho	MW	480	56	1.3×10^{-19}	0.65	5.8	2.5[c]
G327.6+14.6	SN1006	MW	1800	19	3.2×10^{-21}	0.60	14.8	1.7[d]
B0454–67.2	N9	LMC	140 × 120	0.077	2.5×10^{-21}	0.51	31.4	50[e]
B0505–67.9	DEM L71, LHG 10	LMC	88 × 61	0.009	9.1×10^{-22}	0.60	17.8	50[e]
B0508–68.7	N103B, LHG 13	LMC	27 × 29	0.578	4.0×10^{-19}	0.65	6.8	50[e]
B0509–67.5	LHG 14	LMC	32 × 29	0.097	5.7×10^{-20}	0.73	7.4	50[e]
B0519–69.0	LHG 26	LMC	36 × 33	0.132	6.0×10^{-20}	0.64	8.4	50[e]
B0534–69.9	LHG 53	LMC	120 × 110	0.089	3.7×10^{-21}	0.51	27.9	50[e]
B0534–70.5	DEM L238	LMC	222 × 158	0.080	1.2×10^{-21}	0.44	45.4	50[e]
B0536–70.6	DEM L249	LMC	187 × 127	0.070	1.6×10^{-21}	0.52	37.4	50[e]
B0547–69.7	DEM L316A	LMC	122 × 118	0.522	2.0×10^{-20}	0.54	29.1	50[e]
B0547–70.4	LHG 89	LMC	120 × 105	0.063	2.7×10^{-21}	0.56	27.2	50[e]
B0047–73.5	IKT 5	SMC	190	0.070	1.1×10^{-21}	0.49	55.2	60[e]
B0103–72.4	DEM S128	SMC	130	0.060	1.9×10^{-21}	0.56	37.8	60[e]
B0104–72.3	IKT 25	SMC	110 × 80	0.013	8.0×10^{-22}	0.50	27.3	60[e]

*References: [a]Reynolds et al. (2008); [b]Chiotellis et al. (2012); [c]Zhang et al. (2013); [d]Nikolić et al. (2013); [e]Westerlund (1990).

References

Abramowitz, M., Stegun, I. A., 1972, *Handbook of Mathematical Functions*, New York: Dover Publications

Alarie, A., Bilodeau, A., Drissen, L., 2014, *Mon. Not. R. Astron. Soc.*, **441**, 2996

Allen, M. G., Groves, B. A., Dopita, M. A., Sutherland, R. S., Kewley, L. J., 2008, *Astrophys. J. Suppl. Ser.*, **178**, 20

Amato, E., 2011, *Mem. S.A.It.*, **82**, 806

Amato, E., Blasi, P., 2005, *Mon. Not. R. Astron. Soc.*, **364**, 76

Arbutina, B., 2005, *M.Sc. Thesis*, University of Belgrade

Arbutina, B., 2007, *International Journal of Modern Physics D*, **16**, 1219

Arbutina, B., 2015, *Astrophysical Bulletin*, **70**, 214

Arbutina, B., Urošević, D., Stanković, M., Tešić, Lj., 2004, *Mon. Not. R. Astron. Soc.*, **350**, 346

Arbutina, B., Urošević, D., 2005, *Mon. Not. R. Astron. Soc.*, **360**, 76

Arbutina, B., Urošević, D., Andjelić, M., Pavlović, M., 2011, *Mem. S.A.It.*, **82**, 822

Arbutina, B., Urošević, D., Andjelić, M., Pavlović, M., Vukotić, B., 2012, *Astrophys. J.*, **746**, 79

Arbutina, B., Urošević, D., Vučetić, M., Pavlović, M., Vukotić, B., 2013, *Astrophys. J.*, **777**, 31

Arnett, D., 1996, *Supernovae and Nucleosynthesis*, Princeton: Princeton University Press

Axford, W. I., Leer, E., Skadron, G., 1934, *Proceedings of the 15th International Cosmic Rays Conference*, **11**, 132

Baade, W., Zwicky, F., 1934, *Proceedings of the National Academy of Sciences*, **20**, 254

Bandiera, R., Petruk, O., 2004, *Astron. Astrophys.*, **419**, 419

Barbon, R., Boundi, V., Cappellaro, E., Turatto, M., 1999, *Astron. Astrophys.*, **139**, 531

Batejat, F. et al. 2011, *Astrophys. J.*, **740**, 95

Beck, R., Brandenburg, A., Moss, D., Shukurov, A., Sokoloff, D., 1996, *Annu. Rev. Astron. Astrophys.*, **34**, 155

Beck, R., Krause, M., 2005, *Astron. Nachr.*, **326**, 414

Beck, R., 2016, *Astron. Astrophys. Rev.*, **24**, 4

Bell, A. R., 1978a, *Mon. Not. R. Astron. Soc.*, **182**, 147

Bell, A. R., 1978b, *Mon. Not. R. Astron. Soc.*, **182**, 443

Bell, A. R., 2004, *Mon. Not. R. Astron. Soc.*, **353**, 550

Bell, A. R. 2015, *Mon. Not. R. Astron. Soc.*, **447**, 2224

Bell, A. R., Schure, K. M., Reville, B., Giacinti, G., 2013, *Mon. Not. R. Astron. Soc.*, **431**, 415

Berezhko, E. G., Ellison, H. J., 1999, *Astrophys. J.*, **526**, 385

Berezhko, E. G., Völk, H. J., 2004, *Astron. Astrophys.*, **427**, 525

Berkhuijsen, E. M., 1973, *Astron. Astrophys.*, **24**, 143

Blair, W. P., Long, K. S., 2004, *Astrophys. J. Suppl. Ser.*, **155**, 101

Blandford, R. D., Ostriker, J. P., 1978, *Astrophys. J.*, **221**, L29

Blandford, R. D., Eichler, D., 1987, *Phys. Rep.*, **154**, 1

Blasi, P., 2002, *Astropart. Phys.*, **16**, 429

Blasi P., 2010, *Mon. Not. R. Astron. Soc.*, **402**, 2807

Bozzetto, L. M. et al., 2017, *Astrophys. J. Suppl. Ser.*, **230**, 2

Caroll, B. W., Ostlie, D. A., 2006, *An Introduction to Modern Astrophysics - Second Edition*, San Francisco: Pearson

Case, G. L., Bhattacharya, D., 1998, *Astrophys. J.*, **504**, 761

Chevalier, R. A., 1982, *Astrophys. J.*, **258**, 790

Chevalier, R. A., 1983a, *Proceedings of the 18th International Cosmic Rays Conference*, **2**, 314

Chevalier, R. A., 1983b, *Astrophys. J.*, **272**, 765

Chevalier, R. A., 1984, *Astrophys. J.*, **285**, L63

Chiotellis, A., Schure, K. M., Vink, J., 2012, *Astron. Astrophys.*, **537**, 139

Chomiuk, L., Wilcots, E. M., 2009, *Astron. J.*, **137**, 3869

Drury, L'O. C., 1983, *Rep. Prog. Phys.*, **46**, 973

Drury, L'O. C., Strong, A. W., 2015, *The 34th International Cosmic Ray Conference* (arXiv:1508.02675v1)

Dubner, G., 2016, *Radio Emission from Supernova Remnants*, in "Handbook of Supernovae", Eds. Athem W. Alsabti and Paul Murdin, Springer International Publishing

Duric, N., 1990, *IAU Symp.*, **140**, 235

Duric, N., Seaquist, E. R., 1986, *Astrophys. J.*, **301**, 308

Fedorenko, V. N., 1983, *IAU Symp.*, **101**, 183

Ferrand, G., Safi-Harb, S., 2012, *Adv. Space Res.*, **49**, 1313

Filippenko, A. V., 1997, *Annu. Rev. Astron. Astrophys.*, **35**, 309

Fermi, E., 1949, *Phys. Rev.*, **75**, 1169

Filipović, M. D. et al., 2005, *Mon. Not. R. Astron. Soc.*, **364**, 217

Fowler, W. A., Hoyle, F., 1964, *Astrophys. J. Suppl. Series*, **9**, 201

Gaensler, B. M., Wallace, B. J., 2003, *Astrophys. J.*, **594**, 326

Gaisser, T. K., 2012, *Astropart. Phys.*, **35**, 801

Gal-Yam, A., 2012, *Scientific American*, **306**, 44

Gal-Yam, A., Mazzali, P., Manulis, I., Bishop, D., 2013, *Publ. Astron. Soc. Pacific*, **125**, 749

Green, D. A., 1984, *Mon. Not. R. Astron. Soc.*, **209**, 449

Green, D. A., 1991, *Publ. Astron. Soc. Pacific*, **103**, 209

Green, D. A., 2014, *Bulletin of the Astronomical Society of India*, **42**, 47

Green, D. A., Stephenson, F. R., 2002, *Historical supernovae and their remnants*, Oxford: Oxford University Press

Grupen, C., 2005, *Astroparticle Physics*, Heidelberg: Springer-Verlag

Gonzalez Gaitan, S., 2001, *Ph.D. Thesis*, University of Toronto

Gull S. F., 1973, *Mon. Not. R. Astron. Soc.*, **161**, 47

Hamuy, M., 2003, *Astrophys. J.*, **582**, 905

Hoyle, F., Fowler, W. A., 1960, *Astrophys. J.*, **132**, 565

Huang, Y.-L., Thaddeus, P., 1985, *Astrophys. J.*, **295**, L13

Iben, I., Tutukov, A. V., 1984, *Astrophys. J. Suppl. Series*, **54**, 335

Jeffery, D. J., 1999, astro-ph/9907015

Kerzendorf, W. E., Childress, M., Scharwächter, J., Do, T., Schmidt, B. P., 2014, *Astrophys. J.*, **782**, 27

Kesteven, M. J. L., 1968, *Australian Journal of Physics*, **21**, 739

Kirshner, R. P., Kwan, J., 1974, *Astrophys. J.*, **193**, 27

Kothes, R., Foster, T., 2012, *Astrophys. J.*, **746**, L4.

Krause, O., Tanaka, M., Usuda, T., Hattori, T., Goto, M., Birkmann, S., Nomoto, K., 2008, *Nature*, **456**, 617

Krymsky, G. F., 1977, *Dok. Acad. Nauk. USSR*, **234**, 1306

Landau, L. D., Lifshitz, E. M., 1987, *Course of Theoretical Physics Vol. 6, Fluid Mechanics, Second Edition*, Oxford: Butterworth-Heinemann

Leahy, D. A., Green, K. S., 2012, *Astrophys. J.*, **760**, 25

Lequeux, J., 1962, *Ann. D'Astrophys.*, **25**, 221

Lequeux, J., 2005, *The Interstellar Medium*, Berlin Heidelberg: Springer-Verlag

Long, K. S., 2016, *Galactic and Extragalactic Samples of Supernova Remnants: How They Are Identified and What They Tell Us*, in "Handbook of Supernovae", Eds. Athem W. Alsabti and Paul Murdin, Springer International Publishing

Longair, M. S., 2011, *High Energy Astrophysics Third Edition*, Cambridge: Cambridge Univ. Press

Malkov, M. A., Drury, L'O. C., 2001, *Rep. Prog. Phys.*, **64**, 429

Mannucci, F., Della Valle, M., Panagia, N., Cappellaro, E., Cresci, G., Maiolino, R., Petrosian, A., Turatto, M., 2005, *Astron. Astrophys.*, **433**, 807

Mathewson, D. S., Clarke, J. N., 1973, *Astrophys. J. Suppl. Series*, **180**, 725

Mathewson, D. S., Ford, V. L., Dopita, M. A., Tuohy, I. R., Long, K. S., Helfand, D. J., 1983, *Astrophys. J. Suppl. Series*, **51**, 345

Maund, J., Smartt, S. J., Kudritzki, R. P., Podsiadlowski, P., Gilmore, G. F., 2004, *Nature*, **427**, 129

MacFadyen, A. I., Woosley, S. E., 1999, *Astrophys. J.*, **524**, 262

McKee, C. F., Ostriker, J. P., 1977, *Astrophys. J.*, **218**, 148

Milne, D. K., 1970, *Austral. J. Phys.*, **23**, 425

Minkowski, R., 1941, *Publ. Astron. Soc. Pacific*, **53**, 224

Morlino, G., 2016, *High-Energy Cosmic Rays from Supernovae*, in "Handbook of Supernovae", Eds. Athem W. Alsabti and Paul Murdin, Springer International Publishing

Nikolić, S. et al., 2013, *Science*, **340**, 45

Nomoto, K., 1984, *Astrophys. J.*, **277**, 791

Nomoto, K., Jamaoka, H., Pols, O. R., van den Heuvel, E. P. J., Iwamoto, K., Kumagai, S., Shigeyama, T., 1994, *Nature*, **371**, 227

Nomoto, K., Thielemann, F.-K., Yokoi, K., 1984, *Astrophys. J.*, **286**, 644

Onić, D., 2013, *Astrophys. Space Sci.*, **346**, 3

Onić, D., Urošević, D., Arbutina, B., Leahy, D., 2012, *Astrophys. J.*, **756**, 61

Paczyński, B., 1998, *Astrophys. J.*, **494**, L45

Pacholczyk, A. G., 1970, *Radio Astrophysics. Nonthermal Processes in Galactic and Extragalactic Sources*, San Francisco: Freeman & Co.

Pavlović, M. Z., 2017, *Mon. Not. R. Astron. Soc.*, **468**, 1616

Pavlović, M. Z., Urošević, D., Vukotić, B., Arbutina, B., Göker, Ü. D., 2013, *Astrophys. J. Suppl. Ser.*, **404**, 4

Pavlović, M. Z., Dobardžić, A., Vukotić, B., Urošević, D., 2014, *Serb. Astron. J.*, **189**, 25

Perlmutter, S. et al., 1999, *Astrophys. J.*, **517**, 565

Petukhov, Yu. V., Razin, A. V., Razin, V. A., 2006, *Astronomy Letters*, **32**, 747

Pizzochero, P., 1990, *Astrophys. J.*, **354**, 333

Poveda, A., Woltjer, L., 1968, *Astron. J.*, **73**, 65

Reynolds, S. P., 2016, *Dynamical Evolution and Radiative Processes of Supernova Remnants*, in "Handbook of Supernovae", Eds. Athem W. Alsabti and Paul Murdin, Springer International Publishing

Reynolds, S. P., Chevalier, R. A., 1981, *Astrophys. J.*, **245**, 912

Reynolds, S. P., Borkowski, K. J., Green, D. A., Hwang, U., Harrus, I., Petre, R., 2008, *Astrophys. J. Letters*, **680**, L41

Reynolds, S. P., Gaensler, B. M., Bocchino, F., 2012, *Space Sci. Rev.*, **166**, 231

Reynoso, E. M., Dubner, G. M., Goss, W. M., Arnal, E. M., 1995, *Astron. J.*, **110**, 318

Riess, A. G. et al., 1998, *Astron. J.*, **116**, 1009

Riess, A. G. et al., 2007, *Astrophys. J.*, **659**, 98

Rohlfs, K., Wilson, 2004, *Tools of Radio Astronomy*, Heidelberg: Springer-Verlag

Ruiz-Lapuente, P. et al., 2004, *Nature*, **431**, 1069

Rybicki, G. B., Lightman, A. P., 2004, *Radiative Processes in Astrophysics*, Weinheim: Wiley-VCH

Sedov, L. I., 1959, *Similarity and Dimensional Methods in Mechanics*, New York: Academic Press

Scalzo, R. A. et al., 2010, *Astrophys. J.*, **713**, 1073

Schmidt, B. P. et al., 1993, *Nature*, **364**, 600

Shu, F., 1991, *The Physics of Astrophysics, vol. I – Radiation*, Sausalito: University Science Books

Shu, F., 1992, *The Physics of Astrophysics, vol. II – Gas Dynamics*, Sausalito: University Science Books

Shklovsky, I. S., 1960a, *Astron. Zh.*, **37**, 256

Shklovsky, I. S., 1960b, *Astron. Zh.*, **37**, 369

Stanimirović, S., Chomiuk, L., Salter, C. J., Urošević, D., Bhat, R., Lorimer, D. R., 2003, *Publ. Astron. Obs. Belgrade*, **75**, 67

Taylor, G. I., 1950, *Proc. R. Soc. London, A*, **201**, 159

Tian, W. W., Leahy, D. A., 2014, *Astrophys. J.*, **783**, L2

Toptygin, I. N., 2000, *Astronomy Letters*, **26**, 356

Tuohy I. R., Dopita M. A., Mathewson D. S., Long K. S., Helfand D. J., 1982, *Astrophys. J.*, **261**, 473

Urošević, D., 2002, *Serb. Astron. J.*, **165**, 27

Urošević, D., Pannuti, T. G., 2005, *Astroparticle Physics*, **23**, 577

Urošević, D., Pannuti, T.G., Duric, N., Theodorou, A., 2005, *Astron. Astrophys.*, **435**, 437

Urošević, D., Vukotić, B., Arbutina, B., Sarevska, M., 2010, *Astrophys. J.*, **719**, 950

van den Bergh, S., 1988, *Astrophys. J.*, **327**, 156

Vink, J., 2012, *Astron. Astrophys. Rev.*, **20**, 49

Vučetić, M. M., Arbutina, B., Urošević, D., 2015, *Mon. Not. R. Astron. Soc.*, **446**, 943

Webbink, R. F., 1984, *Astrophys. J.*, **277**, 355

Westerlund B. E., 1990, *Astron. Astrophys. Rev.*, **2**, 29

Westfold, K. C., 1959, *Astrophys. J.*, **130**, 241

Wheeler, J. C., 1990, *Introduction of Supernovae*, 6th Jerusalem Winter School for Theoretical Physics: Supernovae, 1

Wheeler, J. C., 2003, *American Journal of Physics*, **71**, 11

Whelan, J., Iben, I. J., 1973, *Astrophys. J.*, **186**, 1007

Woltjer, L., 1972, *Annu. Rev. Astron. Astrophys.*, **10**, 129

Woosley, S. E., Weaver, T. A., 1986, *Annu. Rev. Astron. Astrophys.*, **24**, 205

Woosley, S. E., Langer, N., Weaver, T. A., 1995, *Astrophys. J.*, **448**, 315

Zirakashvili V. N., Aharonian F., 2007, *Astron. Astrophys.*, **465**, 695

Zhang, X., Chen, Y., Li, H., Zhou, X., 2013, *Mon. Not. R. Astron. Soc.*, **429**, L25

CIP- Каталогизација у публикацији
Народна библиотека Србије

524.352/.354

ARBUTINA, Bojan, 1977-

Evolution of Supernova Remnants / Bojan Arbutina. - Belgrade : Astronomical Observatory, 2018 (Belgrade : Donat Graf). - 92 str. : ilustr. ; 25 cm. - (Публикације Астрономске опсерваторије у Београду = Publications of the Astronomical Observatory of Belgrade, ISSN 0373-3742 ; св. 97)

Tiraž 150. - Napomene i bibliografske reference uz tekst. - Bibliografija: str. 87-92.

ISBN 978-86-80019-83-3

а) Супернове

COBISS.SR-ID 268808716

ISSN 0373-3742
ISBN 978-86-80019-83-3